2012

Compact Terahertz Sources Based on Difference Frequency Generation

Pu Zhao
Lehigh University

COMPACT TERAHERTZ SOURCES BASED ON DIFFERENCE FREQUENCY GENERATION

by

Pu Zhao

A Dissertation

Presented to the Graduate Committee

of Lehigh University

in Candidacy for the Degree of

Doctor of Philosophy

in

Electrical Engineering

Lehigh University

September 2012

Approved and recommended for acceptance as a dissertation in partial fulfillment of the requirements for the degree of Doctor of Philosophy.

.

_____
(Date)

_____
Yujie J. Ding
(Dissertation Advisor)

_____
Accepted Date

Committee Members:

_____
Yujie J. Ding
(Committee Chair)

_____
Filbert J. Bartoli

_____
Nelson Tansu

_____
Yong W. Kim
(Physics Department)

Acknowledgements

Of all the people that I am indebted to, foremost among them is my advisor, Prof. Yujie Ding, whom I would like to thank for his support, encouragement and patience throughout the time I worked and studied in his lab at Lehigh University. I'm greatly obliged to Prof. Ding for offering me this Ph.D student position and giving me the chance to pursue this interesting research topic. Prof. Ding is definitely a model of what every researcher should strive to become. His enthusiasm toward science and technology will constantly influence me in the future.

I would also gratefully thank my Ph.D committee members Prof. Filbert J. Bartoli, Prof. Nelson Tansu and Prof. Yong W. Kim for their constructive comments and advice on my Ph.D research.

I also owe a lot of gratitude to the lab colleagues Dr. Xiaodong Mu, Guibao Xu, Yi Jiang, Hongqian Sun, Renbo Song, Suvranta K.Tripathy for their help and training when I firstly started to do research in the lab. Without their generous assistance, it is impossible for my projects to carry out so fluently. Besides, I would also like to express my thanks to other members of the group for the valuable discussion and rewarding collaboration with them, including Dr. Srinivasa Ragam, Baigang Zhang, Lei Wang, Zhaojun Liu and Ph.D students of the group Guan Sun, Da Li, Xiaomu Lin, Ruolin Chen, Zhongyang Li.

Especially, I would like to thank Mr. Ted Bowen for teaching me how to use Labview as well as his help on providing me with all kinds of electronic devices and components. Besides, I would also like to express my thanks and deeply respect to Mr. Herman Baader for his help in the machine shop.

My friends also gave me a lot of help and encouragement during my stay in Lehigh, including Dan Li, Xingjian Zhang, Xiaochen Zhang, Xiaoxiao Ma, Hanzhu Ni, and Xuebin Wu. All the happy moments we spent together will be unforgettable and become the treasure of my memory. Although our story in Lehigh has almost ended, the years long friendship will continue.

In addition, I would like to dedicate this work to my parents and I am also deeply indebted to them for bringing me up and providing me with the best education opportunities. Finally, I would like to thank my fiancée Yi Liu, for her constant love and support. Without the joy she brought to me, my life would not become colorful. Without the encouragement she gave to me, I would not finish this work with so much courage and confidence.

Contents

List of Tables

List of Figures

Abstract

Terahertz (THz, or be called T-ray) wave refers to the electromagnetic wave with the frequency between 0.1 THz (1THz=1000GHz) and 10 THz or wavelength from 30 μm to 3000 μm. In the frequency domain, this region of electromagnetic wave is located between microwave and infrared wave. Different from the great successes in the microwave and infrared light wave, the applications of THz wave are much less investigated in the past few decades. Recently, it has recently been demonstrated that THz wave exhibits several unique features in terms of applications. For example, THz wave can easily penetrate fabrics and plastics, but it will be reflected by metallic materials. Thus, THz wave has a promising application in security screening. In order to realize the applications of THz wave, the compact, efficient, and high power THz sources have become a critical element of researches in THz wave.

Compared with other ways of generating THz, the approach based on difference frequency generation (DFG) has several advantages, such as operating at room temperature, availability of various pump sources, high conversion efficiency etc. In this dissertation, I will investigate the approaches of making compact THz sources based on DFG. Our compact source is pumped by a unique dual-frequency Q-switched Nd:YLF laser operating at 1047 nm and 1053 nm simultaneously. THz wave at 1.64 THz is generated from GaSe crystal based on DFG between these two wavelengths.

The source is operated completely at room temperature and is capable of emitting output power equivalent to a dynamic range of more than 4000 by using a room temperature detector. Such a dynamic range is sufficiently large for a number of applications.

An improved scheme is also explored to scale up the THz output power by 4.7 times. And this is achieved by introducing two solid-state laser crystals as well as two diode pumps. Furthermore, frequency agility of the THz source is also realized based on this unique design. As a demonstration, THz wave at 2.98 THz is generated by using one Nd:YAG and one Nd:YLF crystal as the two laser gain mediums.

To further improve the output power of the compact source, some more novel configurations are investigated, such as intracavity DFG, compact pump source using dual-frequency passively Q-switched laser, novel optical parametric oscillator with dual-signal and dual-idler output. All these efforts, we believe, will be essential to the realization of the applications of our THz sources in the future.

Chapter 1

Introduction

1.1 Introduction to Terahertz Wave

Terahertz (THz, or be called T-ray) wave refers to the electromagnetic radiations with the frequency between 0.1 THz (10^{12} Hz) and 10 THz or wavelength from 30 μm to 3000 μm [1]. This region of radiations is located between microwave and infrared light. Different from the huge application successes for microwave and infrared light, the applications in the THz region are much less investigated in the past several decades. However, researchers have not neglected this region and the intense researches related to THz wave started at the beginning of 1990s. Now, almost twenty years has passed, many applications of THz wave have been demonstrated, showing a lot of advantages and unique characteristics that cannot be found in the region of microwave or infrared light. The researches of THz wave are still on-going and more applications of THz wave will emerge in the near future.

1.2 Characteristics and Applications of THz wave

1.2.1 Characteristics of THz wave

Advantages

(1) THz wave can penetrate fabrics and plastics. (2) THz wave is non-ionizing and may not damage tissue. Thus, THz wave is safer than X-ray. (3) Many materials have unique spectral "fingerprints" in the THz wave region. (4) THz wave has faster frequency than microwaves which means that it can be used in higher-speed communications. (5) Different from the optical region, it is possible to obtain the phase information of the THz electromagnetic radiation.

Disadvantages

The biggest enemy of THz wave is water. The water vapor or molecule has very high absorption coefficient in THz region. Thus, THz wave cannot propagate very far in atmosphere so that its applications in communication would become very difficult. Besides, the penetration depth of THz wave in tissue is also not very deep (eg. 4 mm in skin).

1.2.2 Applications

In the past two decades, many different applications of THz wave have been developed. Some of these applications will greatly change people's life or even bring some evolutions in different fields.

(1) Cosmology and radio astronomy

(2) Imaging (Figure 1.1 shows one example of THz imaging technology [2].)

(3) Atmospheric remote sensing

(4) Plasma fusion diagnostics and heating

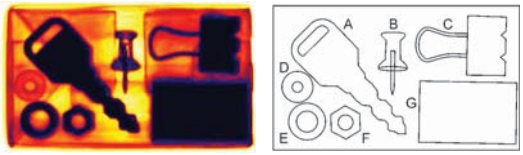

Figure 1.1: THz imaging of a closed cardboard box.

(5) Radar modeling

(6) Material measurement

(7) Local area networks and narrowing

(8) Anti-collision radar for cars

(9) Windshear detection for aircraft

(10) Radar ground movement for aircraft

(11) Concealed weapon detection

(12) Medical sensing

(13) Airport security inspection

1.3 Terahertz Wave Sources

As mentioned in the introduction, the intense researches related to terahertz wave can date back to early 1990s. Now, almost twenty years has passed, most of the applications and explorations are still limited within laboratories and carried out only on optical table. It is easy for us to associate THz wave with the invention of

laser in 1960. Twenty years after that, the researches and applications blossomed at an extremely fast speed. But why is it not so in terahertz domain? One of the most important reasons seems quite obvious. Although different methods have been explored, we are still in short of efficient, compact, powerful terahertz sources that could operate at room temperature.

It is important to list the present THz wave sources and point out their shortcomings and limitations.

1.3.1 Broadband Terahertz Sources

Blackbody Radiation

High-temperature blackbody emitters can provide incoherent radiation in the THz domain. And this kind of sources has already been used in the THz Fourier transform infrared (FTIR) spectrometer. The THz FTIR spectrometer has also been used to fingerprint many different of materials, like DNA's and proteins [3]. However, it is still difficult to create useful terahertz power levels with a blackbody source, because the generated THz power can only reach about 1nW per wave number.

Photoconduction

Terahertz wave photoconduction emitter is based on ultrafast laser pulses. Free carriers-electrons and holes are generated in the photoconductor which is excited by the ultrafast pulses. The static bias fields then accelerate the free carriers and generate a transient photocurrent, resulting in the fast and time changing current which radiates electromagnetic waves in the THz domain. The typical THz wave bandwidth is about 4 THz and the highest output power is about tens of μW.

However, the photoconductor has the drawback of breakdown voltage which greatly limits the output power. [1][4][5]

Optical Rectification

This kind of the method also needs the excitation of ultrafast laser. Optical rectification is a nonlinear optical process which consists in the generation of a DC polarization in a nonlinear optical medium pumped by the ultrafast laser pulses. The output THz wave power is related to the second-order nonlinear coefficient of materials and does not have the upper limit voltage characteristics in photoconduction. The output power will then be limited by the optical damage threshold of the materials and the problem of optical phase-matching. [4]

Air Plasma

This is demonstrated in recent years and will also need very intense ultrafast laser pulses. The advantage is that none special medium is used in the process of generation and air is actually the emitter of the terahertz wave. The ionized plasma is the main mechanism of the efficient THz wave generation and it is actually a third-order nonlinear optical process.[6]

1.3.2 Narrowband Terahertz Sources

Difference Frequency Generation

Difference frequency generation (DFG) is one of the second-order nonlinear optical processes, in which new photon at ω_3 is generated when exciting the nonlinear optical medium both at ω_1 and ω_2 simultaneously ($\omega_3 = \omega_1 - \omega_2$). The generation of THz

wave based on DFG is not a new topic. The experimental demonstration is as early as in the 1970s. However, because of the lack of application in the THz domain at that time, this technique was not further investigated. In recent years, THz wave generation from DFG attracts increasing attentions due to the lack of efficient and powerful THz sources. *Directed by Prof. Ding, our group accomplished a lot of researches in this field and still hold the THz wave peak power record which is 389 W at 203* μm (1.48 THz).[7, 8, 9, 10, 11, 12, 13, 14, 15, 16, 17, 18, 19, 20, 21, 22]. The efficient, tunable, and coherent THz source in our lab can cover as wide as 0.185$\sim$5.27 THz [8].

Upconversion from RF Source

This method is based on the microwave technology and is often obtained by cascading a chain of planar GaAs Schottky-diode multipliers. To achieve THz with higher frequency, the frequency has to be doubled or even tripled with a lot of output power sacrificed each time as this process is applied. And these kinds of THz sources are achievable under 1 THz and are very difficult to reach higher frequency.

CO_2 THz lasers

CO_2 gas THz lasers can give an average output power as high as 100 mW at THz region. This kind of laser use the high power CO_2 gas lasers as the pump source and excites gas molecules emission-line (eg. methanol). Although the high output power is very impressive, the wavelength cannot be tuned continuously and can only cover some discrete emission frequencies. Besides, the whole dimension of the laser is very big and can only be used on optical table in laboratory.

Free-electron Laser

Different from the gas, solid-state, diode lasers, the gain medium in the free-electron laser is relativistic electron beam that moves freely through a periodic magnetic structure. It has the widest tunable wavelength range, which covers from the microwaves to X-rays. The THz domain is included in its tunable range. However, because of its huge dimension and operating complexity, it is only available in some large universities and research institutes. For example, the free electron laser in UCSB can provide kilo-Watt level THz radiation.

Quantum Cascade Lasers

Quantum-cascade laser (QCL) is based on intersubband transitions of electrons inside a quantum-well structure. Unlike other semiconductor light sources, the emitted wavelength is not determined by the band gap of the used material but on the thickness of the constituent layers [23, 24]. QCL obtained complete victory in generating mid-infrared radiation and also is considered to be one of the best candidates for compact THz source. Lots of researches on quantum-cascade terahertz lasers have been reported [25, 26, 27, 28]. The only intrinsic drawback is that quantum-cascade terahertz laser cannot operate at room-temperature.

1.4 Research Objective and Organization

The objective of this research for dissertation is to achieve compact, efficient and high average power terahertz wave source working at room temperature. Because our approach is based on the difference frequency generation technology, these THz sources can completely operate at room temperature. Equation 1.1 shows a basic

expression for the generated terahertz wave power from DFG.

$$P_{THz} \propto \ C \ \frac{P_1 \times P_2}{Area} \ l^2_{coherence} \tag{1.1}$$

C is dependent on the nonlinear optical coefficient of different materials. To generate the THz wave efficiently, we should choose some materials with larger nonlinear optical coefficient, like GaSe, GaP etc. P_1 and P_2 are the pump powers at ω_1 and ω_2, respectively (peak power for pulsed operation; average power for continuous-wave operation). Besides, because the intracavity laser power can be an order of magnitude larger than the extracavity laser power, intracavity DFG can generate much higher THz output power [29]. *Area* is the beam area of the pumps. Although, the area is at the denominator of the expression, it does not mean that we should focus the pump beam size as small as possible. *Area* actually has an optimal value which are connected with the value of $l_{coherence}$. Besides, $l_{coherence}$ covers the information of phase-matching problem which is one of the most important concerned factors in nonlinear optical process.

This dissertation is organized as follows.

In Chapter 2, we propose and demonstrate a compact and portable THz source, based on difference-frequency generation in a GaSe crystal. The two input frequencies, required for achieving frequency mixing, are generated by a single Q-switched Nd:YLF laser incorporating two laser resonators. The average power of the THz output reaches 1 μW at 1.64 THz (182 μm) within a linewidth of 65 GHz. Such a THz source can be packaged into a compact system and operate at room temperature.

In Chapter 3, we investigate power scalability and frequency agility of a THz source by mixing two frequencies generated by solid-state lasers in a nonlinear crystal. They are made possible by introducing two solid-state laser crystals sharing

the same Q-switch and output coupler with the same laser beams decoupled to each other by a polarizer. Following the optimization, we have improved the THz output power to 4.46 μW, which is nearly fivefold compared with the result in Chapter 2 at 1.64 THz. By replacing one of the Nd:YLF crystals with a Nd:YAG crystal, we have produced 2.1 μW at 2.98 THz.

In Chapter 4, we propose a novel intracavity terahertz generator based on compact dual-frequency solid state laser. The laser output coupler, based on multilayer unbonded GaP stack, operates as the nonlinear optical medium for terahertz generation simultaneously. By achieving intracavity scheme and using quasi-phase-matching through alternating each layer of GaP stack, terahertz output power is significantly enhanced compared with the external-cavity approach.

In Chapter 5, we will discuss an approach to dramatically reduce the timing jitter between the pulses at two different wavelengths. In the experiment, when two Nd:YLF crystals share a Cr:YAG crystal functioning as a single passive Q-switch, the timing jitter between each pair of dual-frequency pulses generated by the two crystals has been reduced by a factor of 20. Such a reduction in the timing jitter allows us to generate terahertz pulses by focusing such a passively Q-switched laser beam onto a nonlinear crystal. Such a result represents the first step for us to eventually implement a compact terahertz source based on ultracompact microchip lasers.

In Chapter 6, we propose and implemente a singly resonant optical parametric oscillator based on adhesive-free-bonded periodically inverted $KTiOPO_4$ plates. It has major advantages such as walk-off compensation and oscillation at four wavelengths. The threshold of the oscillation was measured to be 8 MW/cm^2, which is about a factor of 4 lower than that based in two separate $KTiOPO_4$ crystals.

By frequency-mixing the dual-wavelength output in GaP stacks, we generated the terahertz radiation at 2.54 THz. The tuning range of the terahertz output was demonstrated to be 2.19-2.77 THz. Besides, based on the same adhesive-free-bonded $KTiOPO_4$, we also propose and demonstrate an approach to generate THz wave with multiple wavelengths.

In Chapter 7, in order to further reduce the size of compact THz source, we propose a way to generate dual-wavelength radiation from the same laser medium. This is made possible by inserting etalon into the cavity such that the dual-wavelength gain could be selected from the wide emission bandwidth of the laser gain medium. A demonstration will be discussed by using Yb: YAG laser crystal and the following experiment of generating THz wave. Besides, we will also discuss the experiment of generating multi-wavelength laser radiation from Yb: YAG ceramics, which could be used to build the promising pump source for the cascaded DFG process.

In Chapter 8, we would summarize this dissertation and discuss about the future work.

Chapter 2

Compact and Portable THz Source

Parametric processes such as terahertz (THz) parametric oscillation [30] and difference-frequency generation (DFG) [8] have been used to efficiently generate monochromatic THz beams. However, the efficient conversion has been made possible only by using input beams with relatively high peak powers [30, 8, 9], available from a bulky and nonportable Nd:YAG laser and master oscillator/power oscillator [19]. Monochromatic THz frequencies have also been generated from quantum cascade lasers [31, 32] and photomixers [33]. However, THz quantum cascade lasers must be cryogenically cooled, whereas photomixers typically suffer from low output powers owing to the potential damage caused by overheating [34].

In this chapter, we demonstrate a compact and portable THz source that has been implemented by us based on DFG in a GaSe crystal [35]. An average THz output power can be as high as 1 μW at 1.64 THz (182 μm) in a linewidth of 65 GHz, corresponding to the peak power of 20 mW. Such an output power is sufficiently

high for realizing certain applications such as THz imaging [36], chemical sensing [37], and probing intermolecular interaction mechanisms [38].

2.1 Nd: YLF

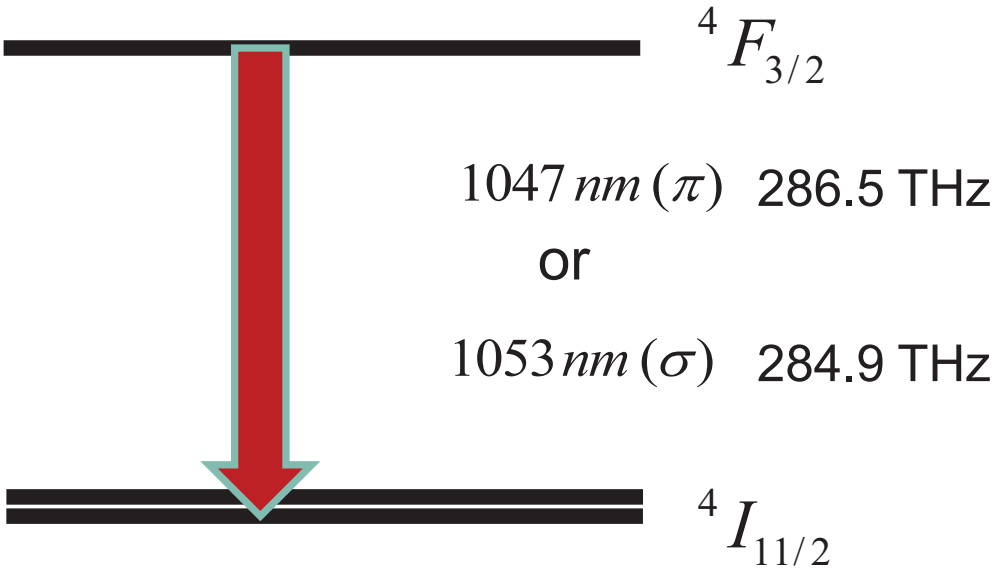

Figure 2.1: Energy level of Nd:YLF.

Neodymium-doped yttrium lithium fluoride (Nd:YLF) is a conventional laser medium and has already been used in different solid-state laser systems for many years. However, in the research, we will prove that Nd:YLF crystal is a quite promising laser medium in the laser pump source for THz generation based on

DFG.

In our experiment, we have chosen a Nd:YLF crystal as the lasing medium because two different frequencies of 286.5 THz and 284.9 THz (wavelengths of 1047 nm and 1053 nm) can be generated from a single Nd:YLF laser. Indeed, because a Nd:YLF crystal is birefringent, it emits two transitions at 1047 nm and 1053 nm with the polarizations being orthogonal to each other, designated by π and σ, respectively. Figure 2.1 shows the schematic plot of the energy levels related to these two transitions which are between the two energy levels $^4F_{3/2}$ and $^4I_{11/2}$, respectively.

Because the two transitions have the stimulated emission cross sections of $1.8 \times 10^{-19}\ cm^{-2}$ and $1.2 \times 10^{-19}\ cm^{-2}$ at 1047 nm and 1053 nm, respectively, it is feasible for us to tailor the output powers at these two wavelengths from a single laser crystal to be close to each other. In such a case, the corresponding THz power reaches an optimal value under the same sum of the two input powers. Moreover, the THz output frequency generated by mixing these two laser beams is 1.643 THz (i.e., the wavelength of 182.42 μm), which is sufficiently close to 200 μm, and therefore, the THz output power is close to the maximum value from a GaSe crystal [8, 9]. Furthermore, a Nd:YLF crystal is known for its low thermal effect and long upper-state lifetime. In the past, a single Nd:YLF crystal was used to simultaneously generate the output beams at 1047 nm and 1053 nm without introducing any optical element inside a single laser resonator [39]. However, the ratio of the powers generated at these two wavelengths could not be controlled at all. In addition, the laser output powers are also too low for the efficient generation of a THz output based on DFG. Although a Q-switched Nd:YLF laser was implemented at 1053 nm [40], the simultaneous lasing of the two wavelengths has not been achieved. Besides the Nd:YLF

crystal, other combinations of the active ions and host materials can emit two different frequencies, see, e.g., [41]. As demonstrated by us below, Q-switched solid-state lasers may be one of the optimal choices for implementing a compact THz source based on DFG.

2.2 Dual-Frequency Nd: YLF Laser

Our experimental setup is shown in Fig. 2.2. The section is a schematic for a dual-frequency Nd:YLF laser. In principle, one can simultaneously generate the coherent beams at 1047 and 1053 nm from a single Nd:YLF laser. Figure 2.3 shows the real setup for the dual-frequency Nd: YLF laser.

However, under such a case, balancing the output powers at the two wavelengths is out of question owing to the strong competition between the gains for the two transitions within the same laser medium. In our experiment, we introduced an intracavity polarizer to separate the two perpendicularly polarized beams into two laser cavities, both of which shared the same lasing medium for alleviating the gain competition. In our design, an input mirror (IM), output coupler (OC1), and polarizer (P) make up the cavity for lasing at 1047 nm (π, o wave), whereas an IM, P, and coupler OC2 make up the cavity for lasing at 1053 nm (σ, e wave). An a-cut 1.0% Nd-doped YLF ($4mm \times 4mm \times 10mm$) crystal was shared arm by the two laser cavities. A plano IM has a coating for producing the high transmittance of T $>$ 95% at 808 nm and simultaneously a high reflectivity of R $>$ 99.5% at 1047 and 1053 nm. The polarizer has a coating in such a way that when being placed at a Brewster angle relative to the input beam, the -polarized beam has a high transmittance of T $\approx$ 98%, whereas the -polarized beam has the high reflectivity of R $>$ 99.9%. The

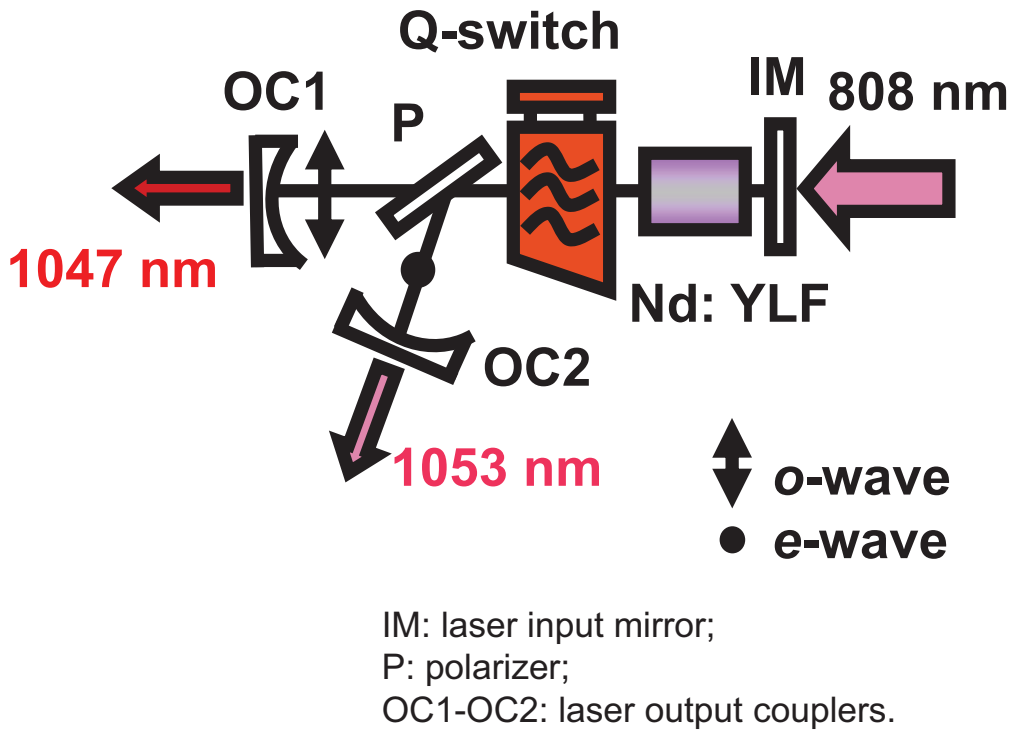

Figure 2.2: Experimental setup for the dual-frequency Nd: YLF laser.

Nd:YLF crystal was pumped by a diode laser via a fiber pigtail after the laser beam was collimated by a lens assembly. Such a diode laser has dimensions of 1.75" $\times$1.25" (4.45 cm $\times$ 3.18 cm), which is portable. Considering the fact that the stimulated emission cross section for the 1047 nm transition is 50% larger, one of the most effective approaches for balancing the output powers of the two transitions is to introduce an additional amount of loss in the cavity for the 1047 nm beam. First, we have specifically chosen the different reflectivities for the two output coupler to be 75% and 80% at 1047 nm (OC1) and 1053 nm (OC2), respectively. As a result, the lasing thresholds for the two transitions become closer to each other.

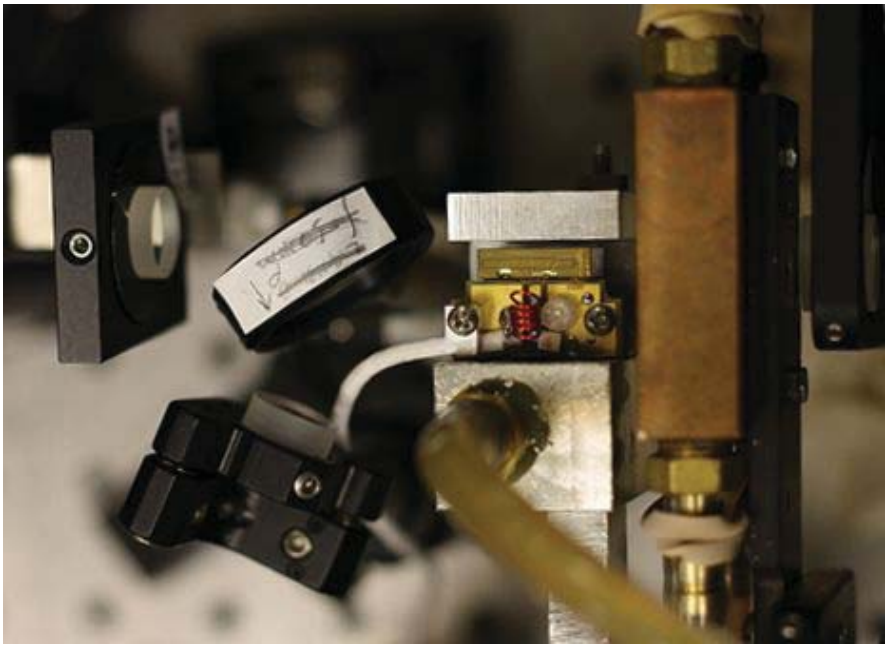

Figure 2.3: Real setup for the dual-frequency Nd: YLF laser.

Second, OC1 was slightly tilted to introduce an additional amount of the loss at 1047 nm. To generate sufficiently high peak powers, an acousto-optic Q-switch was placed next to the Nd:YLF crystal in such a way that it was shared by the two beams oscillating in the two cavities. This represents an important method for us to synchronize the output pulses generated from the two laser cavities. The typical dimension of the entire THz source illustrated by Fig. 2.6 is about 12" × 12" × 6" ($30.48cm \times 30.48cm \times 15.24cm$). Through further optimization, it can be reduced to 12" × 6" × 4" ($30.48cm \times 15.24cm \times 10.16cm$).

In addition, such a compact THz source currently consumes the electrical power of $\leq$20 W. Therefore, it can be readily packaged into a portable system.

Figure 2.4 shows the dependence of Q-switched output powers at 1047 nm and

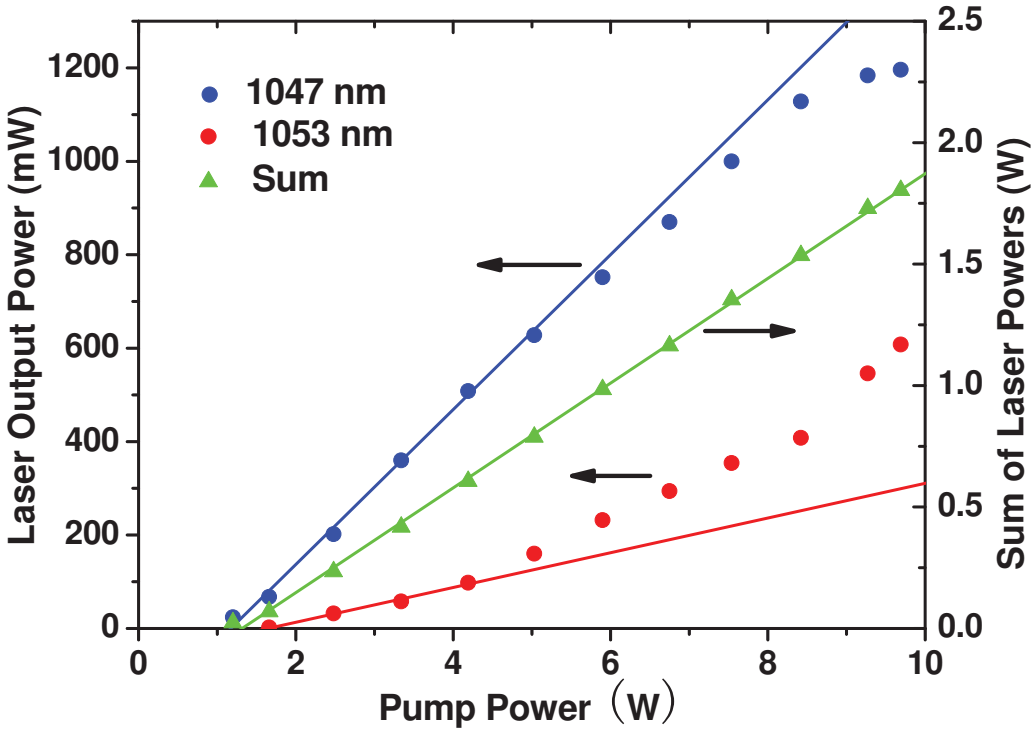

Figure 2.4: Dependence of powers from dual-frequency Q-switched Nd:YLF laser on pump power from laser diode.

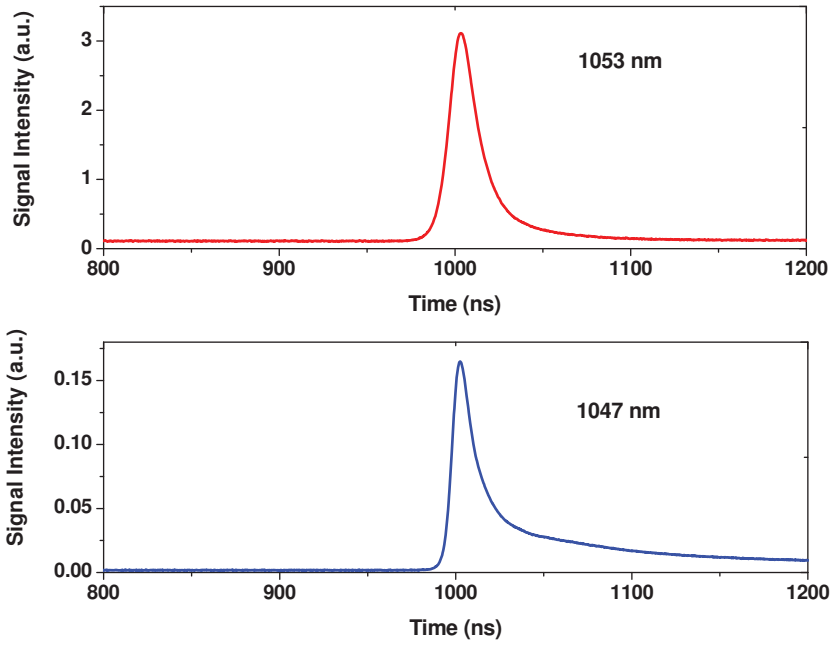

Figure 2.5: Temporal profiles of dual-frequency output pulses generated by from Q-switched Nd:YLF laser. Ch1: 1053 nm and Ch2: 1047 nm.

1053 nm and the sum of the output powers on the output power from the laser diode. The lasing thresholds were measured to be 1.17 and 1.64 W at 1047 and 1053 nm, respectively. From Fig. 2.4, we can see that below the pump power of 5 W, both of the output powers increased linearly with the pump power. In addition, the powers at 1047 nm are significantly higher. Above 5 W, however, the output power at 1047 nm became slightly saturated, whereas the output power at 1047 nm was increased at a higher rate. This is due to the fact that the two transitions

accessed the same population of the electrons in the upper lasing level. When the gain for one transition was saturated, the gain for the second one was increased. Therefore, the dependence for the sum of the output powers is still linear, which agrees well with the theory for the solid-state laser [42]. By measuring the output powers as a function the repetition rate, we found an optimal repetition rate of 3.9 kHz for the Q switch in terms of the THz output powers. At the pump power of 9.69 W, we generated the output powers of 1.196 and 0.608 W at 1047 and 1053 nm, respectively, corresponding to the net conversion efficiency of 18.6%. The ratio of the output powers at the two wavelengths is measured to be around 2:1. By further optimizing the design of the optical cavities, we can reduce the ratio to nearly 1:1. The M^2 factors were measured to be 5.18 and 3.07 for 1047 and 1053 nm, respectively, at the pump power of 5.9 W. The poorer beam quality at 1047 nm is attributed to the tilting of its cavity mirror, which was used by us to reduce the ratio of the output powers for the two transitions. The pulse shapes of the two output beams are shown in Fig. 2.5. The two pulse trains were measured simultaneously by using two photodiodes. According to Fig. 2.5, the two pulses were synchronized. At the pump power of 9.69 W, the pulse widths were measured to be 15.5 and 18.6 ns at 1047 and 1053 nm, respectively.

2.3 Compact THz Source based on DFG

Using two convex lenses with the same focal length, the two beams were collimated and then combined by a polarization cube, as shown in Fig. 2.6. It was adjusted in such a way that the optical paths at the two wavelengths were exactly the same. As a result, the two input beams were overlapped in both time and space and

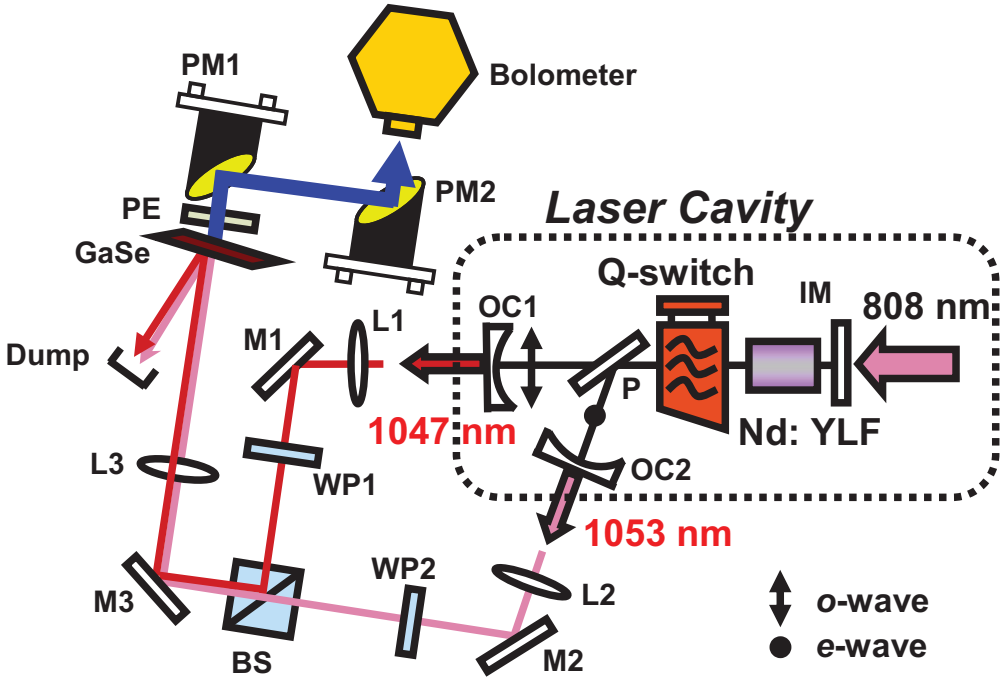

Figure 2.6: Experimental setup for the THz DFG based on a compact and portable dual-frequency Nd:YLF laser having dual cavities: L1-L3, convex lenses; M1-M3, highreflection mirrors; WP1-WP2, half-wave plates; PE, high density white polyethylene filter; and PM1-PM2, parabolic mirrors.

focused on the 15 cm long GaSe crystal by using a convex lens (L3). After DFG, the residual pump beams were blocked by using a white polyethylene filter and the reflected pump beams were collected by a beam dump. The generated THz beam was collected by two off-axis parabolic mirrors and then focused onto a power meter. The input beams at 1047 nm and 1053 nm were ordinary and extraordinary waves inside the crystal, whereas the THz wave was an extraordinary wave. The external

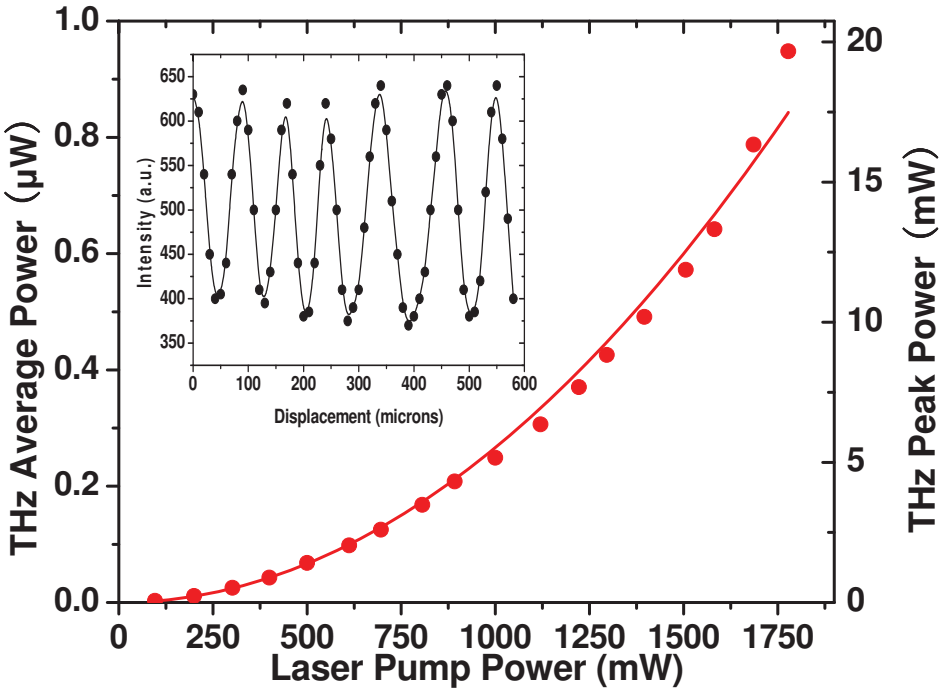

Figure 2.7: Dependences of average and peak output powers on sum of the output powers generated by the single Nd:YLF laser. Solid curve corresponds to quadratic fit to data points. Inset: plot of power being transmitted through a Si etalon vs. distance between two Si plates in the etalon.

phase matching angle was measured to be 11.5°, which is close to the theoretical value of 11° [43]. The azimuthal angle was optimized in our experiment in order to reach the optimal value of the effective nonlinear coefficient [43]. The output wavelength was measured by scanning a Si-based etalon, shown in the inset of Fig. 2.7. The output wavelength was measured to be 183.3 μm, which agrees well with 182.4 μmm, calculated from the two input wavelengths of 1.04666 and 1.0527 μm [42]. We plotted the dependence of the average and peak output powers on the sum of the output powers generated by the Nd:YLF laser as the input powers for DFG; see Fig. 2.7. The solid curve corresponds to the quadratic fit to the data points, which is consistent with the characteristics of DFG. Our experimental result indicated that the average output reached optimal values at the repetition rate of 3.9 kHz. When the sum of the input powers was 1.8 W, the average output power from the GaSe crystal was measured to be 0.948 μW. The pulse width for the THz beam was deduced to be 12.36 ns by measuring the temporal profile of the sum-frequency signal in a KTP crystal. Based on such a pulse width, the highest THz peak power was determined to be 19.7 mW. The linewidth of the THz wave was estimated to be 65 GHz by measuring the linewidth of the sum-frequency signal (i.e., 0.06 nm). A DLATGS pyroelectric detector operating at room temperature can have a noise equivalent power of as low as 230 pW. Therefore, the output power of 0.948 μW corresponds to a dynamic range of 4120, which is sufficiently high for realizing the key applications mentioned above. We can further improve the output powers to at least 100 μW by placing a nonlinear crystal inside the optimized Nd:YLF laser cavities.

In conclusion, we have implemented a compact and portable THz source operating at room temperature. Such a device is based on the mixing of two frequencies

generated from a single solid-state Nd:YLF laser in a GaSe crystal. The highest average output power was measured to be 1 μW at 1.64 THz (182.4 μm) in a linewidth of 65 GHz, at the repetition rate of 3.9 kHz.

Chapter 3

Power Scaling and Frequency Tuning

As mentioned in chapter 1, although the quantum cascade lasers have their own advantage due to their compact sizes [36] and tunability [44], these lasers still must be cryogenically cooled in order to generate radiations in THz band.

On the other hand, solid-state lasers such as those based on neodymium-doped laser crystals can be used to generate very high output powers in the near-infrared region, especially if they are Q-switched [42]. Recently, by mixing the dual-frequency output from a neodymium: yttrium lithium fluoride (Nd:YLF) laser at 286.5 and 284.9 THz in a nonlinear crystal, we generated a THz output at the frequency of 1.643 THz [35]. Since a Nd:YLF laser can be made to be rather compact, such a demonstration opened a new route to a compact THz source. Besides the compactness, such a THz source is operated at room temperature. However, since the two lasing transitions share the same upper level inside in a single Nd:YLF laser crystal [35], they compete for the output powers. Namely, when the output power at one

frequency grows at a higher rate, the power at the other frequency must grow at a lower rate or it can be even saturated. Such a competition severely limits the product of the output powers at the two frequencies, necessary for further scaling up the THz power. Moreover, it causes the instability of the dual-frequency laser output. Furthermore, since such a laser can only emit two specific frequencies, only a single THz output frequency can be generated, which limits the applications of the THz source.

In this chapter, we will explore the approach to do power scaling for THz generation and achieve frequency tuning for the THz radiation based on DFG [45].

3.1 Dual-Frequency Dual-Gain-Medium Nd:YLF Laser

In order to solve the problem of gain competition between the transitions at 1047 nm and 1053 nm in Nd:YLF laser crystal, we introduced two laser crystals to generate two different output frequencies. Our experimental result illustrates that the output powers of the solid-state lasers based on two crystals are significantly improved. Consequently, we have improved the THz output power by mixing the two laser frequencies in a nonlinear crystal. After the second laser crystal is introduced, the THz source still maintains its compactness. Moreover, such a configuration can be used to extend to the combinations of different laser crystals for generating different output frequencies.

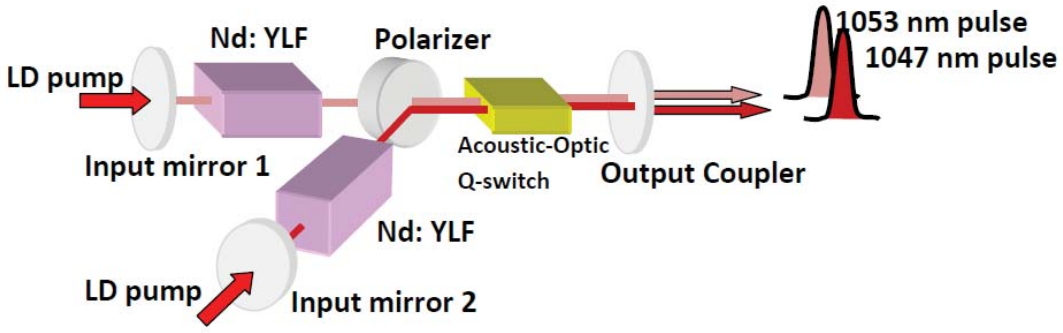

Figure 3.1: Experimental setup for the dual-frequency dual-Nd: YLF crystals laser.

3.1.1 Experimental Setup

The experimental setup for the new configuration of laser cavities is shown in Fig. 3.1. The input mirror 1, polarizer, output coupler make up the first cavity for lasing at 1053 nm while the input mirror 2, polarizer, output coupler make up the second cavity for lasing at 1047 nm. This cavity configuration is completely different from our previous one [35]. Indeed, in the previous work [35], the Nd:YLF crystal was placed at the arm sharing the 1047 and 1053 nm cavities. As a result, the two radiation beams at 1047 and 1053 nm transition accessed the same population inversion within a single Nd:YLF crystal pumped by the same diode laser. Since the 1047 and 1053 nm beams have perpendicular polarization directions, we introduced an intracavity polarizer to separate the two beams into the two cavities. This approach alleviated the gain competition between the 1047 and 1053 nm radiation beams inside the Nd:YLF crystal. However, due to the competition, we observed the unbalanced powers between the two frequencies [35]. In our configuration, we introduced two Nd:YLF crystals (α-cut, Nd doped at 1.0%, and $4 \times 4 \times 10 mm^3$),

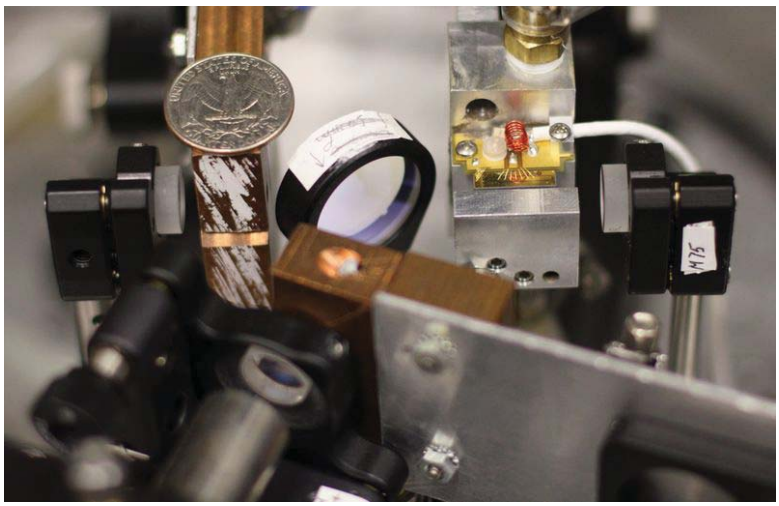

Figure 3.2: Real setup for the dual-frequency dual-Nd: YLF crystals laser. The quarter size can show the compactness of the system

labeled as laser crystals 1 and 2 in Fig. 3.1. The two laser crystals were placed at the two divided arms decoupled by the polarizer. As a result, the 1047 nm and 1053 nm transition beams now access the population inversions from two separate gain media, representing an ultimate solution to the gain competition. An acoustic-optic Q-switch was placed at the shared arm of the two laser cavities. Thus, the dual-frequency pulses are synchronized by simultaneously modulating the losses of the two cavities. The other improvement of the cavities is an output coupler shared by the two cavities, i.e., a concave mirror (curvature=15 cm) having a reflectivity of R=75% at both 1047 nm and 1053 nm. It is mentioned that although we introduced two laser crystals into the cavity, the compactness of the laser is not influenced. Figure 3.2 shows the real setup for the dual-frequency dual-Nd: YLF crystals laser. As we can see in the picture, the laser is rather compact.

The two diode pump beams at 808 nm are collimated and focused onto the

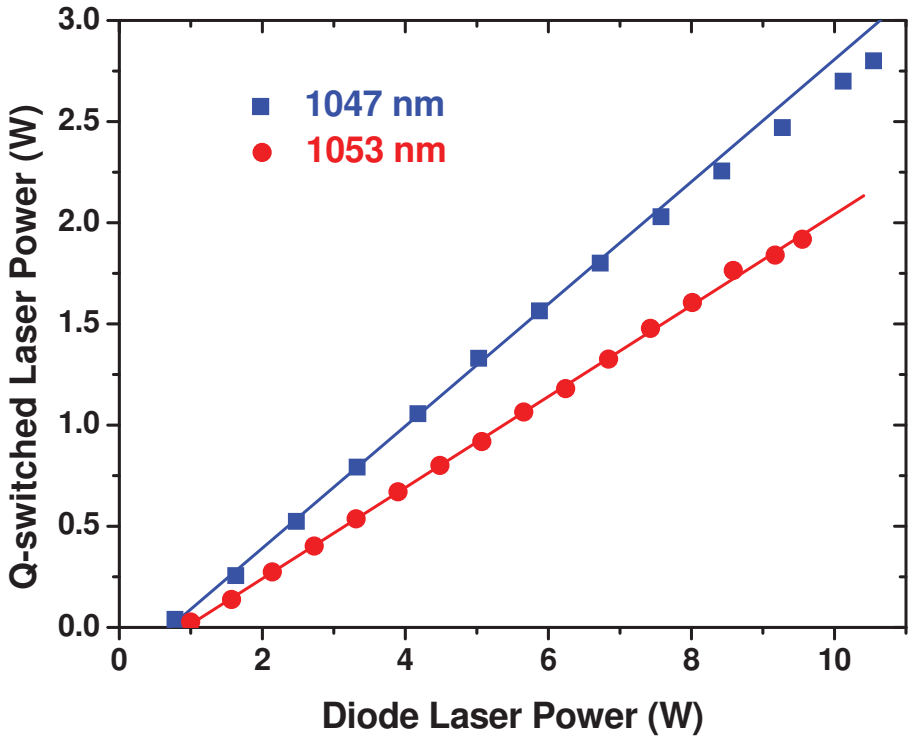

Figure 3.3: Q-switched output power vs pump power at 1047 and 1053 nm. Dots and squares correspond to data points; straight lines correspond to linear fits to data points.

Nd:YLF crystals through a couple of convex lenses, respectively. The diode pump power can be tuned separately. This feature is quite critical for synchronizing the dual-frequency pulses when the lasers are operated at the pulsed mode. In such a case, the pulse build-up times for the two lasers must be exactly the same. After the acoustic-optic become highly transparent, the laser pulse is not generated instantly. The pulse build-up time is the time it takes to generate the laser pulse when the Q-switch is instantly open. This value is determined by the stimulated emission cross section of the laser gain medium, loss of the cavity, output coupling coefficient, and pumping level above threshold. In fact, once the laser crystals are chosen and the cavity is well aligned, the former three factors cannot be changed. As a result, the only way for changing the pulse build-up time is the pump power level. In our configuration, we can separately change the pump power levels of the two lasers simply by varying the driving currents of the lasers.

3.1.2 Power Dependences Based on Two Gain Mediums

When the repetition rate of the Q-switch is set at 5 kHz, we have measured the dependence of the Q-switched output powers on the pump powers at both 1047 and 1053 nm, see Fig. 3.3. Both of the output powers at 1047 nm and 1053 nm have increased linearly. As a result, we have completely solved the issue of the gain competition in our previous geometry [35]. At the pump power of 10.55 W and 9.55 W, we have obtained the output powers of 2.8 W and 1.918 W at 1047 and 1053 nm, corresponding to net conversion efficiencies of 26.5% and 20.1%, respectively. The corresponding slope efficiencies are 29.8% and 22.5%, respectively. Compared with the previous results,5 the total output power has been improved by more than twice. In addition, the ratio of slope efficiencies between 1047 and 1053 nm is 1.32.

This value is close to the ratio of the corresponding stimulated cross sections (i.e., 1.5) [35].

3.2 Power Scaling for THz Generation

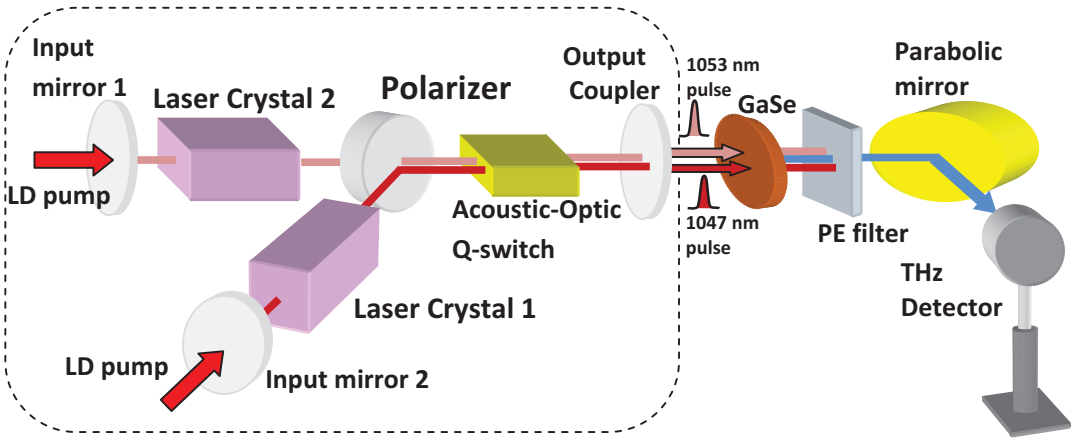

Figure 3.4: Experimental layout for a configuration of the dual-frequency solid-state laser and compact THz source. The dual-frequency laser cavities are marked by the dashed border line.

Since the dual-frequency beams are emitted from the same output coupler, see Fig. 3.1, the two beams are collinearly propagating. In order to generate a THz output based on frequency mixing, we can simply place a nonlinear crystal right after the output coupler. Therefore, the THz source is truly compact.

We have used a 15-mm-long GaSe crystal to measure the THz output by mixing the two laser beams, see Fig. 3.4. The GaSe crystal is placed directly after the output coupler. This setup is different from our previous one where a beam splitter was used to combine the two dual-frequency beams onto a nonlinear crystal. Obviously,

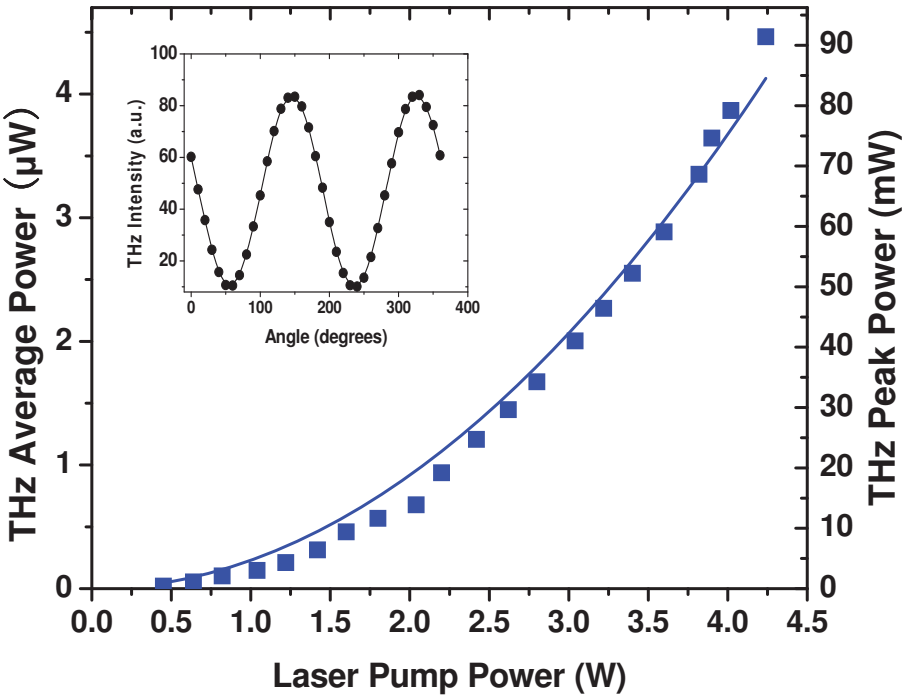

Figure 3.5: THz average and peak power dependence on the combined power at 1047 and 1053 nm; straight lines correspond to quadratic fits to data points. Inset is the intensity of the THz radiation as a function of the azimuthal angle of a THz polarizer.

our configuration shown by Fig. 3.4 is much more compact. We have measured the power dependence, see Fig. 3.5. At the highest incident power of 4.24 W, we have achieved an output power of 4.464 μW at 1.643 THz (182.4 μm). According to Fig. 3.5, the dependence is nearly quadratic, which is characteristic for DFG. Compared with the previous result, we have increased the output power by 4.7. Such an enhancement is attributed to the improvement of the laser powers at 1047 and 1053 nm. The pulse widths at 1047 nm and 1053 nm are measured to be 17.7 ns and 11.71 ns, respectively. The laser linewidths are measured to be 77.5 GHz and 76.5 GHz, respectively. Assuming the pulse shape is Gaussian, the pulse width of THz radiation is estimated to be 9.766 ns. We have also measured the polarization of the THz radiation as a function of the azimuthal angle of a THz polarizer, shown by inset to Fig. 3.5. Based on the sinusoidal oscillation, the THz polarization can be determined.

3.3 Frequency Tuning for THz Wave

3.3.1 Nd-doped Laser Crystals

In the previous parts, we only used Nd: YLF laser crystals as the gain medium in the solid-state lasers as the pump sources for THz source. Actually, more than 100 Nd-doped laser materials or ceramics have been studied with their wavelengths covering from 1.03 μm to 1.1 μm [46]. Nd:YLF is just one of these materials (see Table 3.1). One of the advantages for our configuration lies in the fact that we can generate the THz output frequency simply by choosing two different laser crystals. As a result, it is conceivable for us to generate any THz output wavelength.

Wavelength (μm)	**Material**
1.0369	$CaF_2 - SrF_2$
1.0370	CaF_2
1.0370	SrF_2
1.042-1.075	$Na_{0.4}Y_{0.6}F_{2.2}$
1.0445	SrF_2
1.046-1.064	$LiNdP_4O_{12}$
1.0461	$CaF_2 - YF_3$
1.0461-1.0468	CaF_2
1.047	$LiGdF_4$
1.047	$LiNdP_4O_{12}$
1.047	**$LiYF_4$**
1.047-1.078	NdP_5O_{14}
1.0471	$LiYF_4$
1.0472	$LiLuF_4$
1.0475	$LaBGeO_5$
1.0477	$Li(Nd, La)P_4O_{12}$
1.0477	$Li(Nd, Gd)P_4O_{12}$
1.048	$Li(Bi, Nd)P_4O_{12}$
1.053	**$LiYF_4$**
...	**...**

Table 3.1: Part of the Nd-doped laser materials.

3.3.2 Dual-Frequency Nd: YLF/YAG Laser

In order to demonstrate the THz frequency tuning, we chose Nd:YAG and Nd:YLF crystals. The experimental setup is similar with the setup in Fig. 3.1. In the cavity, a Nd:YLF crystal (α-cut, Nd doped at 1.0%, and $4 \times 4 \times 10mm^3$) was placed at one arm of the cavity and a Nd: YAG crystal (Nd doped at 1.0%, $\Phi 5mm$, 10 mm long) was placed at the other arm of the cavity, see Fig. 3.6. All the rest of the optical components remain the same. At the diode pump powers of 9.55 W and 8.653 W, we have generated the output powers of 1.981 W and 1.706 W at 1053 nm

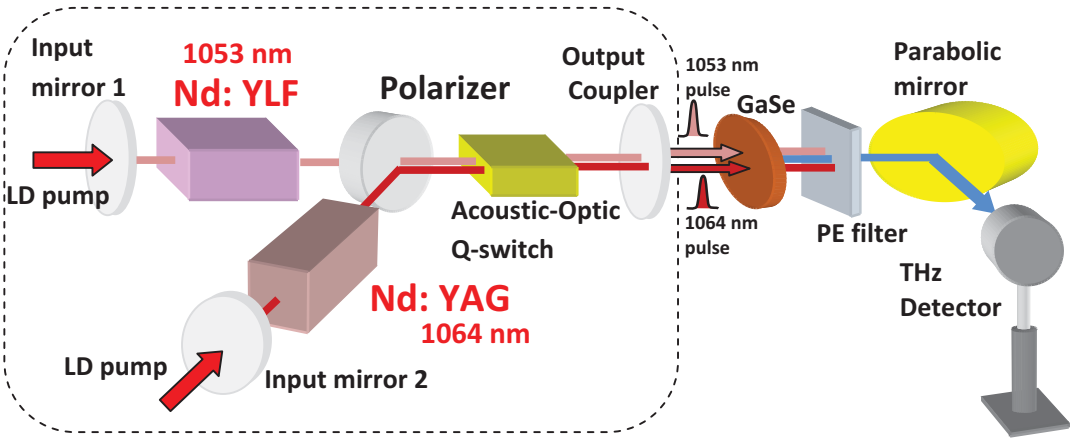

Figure 3.6: Experimental setup for the dual-frequency based on Nd: YAG and Nd: YLF as well as the setup for THz generation.

and 1064 nm, respectively, corresponding to the net conversion efficiencies of 20.7% and 19.7%. At the repetition rate of 5 kHz, the pulse widths are measured to be 9.92 ns and 12.48 ns, respectively. The laser linewidths are measured to be 76.5 GHz and 75.0 GHz, respectively.

3.3.3 Frequency Tuning for THz Wave

By mixing the two laser beams on the GaSe crystal, we have generated the THz radiation at 2.983 THz (100.5 μm). The external phase-matching angle for the type II DFG is measured to be 18.3°, which is consistent to the theoretical value [43]. The highest output power is 2.09 μW. Figure 3.7 shows the THz average power dependence pumped by the dual-frequency lasers based on Nd: YAG and Nd: YLF. The lower output power at such a frequency, compared with that at 1.64 THz, is due to the increased absorption of the THz radiation by the GaSe crystal.

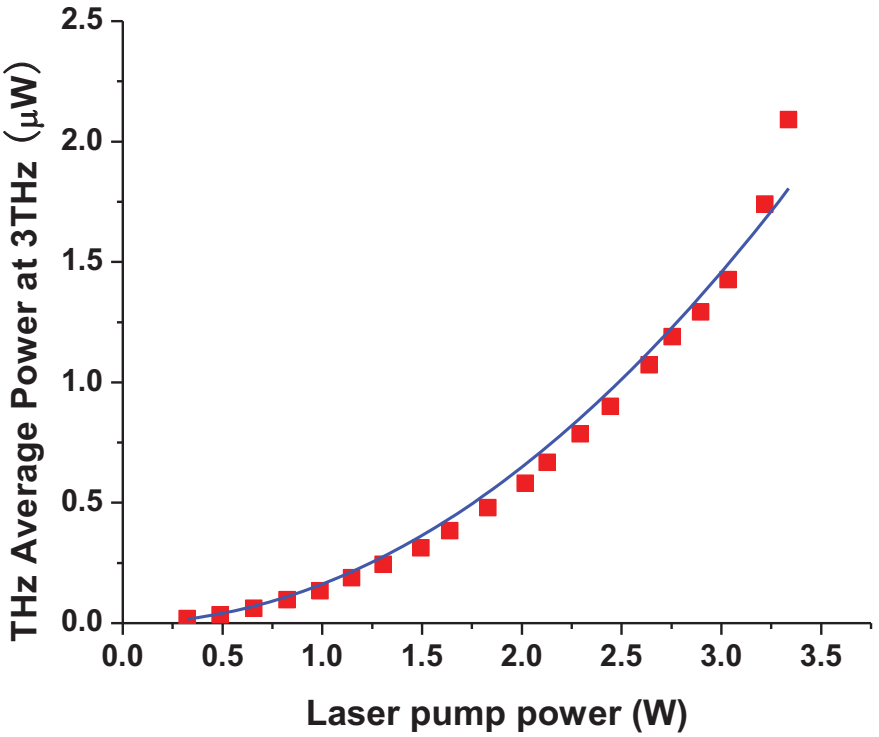

Figure 3.7: THz average power dependence pumped by the dual-frequency lasers based on Nd: YAG and Nd: YLF.

The estimated THz pulse width is 7.766 ns. We have measured the THz output wavelength by scanning a Si-based etalon, see Fig. 3.8. According to Fig. 3.8, the output wavelength is to be 98 μm, which is close to 100.5 μm, calculated from the two pump wavelengths. The THz linewidth is deduced to be 42 GHz from Fig. 4. This value is close to 53.5 GHz, estimated from the laser linewidths. Using surface-emitting geometry [47, 48], it is feasible for us to extend the output wavelengths to the far-infrared region.

In conclusion, by introducing the second solid-state laser gain medium, we have significantly improved the output powers from the two lasers sharing the same Q

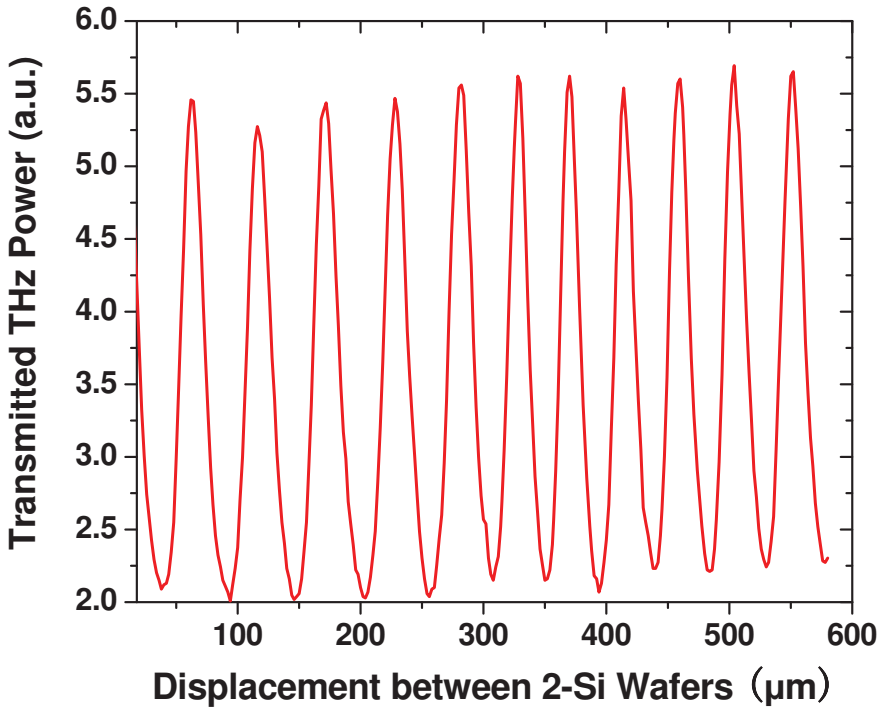

Figure 3.8: THz power at 100.5 μm being transmitted through a Si etalon as a function of the displacement between two Si wafers.

switch and output coupler. Consequently, we have improved the THz output power almost fivefold at 1.64 THz. Such a configuration allows us to generate different THz output frequencies by replacing one Nd:YLF laser medium by other solid-state laser crystal. As an example, we have generated an output power of 2.1 μW at 2.98 THz after replacing the Nd:YLF crystal by neodymium-doped yttrium aluminum garnet (Nd:YAG) crystal.

Chapter 4

Intracavity DFG for THz Generation

In this chapter, we propose and demonstrate a novel intracavity terahertz generator based on compact dual-frequency solid state laser [49, 50]. The laser output coupler, based on multi-layer unbonded GaP stack, operates as the nonlinear optical medium for terahertz generation simultaneously. By achieving intracavity scheme and using quasi-phase-matching (QPM) through alternating each layer of GaP stack, terahertz output power is significantly enhanced compared with the external-cavity approach.

4.1 Background of Intracavity DFG

Intracavity frequency mixing is the technology that can achieve dramatically high efficiency in frequency conversion process. In such an approach, the frequency converter is placed inside the cavity of an optical oscillator with extremely high power fundamental wave oscillating back and forth. The typical example is the intracavity

second harmonic generation (SHG) [51]. And this technology has been widely used to generate high power visible solid-state lasers or very compact laser like the green laser pointer [52, 53]. Recently, it has been demonstrated that both the intracavity parametric process [54] and intracavity difference frequency generation (DFG) [55] can be used to generate terahertz (THz) radiation efficiently. However, due to the high absorption of THz wave in most nonlinear mediums, the surface emitting scheme is employed in these experiments [54, 55], in which the THz propagates at a very big angle or even vertically along the direction of the pump beams. Compared with this scheme, the collinear approach is easier for the alignment of cavity and the collection of THz radiation. To achieve this aim, the nonlinear optical medium must be transparent for both the THz wave and the pump beams that are oscillating inside the cavity. This approach has been demonstrated using GaAs inside the cavity of optical parametric oscillator in which the wavelength of the beams for DFG has reached for more than 2 μm [29]. Since more than 100 Nd-doped crystals or ceramics can have lasing wavelengths between 1.03 μm and 1.1 μm [46], any THz wavelength can be generated by properly choosing two different gain mediums [45]. It would be of great interest for achieving intracavity THz generation within these lasers. However, due to the severe two-photon absorption (TPA) around 1 μm, GaAs cannot become the suitable candidate for intracavity THz generation in most lasers using Nd-doped laser mediums.

In contrast, GaP has rather low TPA coefficient around 1 μm. Recently, it has been demonstrated that GaP could be very efficient in generating terahertz radiation pumped by laser pulses around 1 μm [19, 18]. Besides, it is also proved that GaP could be used in cavity enhanced DFG [56]. As a result, GaP could be promising for intracavity application whereas a sufficiently high damage threshold is

a prerequisite property. In this chapter, to the best of our knowledge, we have firstly demonstrated the terahertz intracavity generation in GaP based on Q-switched dual-frequency solid-state laser with emission wavelengths around 1 μm. The terahertz average power that is generated from intracavity scheme has been enhanced a lot in terms of the power generated from external-cavity scheme.

4.2 GaP Stack as Laser Mirror

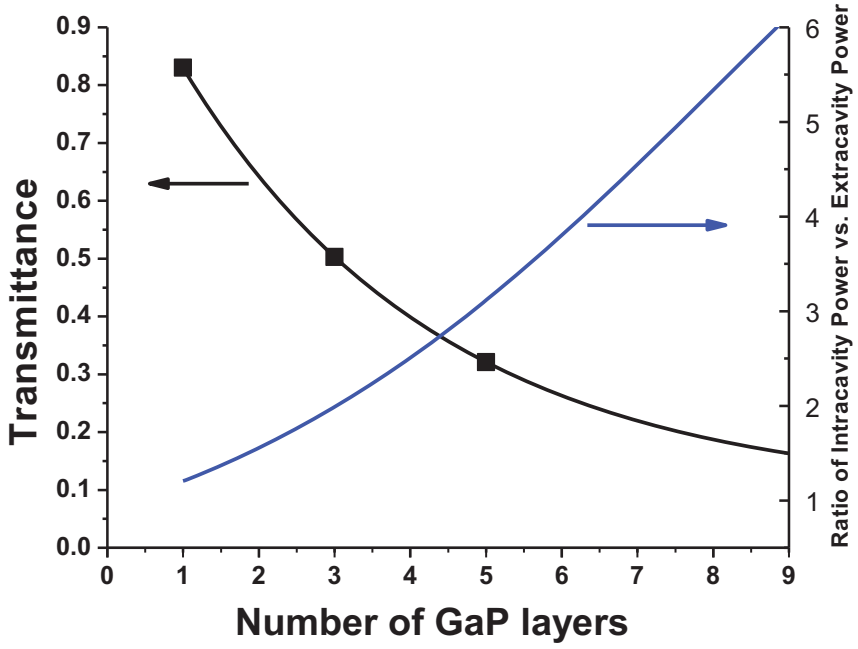

Figure 4.1: Transmittance of laser beam through GaP stacks with different number of layers and the estimated ratio of intracavity intensity vs extracavity intensity.

Specifically, we also present a unique design of intracavity DFG compared with the traditional approach. In this design, several stacked uncoated GaP plates are

used as the key component for THz generation. In the mean time, the plates could also be used as the output coupler for the dual-frequency laser. This is made possible by achieving a high reflection coefficient through the multiple reflections in the GaP plates stacked in series. Starting from the first plate, the intracavity intensity reduces gradually through the multiple plates. Thus the equivalent intensity inside the stack is much higher compared with the intensity from the beam finally emitted from the laser.

Each of the GaP plates used in the experiment was cut and polished along the [110] direction. The diameter of each plate is 48.5 mm and the thickness is 663 μm. To achieve sufficient reflection coefficient for the output coupler, as many as nine GaP plates were stacked. We used a neodymium: yttrium lithium fluoride (Nd:YLF) laser to test the reflection coefficient of GaP plates with different stacking numbers. The transmission coefficient dependence is shown in Fig. 4.1. The solid line corresponds to the exponential fitting, showing that the transmittance reduces as we increase the number of stacked plates. It is estimated that the reflection coefficient of nine GaP plates stack could reach more than 80% which is sufficient as an output coupler.

4.3 Novel THz Generation Based on Intracavity DFG

4.3.1 GaP Stacking Configuration based on QPM

In order to achieve efficient DFG, the polarization direction of these two wavelengths should be directed parallel to $[1\bar{1}0]$ and [001]onto the GaP. Besides, considering the

coherence length of the DFG process, we could figure out the orientation direction of each GaP plate before stacking. In addition, different from the approach of diffusion bonding [56], the GaP plates used in the experiments are only stacked such that the orientation direction of each plate is still changeable. Thus, in order to achieve quasi-phase-matched (QPM) DFG and optimize the conversion efficiency, it is convenient to realign the orientation of GaP plates in terms of different coherence lengths at different THz wavelengths.

By using the experimental setup in Fig. 3.1, the dual-frequency beams at 1047 nm and 1053 nm were directed onto the GaP stacks with these configurations and generated THz radiation by DFG. In each configuration, we also tested the GaP stacks with different number of plates. The THz intensity in terms of these configurations is shown in Fig. 4.2. In addition, under the assumption that the coherence length is about 2 mm, we plot the theoretical THz power dependences on the number of stacked GaP plates, see Fig. 4.2. It is noted that considering the reduction of laser power after transmitting through different number of plates, we also used the fitted exponential expression in the theoretical calculation. The experimental data agree well with the theoretical value, which shows that the third configuration is the optimized for the orientation of the stacking of GaP plates (see the schematic figure of GaP stack in Fig. 4.2).

4.3.2 Experimental Setup

The experimental setup for the unique configuration of intracavity DFG is shown in Fig. 4.3. The laser cavity configuration excluding the output coupler is similar with setup in Ref. [45]. However, the introduction of GaP stack as the output coupler makes the whole design completely different and much more compact. The cavity

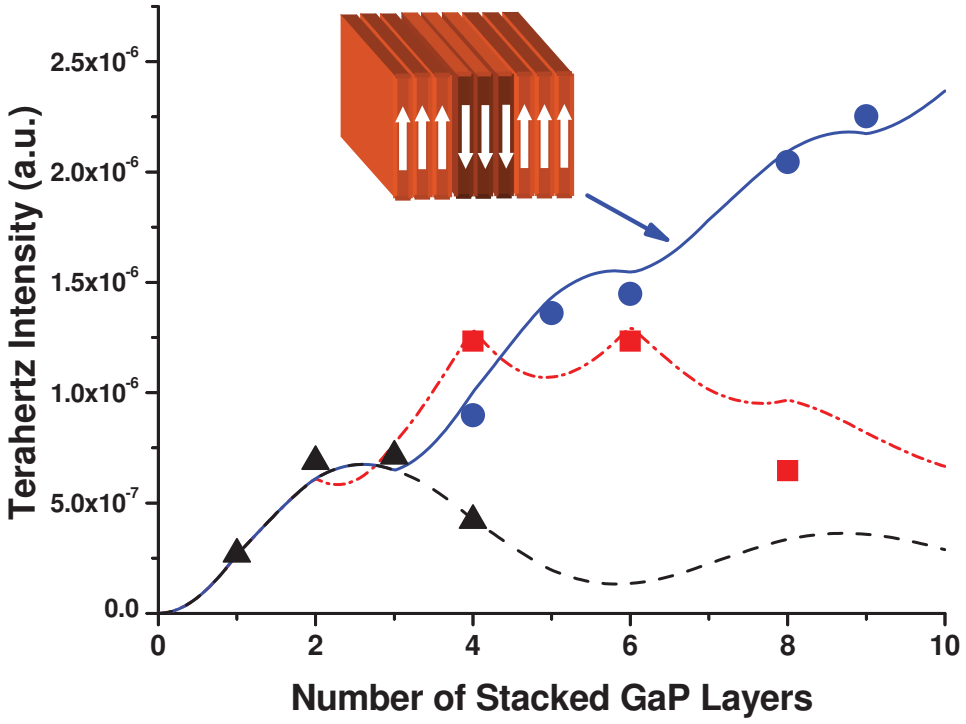

Figure 4.2: THz intensity generated from GaP stacks in terms of different stacking configurations. Triangle, stacked in the same direction (no layer reversed); rectangular, every two-layer reversed; round, every three-layer reversed.

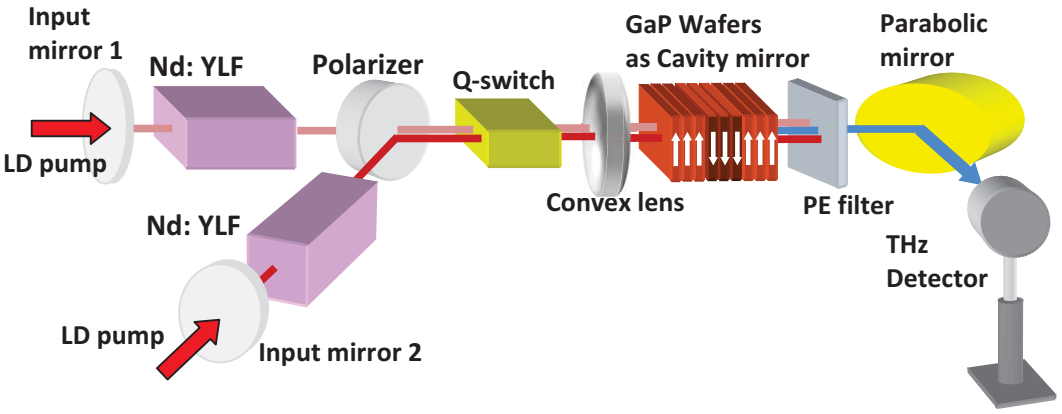

Figure 4.3: The experimental setup for the configuration of intracavity DFG. PE filter, high density white polyethylene filter.

of 1053 nm is composed of input mirror 1, polarizer, convex lens and GaP stack while the cavity of 1047 nm is composed of input mirror 2, polarizer, convex lens and GaP stack. The intracavity polarizer is high transmission for the light with horizontal polarization and high reflection for the light with vertical polarization. As laser gain mediums, two α-cut Nd: YLF (Nd doped at 1.0%, and $4\times4\times10mm^3$) crystals were placed onto the separate arms connected through the polarizer. Due to the perpendicular polarization direction of 1047 nm and 1053 nm, these two crystals could provide the gains for these two wavelengths respectively. Between the polarizer and the GaP stack which is the shared arm of 1047 nm and 1053 nm cavities, we placed an acoustic-optic Q-switch such that the laser pulses at the two wavelengths could be synchronized. In addition, a bi-convex lens (focus length f=10 cm) was placed beside the Q-switch, yielding a beam waist on the GaP stack. Indeed, as the laser pulses at 1047 nm and 1053 nm are oscillating in the cavities, the intracavity

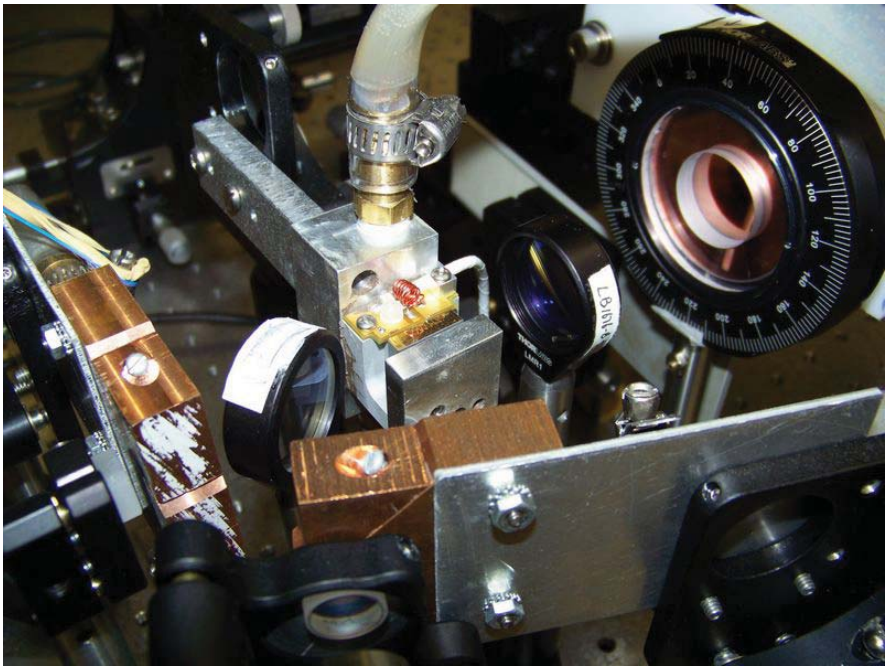

Figure 4.4: Real setup for the configuration of intracavity DFG. In the picture, the sample fixed by the round holder in the upper-right corner is the GaP stack.

laser modes will also penetrate through the stacked GaP plates. Therefore, the DFG process will happen simultaneously as the laser oscillates. As the DFG component GaP stack is part of the cavity, this is truly real intracavity DFG (see the real setup in the Fig. 4.4). After the GaP stack, white polyethylene filter was placed to block the beams of 1047 nm and 1053 nm. THz radiation is then collected through a parabolic mirror and measured by a THz power meter.

4.3.3 Experimental Results

The repetition rate of the Q-switch is set at 4 kHz. Both of the two Nd:YLF crystals are pumped by two 808 nm laser diodes separately. At the pump powers of 3.327

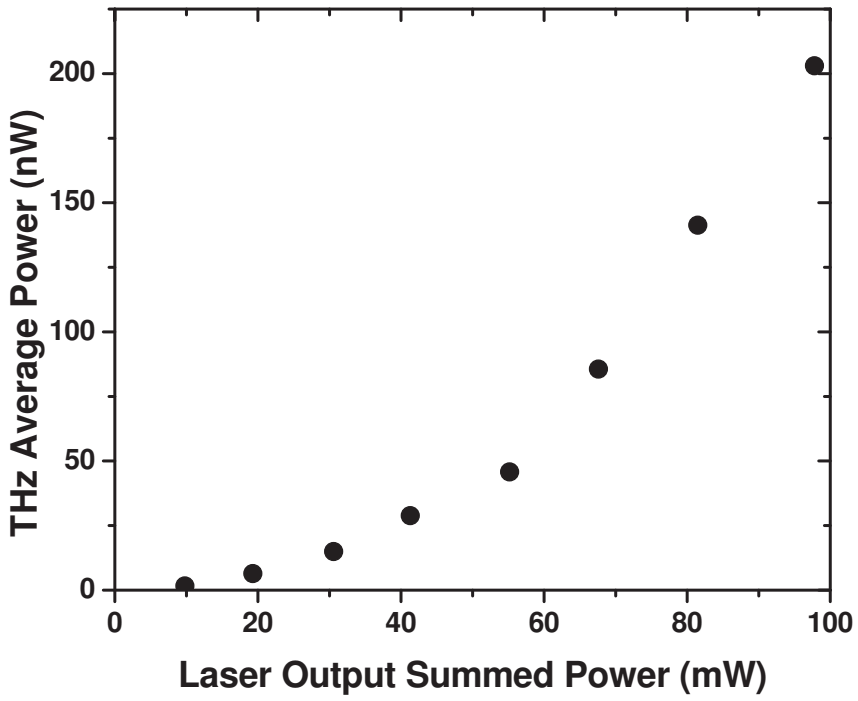

Figure 4.5: THz power dependence vs. corresponding laser powers emitted from the GaP stack.

W and 3.298 W, we have achieved 41.8 mW at 1047 nm and 56 mW at 1053 nm, respectively. The corresponding pulse widths are 280 ns and 170 ns. Both of two output powers were measured from the laser beams emitted from the GaP stack. At these two laser output powers, the terahertz average power was measured to be 203 nW. Besides, we have measured the THz power dependence, see Fig. 4.5. It is mentioned that this dependence was obtained after we optimized the position of the GaP stack for THz generation. Namely, as the lasers were kept operating, we

scanned the surface of the GaP stack in two dimensional directions and measured the THz power at the same time. Variation of THz power was observed as we carried out this scanning. The reason, we believe, is due to the variation of reflection coefficient at the laser wavelengths caused by the inhomogeneous air gaps among different GaP plates. As we prepared the GaP stack, we observed the interference fringe pattern between different layers. This is caused by the variable air gaps between these GaP plates. We estimated that the distances of these gaps are in the order of hundreds of nanometer. Based on the transmission matrix approach dealing with nonperiodic dielectric stack [57], we theoretically estimated the equivalent reflection coefficient of the GaP stack. It was assumed that the thickness of each GaP plate was exactly 663 μm and the two surfaces of each plate were perfectly parallel. However, as nine GaP plates were stacked, there would be eight different air gaps formed. Correspondingly, we would have eight variables in the simulation in terms of the air gaps. The simulation result shows that the variation of equivalent reflection coefficient could be as large as almost 20%. For some instances, the value of the reflection coefficient could be more than 99%, which is perfect for intracavity application.

In order to characterize the performance of the GaP stack in intracavity THz generation, we compared the result with the result achieved in external-cavity THz generation. The GaP stack was replaced with a plano cavity mirror at a coupling efficiency of 5%. At the pump powers of 5.876 W and 3.826 W, we have achieved 902 mW at 1047 nm and 510 mW at 1053 nm, respectively. The corresponding pulse widths are 150 ns and 170 ns, respectively. Then, the synchronized two beams were focused and directed onto the same GaP stack with nine plates. It is noted that the beam sizes are focused to the same values as those in the intracavity scheme. THz average power was measured to be only 2 nW, which is much lower

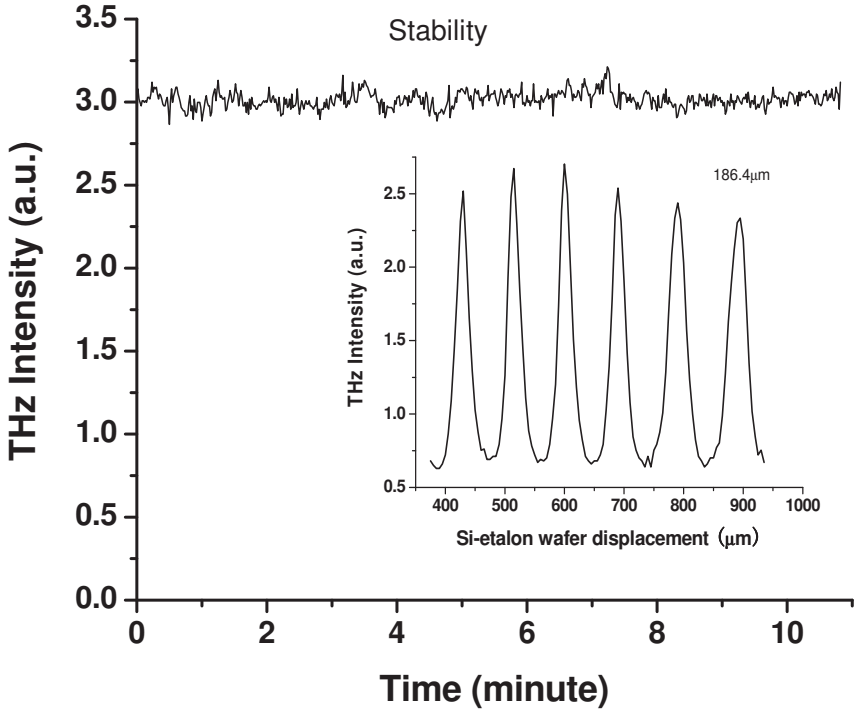

Figure 4.6: Temporal stability of THz intensity. Inset, THz power being transmitted through a Si etalon as a function of the displacement between two Si wafers.

than the value achieved in the intracavity scheme. Thus, the key advantage of the intracavity scheme is the intense intracavity pump power that can be used to improve the efficiency for DFG. Considering the different power and pulse widths from the pump beams in the intracavity and external-cavity scheme, we estimated that the equivalent intracavity power for 1047 nm and 1053 nm are 8.361 W and 11.202 W, respectively. Besides, the equivalent reflection coefficient of the GaP stack reached about 99.5%. It is shown that to achieve efficient intracavity DFG,

the reflection coefficient of the output coupler should be as high as possible. In addition, it is mentioned that as the intracavity laser beams oscillate back and forth inside the GaP stack (see Fig. 4.3), the THz is also generated in the opposite direction relative to the laser output. In order to collect the THz power from this direction, we placed a parabolic mirror inside the cavity. The measured THz power is even 10% higher compared with the power collected from the side outside the cavity. Thus, it is expected that the THz power could be doubled if we can find certain approach to collect the THz from both sides.

It is known that the one of the important concerns in intracavity nonlinear process is the stability. We have also measured the stability of THz output in the experiment, see Fig. 4.6. In the measurement time of 10 minutes, the stability is within $\pm 5.7\%$, which is sufficient for a lot of applications. Shown in the inset of Fig. 4.6, we have also measured the wavelength of the THz beam through the two-wafer Si-etalon. The wavelength is measured to be 186.4 μm, which is close to 182.4 μm, determined from the wavelengths of the two pump laser beams.

In conclusion, we have proposed and demonstrated a novel scheme for generating THz in the intracavity scheme. The GaP stack operates both as cavity output coupler and the component for THz generation. This design greatly simplifies the structure for THz generation based on dual-frequency solid state laser. In addition, the THz power has been improved dramatically compared with the result in external-cavity scheme.

Chapter 5

Passively Q-Switched THz Source

As is known to all, the most compact solid-state-laser is the microchip laser [58]. Figure 5.1 shows a typical structure of microchip passively Q-switched laser. The laser gain medium, passively Q-switch and output coupler are bonded together. As a result, the whole size is extremely compact.

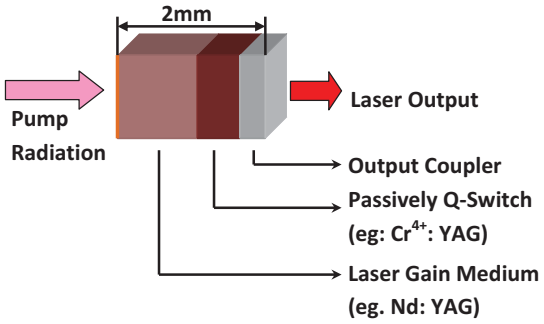

Figure 5.1: Typical setup for passive Q-switched microchip laser.

Is it possible to realize microchip THz source with this kind of compact size? The answer is ′yes′! In this chapter, we are going to explore the possibility of achieving

THz source based on DFG pumped by using passive Q-switched solid-state lasers [59].

5.1 Fundamentals of Passively Q-switched Laser

The key component in the passively Q-switched laser is the saturable absorber. The most common saturable absorber for laser is Cr^{4+}:YAG. There is an initial transmission loss for laser light when the intensity is weak, as shown in Fig. 5.2. Because of this loss, the laser emission will be delayed. As a result, the population inversion in the upper energy level can be accumulated within this time of delay. However, light intensity is still slightly increasing in the laser cavity (the laser oscillation has not been reached, but the radiation from the stimulated emission will accumulate). As the intensity reaches certain value, the transmission loss will be much reduced. Namely, the Q-factor in the cavity is changed, and the laser pulse could build up immediately.

However, the pulses generated by these lasers suffer from large timing jitters, see Fig. 5.3. This is due to the reason that the there is no fixed modulation repetition rate of the alternation of Q-factor within passive Q-switch. Besides, the variation of transmittance of the passive Q-switch would also be influenced by environmental factors which have lots of uncertainties. Such a disadvantage severely limits their applications in differential optical absorption spectroscopy [60] and terahertz (THz) generation [35]. In the past, several approaches for reducing the timing jitter were investigated [61, 62, 63, 64, 65]. In order to synchronize each pair of the pulses generated by two passively Q-switched lasers, specific cavities were exploited [66, 67, 68].

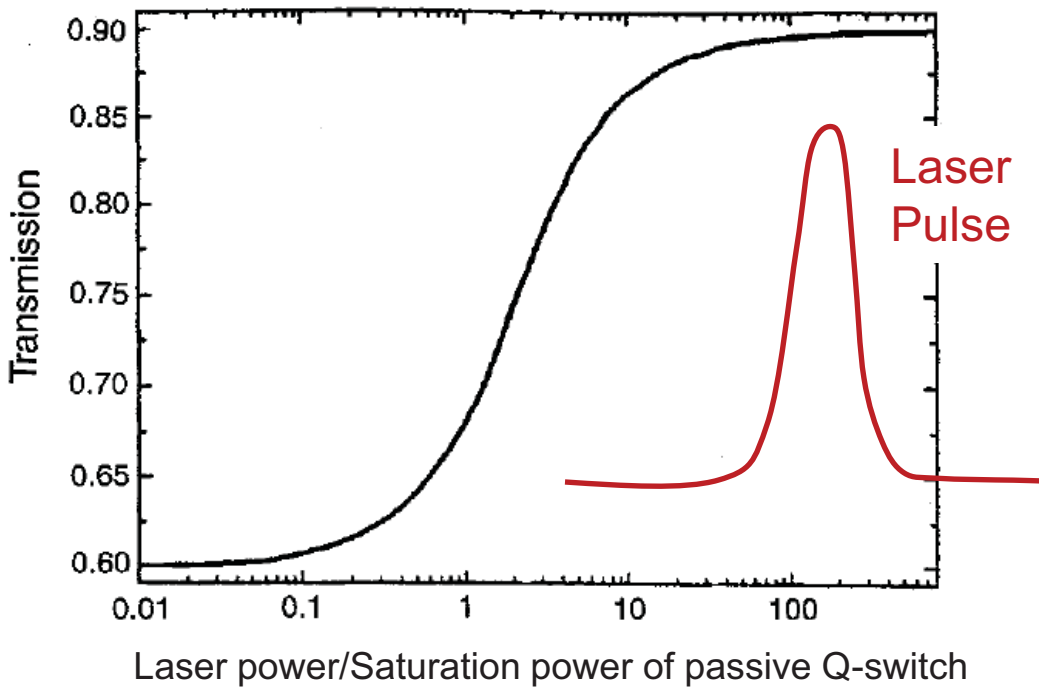

Figure 5.2: The change of transmittance in saturable absorber as a function of the cavity intensity vs the saturation power of the material.

5.2 Dual-Frequency Passively Q-switched Laser

In this chapter, we introduced our demonstration of THz generation by mixing the passively Q-switched laser pulses in a nonlinear crystal. Our success in THz generation is primarily attributed to our novel design of the cavity for the passively Q-switched dual-frequency Nd:YLF laser; see Fig. 5.4.

The laser consists of two cavities being jointed together by a polarizer (P). The two cavities are used to generate two beams at 1047 and 1053nm with the orthogonal polarizations (π and σ). The polarizer being placed at Brewsters angle has a high

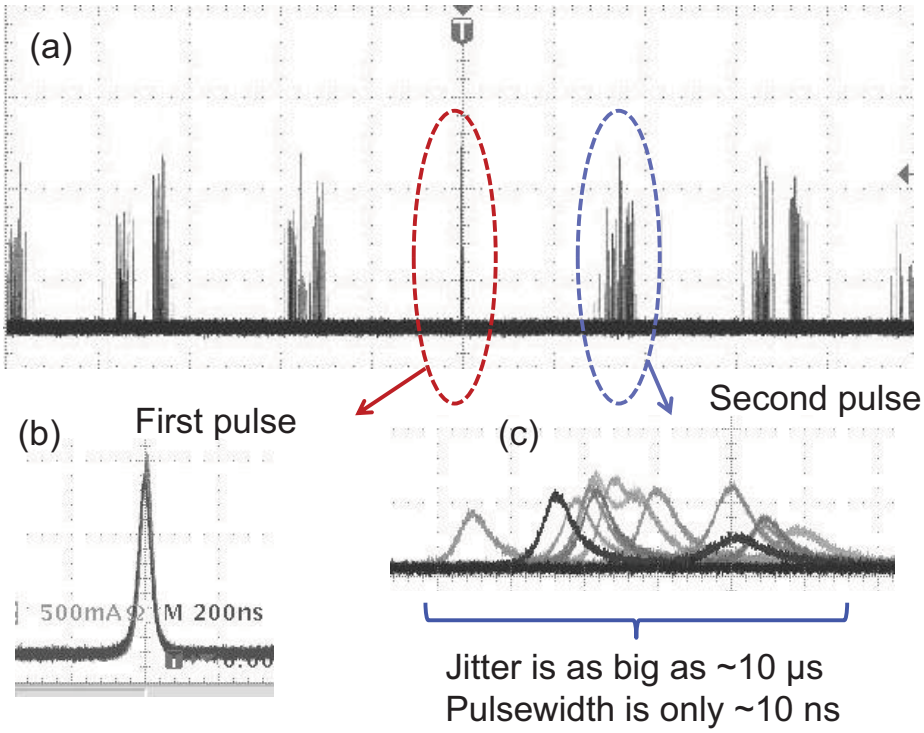

Figure 5.3: Schematic plot of timing jitter measured from output pulses from passively Q-switched lasers.

transmittance of T ≈ 98% for the π-polarized beam and a high reflectivity of R > 99.9% for the σ-polarized beam. This configuration is different from our previous work [45]. In this cavity, a passive Q switch made of a 1mm thick Cr^{4+}:YAG crystal with an initial transmittance of 90% (i.e., under a sufficiently low input intensity) is shared by the two cavities. Without introducing any complicated circuit and electronic driver, such a passive Q switch can be fully integrated with the laser crystal [58]. Thus, the dimension of the entire laser can be reduced to 1-2 in.

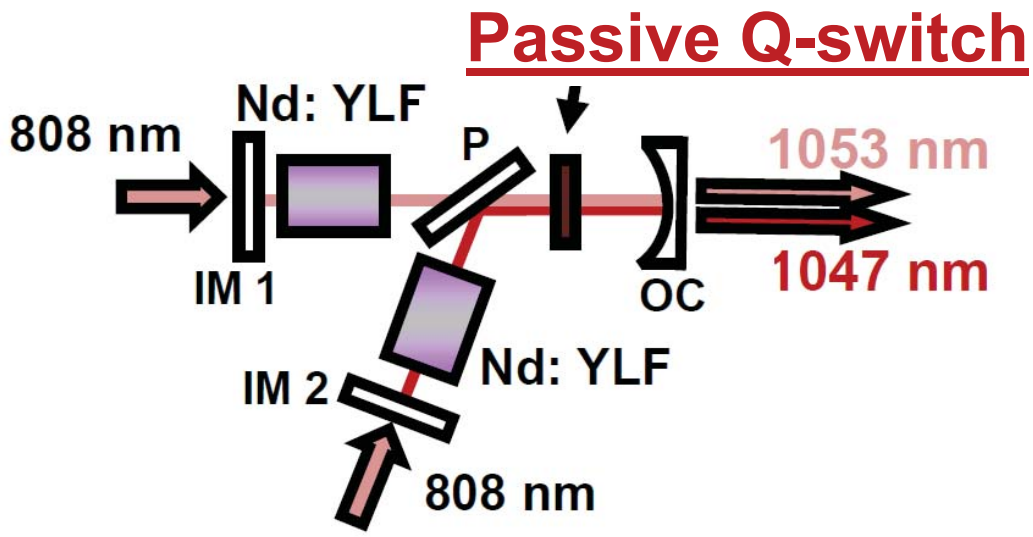

Figure 5.4: Experimental setup of the dual-frequency passively Q-switched Nd: YLF solid-state laser. IM 1 and IM 2, input mirrors; P, polarizer; OC, output coupler.

Before the dual cavities simultaneously reached the lasing conditions, we tested

the timing jitter of the laser pulses at 1047 nm. While the pulse width of the laser was measured to be about 80 ns, the timing jitter was higher than 400 ns. Since the corresponding pulses at the two wavelengths are no longer synchronized, such a dual-frequency laser system is not suitable to THz generation based on difference-frequency generation (DFG) or sum-frequency generation (SFG). Because of the unique design of the cavities, we effectively reduced the timing jitter between the laser pulses at the two frequencies. First, the dual-frequency laser pulses are self-triggered through the occurrence of multiple pulsing [42], see Fig. 5.9. The opening time of the Q-switch is shorter than the pulse build-up time. When the first pulse is generated, the loss of the Q-switch has not reached the minimum. However, the population inversion has not been depleted completely. As the loss the Q-switch is reduced further, an additional pulse is generated shortly after the first one. Via our unique design, multiple pulsing is used to our advantage. As the first pulse is generated in the 1047 nm laser, the passive Q-switch becomes saturated and changes the cavity loss for both of the 1047 and 1053 nm laser oscillators. The pulse at 1053 nm is generated shortly after the first pulse at 1047 nm. In the meantime, due to the multiple- pulsing effect, the second pulse at 1047 nm is also generated. As a result, the second pulse at 1047nm and pulse at 1053nm can be synchronized, and therefore, they can be used as the input mixing signals for DFG and SFG.

Besides, we were able to manipulate the instance when each pulse is generated. This was accomplished by controlling the pumping current for each output frequency, and therefore, we have synchronized the pulses at the two different frequencies. In our experiment, we varied the pump current for the laser at 1053 nm while keeping

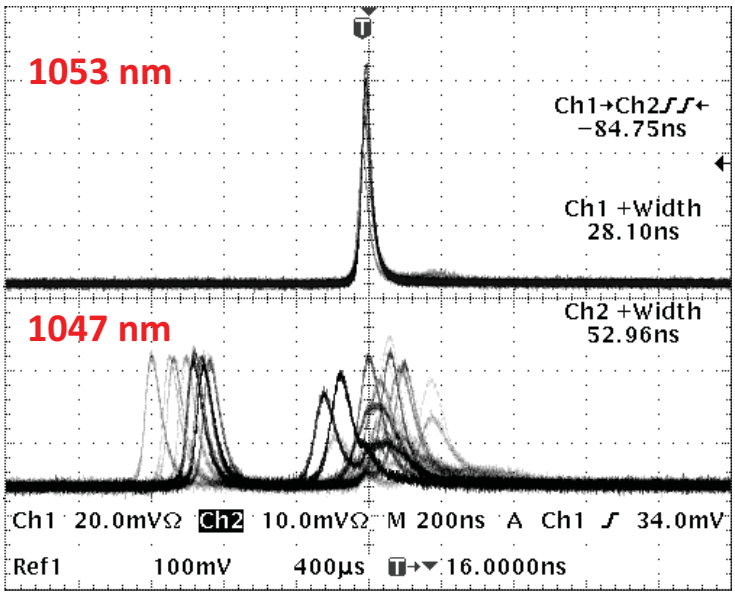

(a) Dual-freqeuncy pulses at 1047 nm and 1053 nm that are self-triggered by pulses at 1047 nm.

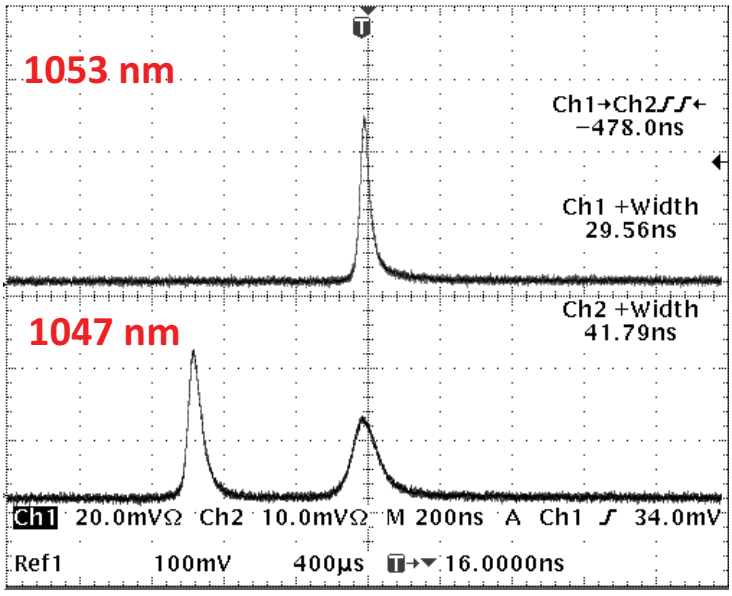

(b) One snap of dual-freqeuncy pulses at 1047 nm and 1053 nm

Figure 5.5: Dual-freqeuncy pulses at 1047 nm and 1053 nm.

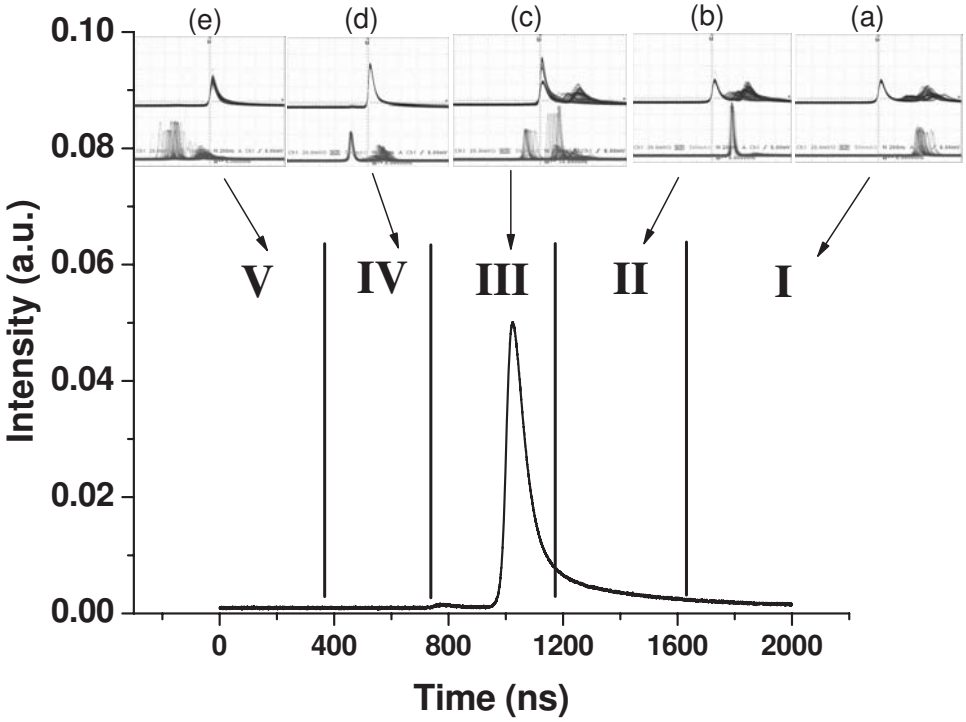

Figure 5.6: Temporal profiles of dual-frequency laser pulses. (a)-(e) five different stages.

the pump current for the laser at 1047 nm at a fixed value. The temporal profiles are shown in Fig. 5.6; all of the measurements were triggered by the laser pulses at 1047 nm. From insets (a)-(e) (zone I - V) in Fig. 5.6, we observed five different regions for the dual-frequency pulses. When the pump current was low, the laser pulse at 1053 nm exhibited a random temporal profile, and therefore, the timing jitter between the dual-frequency pulses is expected to be large. As the pump current for the laser at 1053 nm was increased, the laser pulse at 1053 nm moved slowly toward the laser pulse at 1047 nm. At some current, the laser pulse at 1053 nm became stable, and therefore, the timing jitter was reduced to about 40 ns, see inset (b) (zone II). This represents the reduction of the timing jitter by 20 times. Such reduction is attributed to the presence of the passive Q-switch. Indeed, the laser pulse at 1047 nm was generated ahead of the laser pulse at 1053 nm due to a higher pump level for the laser cavity at 1047 nm. The laser pulse at 1047 nm saturated the passive Q-switch, and therefore, reduced the loss for the Q-switch from 10% to a negligible amount. Since the laser cavity at 1053 nm shared the same Q-switch, the laser at 1053 nm started to emit pulses shortly after the laser pulses at 1047 nm were emitted. Based on our experiment, such a mechanism can be used to significantly reduce the timing jitter for the laser pulses at 1053 nm relative to the laser pulses at 1047 nm. However, as the pump current was further increased, the laser cavity at 1053 nm can reach the lasing threshold without the loss modulation by 1047 nm pulse. As a result, it was not possible for us to precisely control the instance when the laser pulses are generated at 1053 nm, see inset (c) (zone III). Besides, it is hard to determine which pulse is generated first at 1047 nm or 1053 nm. But once the first pulse is generated, the loss in the Q-switch will be saturated and the pulse at the other wavelength will be correspondingly triggered. When the pump current

reached a certain value, the laser pulses at 1053 nm were generated first. Since the loss in the Q-switch was reduced, the laser pulses at 1047 nm were subsequently generated. As a result, the temporal profile became relatively stable again, see inset (d) (zone IV). When the pump current became even higher, the temporal profile became relatively unstable, see inset (e) (zone V), similar to the state in inset (a).

5.3 Passively Q-Switched THz Generation

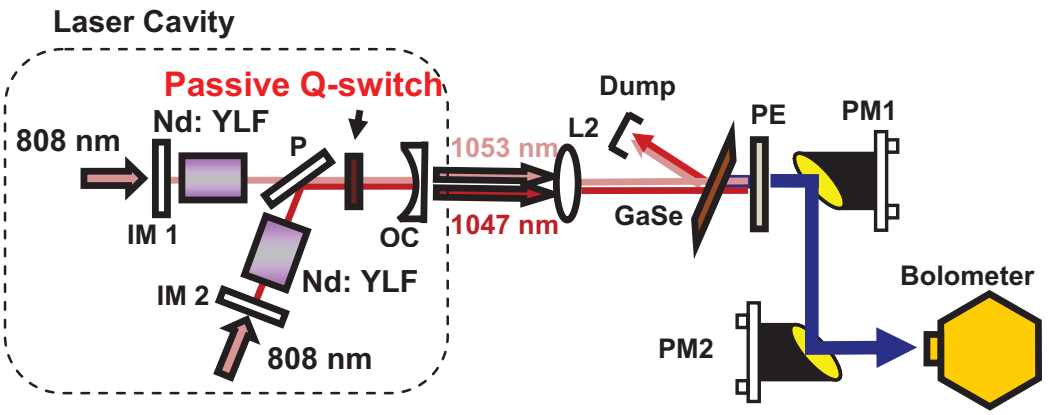

Figure 5.7: Experimental setup of THz generation pumped by passively Q-switched dual-frequency pulses.

Due to the significant reduction of the timing jitter between each pair of the dual-frequency pulses, we can use them for THz generation based on frequency mixing, see the setup in Fig. 5.7. Indeed, we have successfully generated THz pulses from a 15 mm GaSe crystal. This is the first demonstration of THz generation from passively Q-switched dual-frequency laser pulses. While keeping the pump current for the laser cavity at 1047 nm as a constant, we have varied the pump current for

the laser cavity at 1053 nm. According to Fig. 5.8, the behavior of the THz output power vs. the pump current is peculiar. It is strongly correlated with the timing jitter between each pair of the dual-frequency laser pulses. Indeed, the first THz peak from the low-current side in Fig. 5.8 corresponds to the region between insets (a) and (b) in Fig. 5.6 where the second pulse at 1047 nm synchronizes well with the pulse at 1053 nm. Then, as the pump current increases, the pulse at 1053 nm moves to the center part between the two pulses at 1047 nm whereas none of the pulses at these two wavelength could be synchronized. This corresponds to the first dip in terahertz power around the pump current 1.2 A. As the pump current is further increased, either 1053 nm or 1047 nm pulse may be generated first, shown in Fig. 5.6 (c). However, once triggered by the first pulse at one wavelength, the second pulse can still be synchronized with the pulse at the other wavelength. As a result, the terahertz radiation can still be efficiently generated. This region corresponds to the second peak in terahertz power in Fig. 5.8. Then, after the current around 1.4 A, the pulse 1053nm will be generated first and become dominant as the triggering pulse. Similarly, as the pulse at 1047 nm moves around the center point between the two 1053 nm pulses, few pulses at the two wavelength will be synchronized. Accordingly, the terahertz power will have the second dip. The last peak in terahertz power is attributed to the mixing between 1047 nm pulse and second pulse at 1053 nm.

5.4 Synchronized Dual-Frequency Pulses Based on SFG

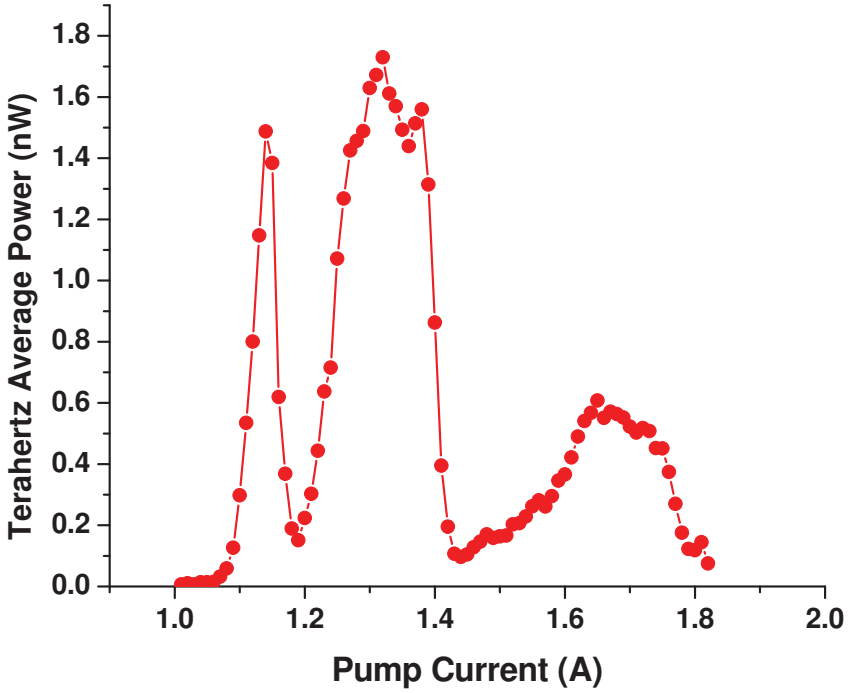

Figure 5.8: THz intensity versus pump current of the 1053nm laser.

Besides the THz generation, we have also demonstrated SFG by using this dual-frequency passively Q-switched laser as the two mixing beams. In order to understand the synchronization between the sum-frequency (SF) pulses and second-harmonic (SH) pulses, a dual-frequency laser beam was divided into two beams using a beam splitter. Each SF pulse was generated by a KTP crystal by one of the split beams. The other split beam, used for second harmonic generation (SHG), was sent through a half-wave plate and a cubic polarizer. Because of the perpendicular polarizations of the beams at 1047 and 1053 nm, either the 1047nm beam or 1053nm

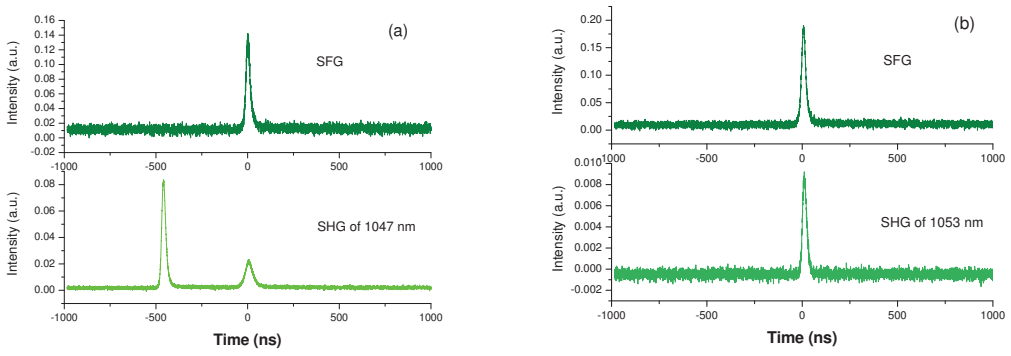

(a) (b)

Figure 5.9: (a) Synchronized pulses of SFG and SHG of 1047 nm; (b) synchronized pulses of SFG and SHG of 1053 nm.

beam can be blocked completely by rotating the half-wave plate. Another KTP crystal was used for achieving SHG. In Fig. 5.9(a), the first pulse of the SH beam at 1047nmwas generated by the first pulse at 1047nm that triggered the following pulses at 1047 and 1053 nm. Figure 5.9(b) shows the pulse profiles of the SF and SH beams. Our measurement yielded a timing jitter of 5 ns, which is much smaller than the value for the timing jitter between each pair of the pulses at 1047 and 1053 nm. Figure 5.10 shows the distribution of jitter measurement between SFG and SHG of 1053 nm pulses. In this approach, we synchronized the pulses at two different wavelengths based on a passively Q-switched laser.

In conclusion, we have demonstrated THz generation by using the pulses generated by a passively Q-switched solid-state laser. Following our novel design of the laser cavities, timing jitter between two lasers has been reduced by a factor of 20. Through further optimizations, such an approach can be utilized to implement an efficient, compact, and portable THz source.

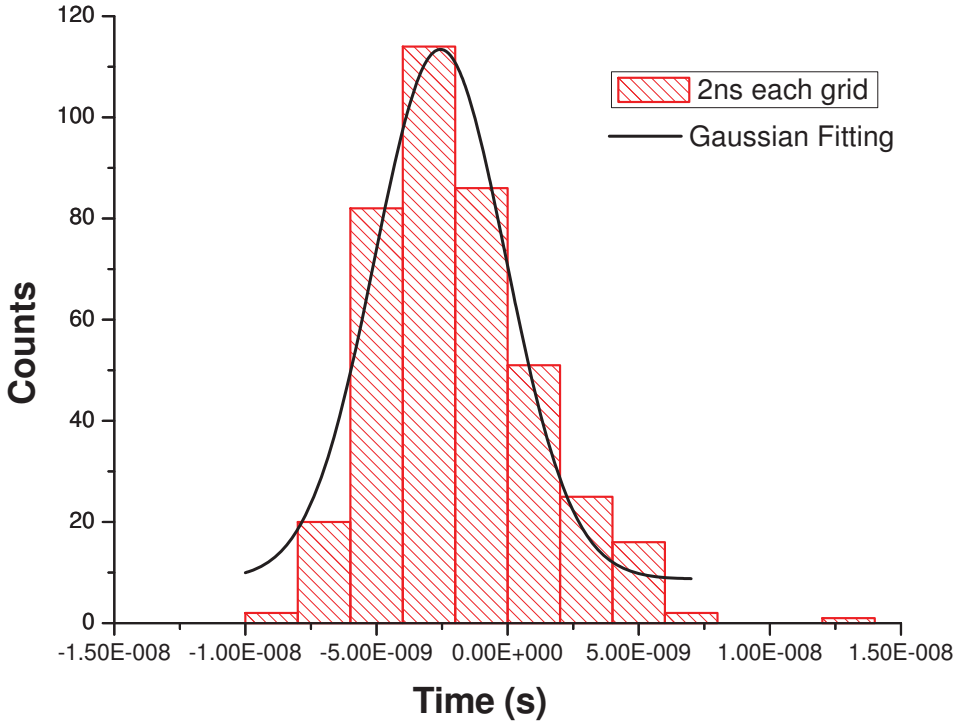

Figure 5.10: Distribution of jitter measurement between SFG and SHG of 1053 nm pulses.

Chapter 6

THz Source Based on AFB-KTP OPO

A coherent infrared source being capable of generating dual wavelengths have a variety of applications such as differential absorption lidar [69], Doppler lidar measurement [70], coherent anti-Stokes Raman scattering microscopy [71], and generation of mid-infrared [72] and terahertz (THz) [73] waves. Apart from the solid-state lasers that can emit coherent dual-frequency radiations, optical parametric oscillator (OPO) is also a very promising approach to achieve this kind of source. Although conventional OPO is capable of generating signal and idler wavelengths, spatial walk-off in a nonlinear crystal not only increases the threshold for the oscillation but also sacrifices the beam quality. Recently, it was demonstrated that periodically-orientated stacks based on adhesive-free-bonding (AFB) can be used to compensate spatial walk-off for the generation of about 2 μm due to quasi-phase-matching (QPM) [74]. In comparison, conventional QPM crystals have very small aperture sizes. Besides, compared with two separate nonlinear optical crystals [72, 73], such

a crystal composite has a significantly higher gain, i.e. a factor of $16/\pi^2$ higher [74]. In addition, because the dual-signal or dual-idler wavelengths (i.e. four output wavelengths) are generated simultaneously inside the same crystal, each pair has almost the same intensity and the temporal profiles which are completely synchronized.

In this chapter, we will discuss about several novel researches on THz generation based on our specially designed AFB-KTP crystal that is the key component in the OPO [75].

6.1 Dual-Signal-Idler OPO Based on AFB-KTP

In this section, we report our results on the oscillations at the dual-signal and dual-idler wavelengths at around 1 μm. By mixing the dual-idler output at 1084.1 nm and 1093.9 nm from the OPO, we generated a THz wave at 118 μm based on difference-frequency generation (DFG).

Each KTP plate was cut according to $\theta = 90^\circ$ and $\varphi = 0^\circ$ (i.e. x-cut). As a result, at these angles the OPO can be noncritical-phase-matched at the pump wavelength of around 532 nm. All the crystal axes of the adjacent plates are opposite to each other in order to periodically switch all elements of second-order nonlinear susceptibility tensor of KTP to realize QPM based on d_{24}. The structure of the KTP plates studied here is quite different from that in Ref. [74]. Indeed, in Ref. [74], z axes of the adjacent KTP plates were bonded in a head-to-tail configuration (i.e. $\theta = 50.2^\circ$) to achieve not only the walk-off compensation but also QPM. It is worth noting that a singly resonant OPO is inherently more stable than a doubly resonant OPO implemented in Ref. [74]. Moreover, the thickness of each KTP plate, dictated by the frequency separation of the dual signals, is different from that

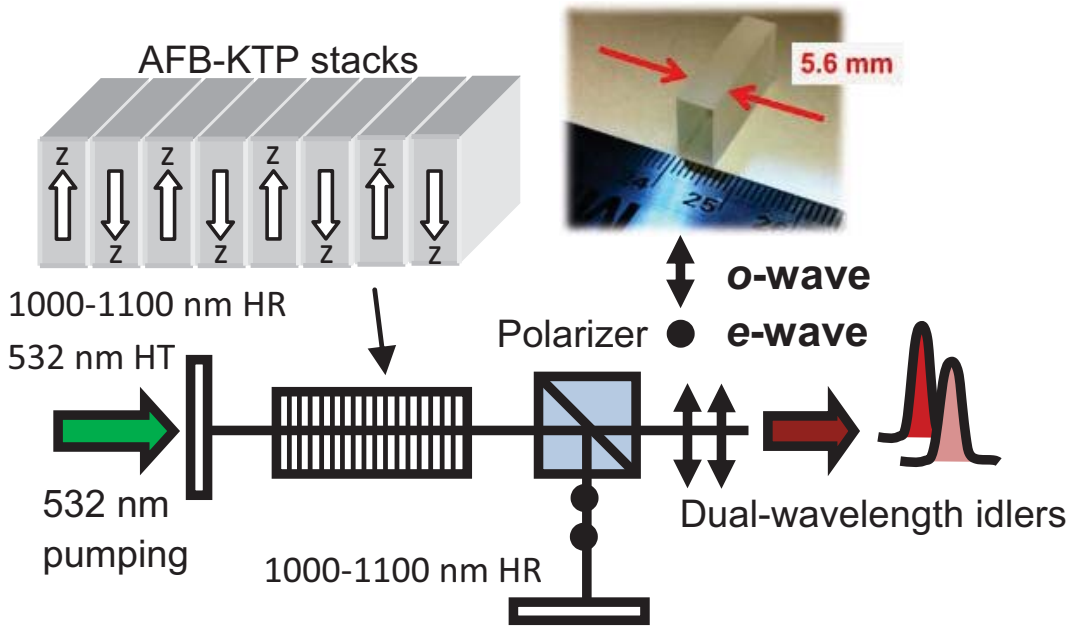

Figure 6.1: Experimental setup for singly resonant OPO.

in Ref. [74] (i.e. 2 mm).

The experimental setup for the singly-resonant OPO is shown by Fig. 6.1. The AFB KTP stacks, fabricated at Onyx Optics, consist of 20 x-cut KTP plates, each of which has a thickness of 1.19±0.01 mm, with their z axes being periodically switched as shown by Fig. 6.1; they were adhesive-free-bonded together as a composite for realizing QPM simultaneously at the dual-signal and dual-idler wavelengths. As a result, the QPM condition is given by $\Delta kl = \pm\pi$, where l is the thickness of each KTP plate. It is noted that the expression $\Delta kl = \pm\pi$ is invalid when the number of KTP plates is small (see our discussion in appendix). In our case, the expression is still precise for 20 KTP plates. Consequently, a pair of the signals having slightly different wavelengths satisfies the QPM condition above. The two corresponding

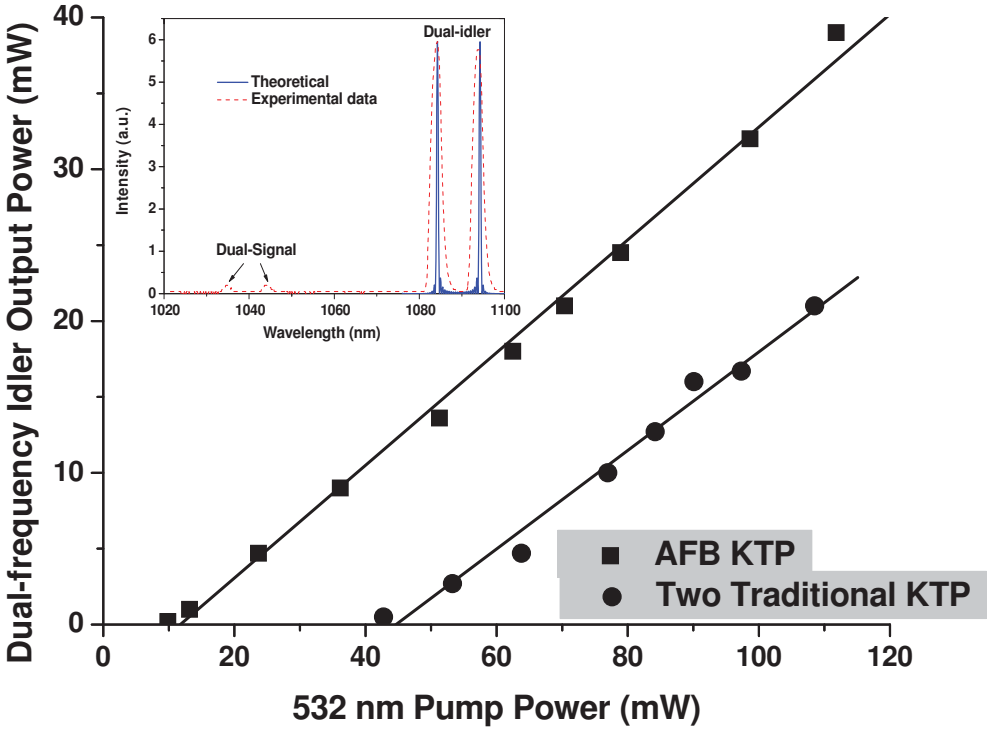

Figure 6.2: Average output power of dual-idler beams vs. pump power at 532 nm based on both in AFB KTP and two bulk KTP crystals. Solid lines correspond to linear fits. Inset: spectra of signals and idlers generated by AFB KTP OPO.

idler wavelengths satisfy the QPM condition.

In comparison, only a single signal wavelength satisfies the birefringence-phase matching condition (i.e. $\Delta kl = 0$) if a single KTP crystal is used instead. Our composite has a clear aperture of 5.6 mm×10.5 mm and a total interaction length of 23.8 mm. As one can see, the aperture size is much larger than the QPM KTP crystals commercially available. As a result, such an AFB crystal composite holds great promise for the generation of high powers, which requires large laser beam sizes. For our composite, both the input and output facets were high-transmission (HT)-coated at the wavelengths of around 532 nm and 1000-1100 nm. To demonstrate the tunability of our OPO based on the KTP composite, we tuned the pump wavelength around 532 nm. Based on our experimental results, low-cost pulsed pump source at 532 nm, commercially available, was sufficient to achieve stable oscillations in the composite. The configuration for the OPO cavity is shown by Fig. 6.1. Two flat mirrors with high reflection (HR) coating in the range of 1000-1100 nm were designed as the cavity mirrors. To ensure the oscillations only at the signal wavelengths, a cubic polarizer was placed inside the cavity. It allows the o-polarized idler beams to pass through (i.e. T $\approx$ 97%) and reflects almost all of the e-polarized signal beams ($R > 99\%$). Since the polarization of each signal was perpendicular to that of the corresponding idler, we were able to oscillate just the dual signals inside the cavity. Almost all the powers of the dual-idler beams were transmitted through the polarizer. The inset to Fig. 6.2 illustrates the spectra of the dual signals and dual idlers generated by the OPO at the pump wavelength of 532 nm. The dual signals appearing in the spectra were caused by their weak transmissions through the polarizer. The wavelengths of the dual signals oscillating in the OPO cavity were measured to be 1034.8 nm and 1044.2 nm, whereas the wavelengths of the dual

idlers were 1084.1 nm and 1093.9 nm, respectively. These measured wavelengths coincide with the calculated values.

When a pump beam at 532 nm with the repetition rate of 10 Hz and the pulse width of 4.8 ns was slightly focused onto the AFB KTP composite (a beam diameter of about 2 mm, measured by us), we measured the total output power from the OPO vs. the pump power, see Fig. 6.2. By linearly fitting the data points in Fig. 6.2, we deduced the threshold power for the OPO to be 12 mW (the corresponding energy of 1.2 mJ per pulse). Such a threshold power corresponds to an intensity of 8 MW/cm^2. At the pump power of 111.8 mW, the OPO output power reached 39 mW, corresponding to a conversion efficiency and slope efficiency of 34.9% and 37.1%, respectively. To demonstrate the advantage of a higher gain in the AFB KTP composite, we measured the power dependence from an OPO based on two traditional KTP crystals which were placed in the setup similar to Ref. [73], see Fig. 6.2.

Each of the two KTP crystals generated a pair of signal and idler around 1 μm with slightly different wavelengths. The length of each crystal is 10 mm such that the total length is 20 mm, which is close to the length of the AFB KTP. At the pump power of 108.5 mW, the dual-idler output power was 21 mW which was 53.8% of the output power generated from AFB KTP. This value is close to an estimate of 42.8%, considering the slightly length difference between the AFB KTP composite and two traditional KTP crystals. Since the implemented OPO is singly resonant, the spectrum and power of the dual-idler beams is rather stable based on our observation.

6.2 THz Generation Pumped by AFB-KTP OPO

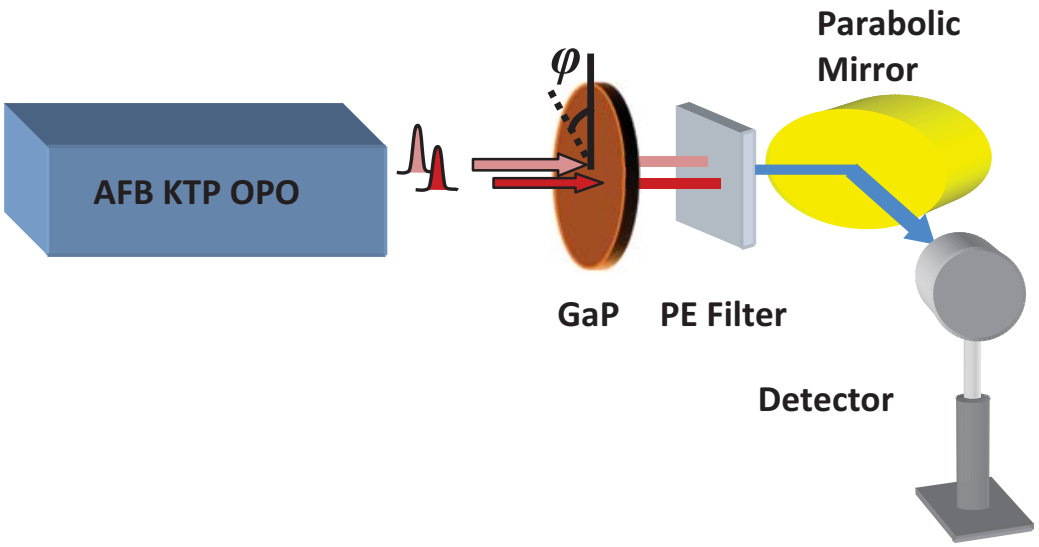

Figure 6.3: An experimental setup for THz generation.

By mixing the dual-idler beams from the OPO based on DFG [19, 18, 56] in four-piece alternatively-rotated GaP plates, we generated the THz wave based on the setup shown by Fig. 6.3. Each GaP plate cut along the (110) plane had a thickness of 663 mum. The polarizations of the dual-idlers were along the same direction which is different from the condition in Refs. [19, 18]. As we rotated the azimuthal angle of a single GaP plate, the THz intensity exhibited a unique dependence, see Fig. 6.4. This is caused by the dependence of the second-order nonlinear coefficient on the polarization directions of the mixing beams relative to the azimuthal angle of the plate. Considering the above conditions and cut angle of GaP plate, the THz intensity is proportional to $cos^4(\varphi) + sin^2(2\varphi)$, where φ is the

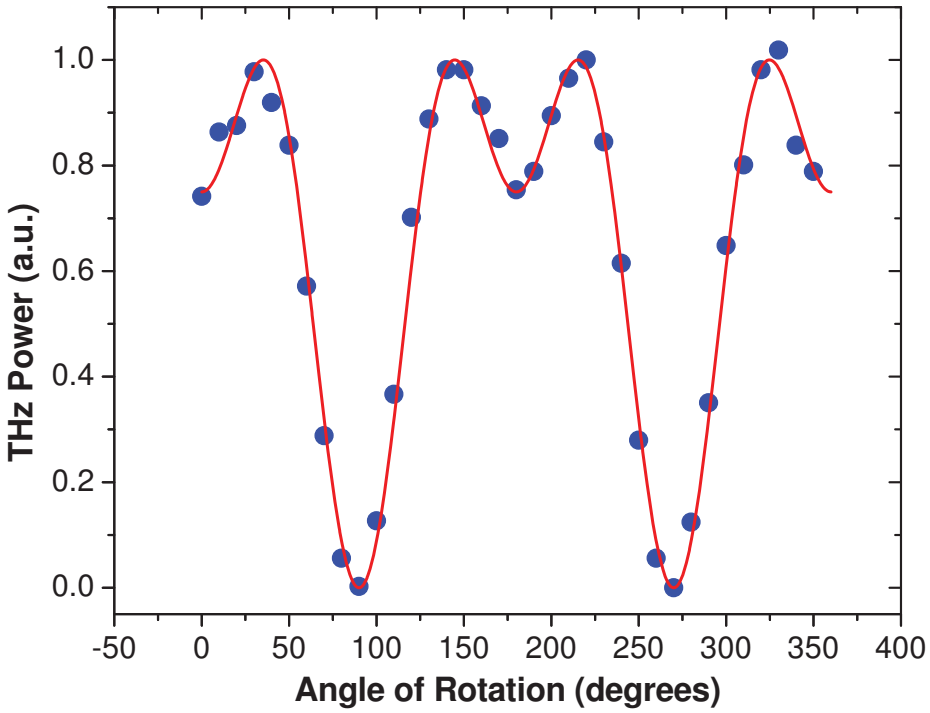

Figure 6.4: THz power as a function of azimuthal angle in GaP plate. Dots correspond to experimental results. Solid curve corresponds to theoretical result.

azimuthal angle. As we can see from Fig. 6.4, the measured data agree quite well with the theoretical values.

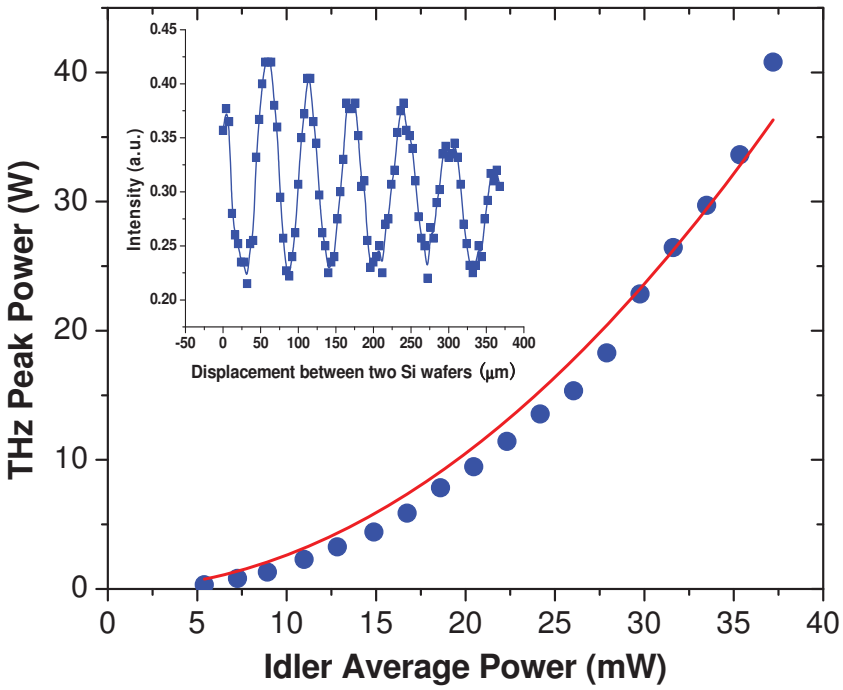

Figure 6.5: Dependences of THz peak power on the dual-idler average power emitted from the OPO. Solid curve corresponds to the quadratic fit. Inset: the power being transmitted through a Si-based etalon versus the distance.

We measured the THz power generated by the four-piece alternatively-rotated GaP stacks vs. the average power of the dual idlers from the OPO, see Fig. 6.5. At 37.2 mW, the THz peak power was measured to be 40.8 W. We fitted the data points using a quadratic dependence, which corresponds to the solid curve in Fig.

6.5. Obviously, the measured data clearly exhibit a quadratic dependence which is the typical characteristics of DFG. Based on the data presented in Fig. 6.5 the THz output power is stable.

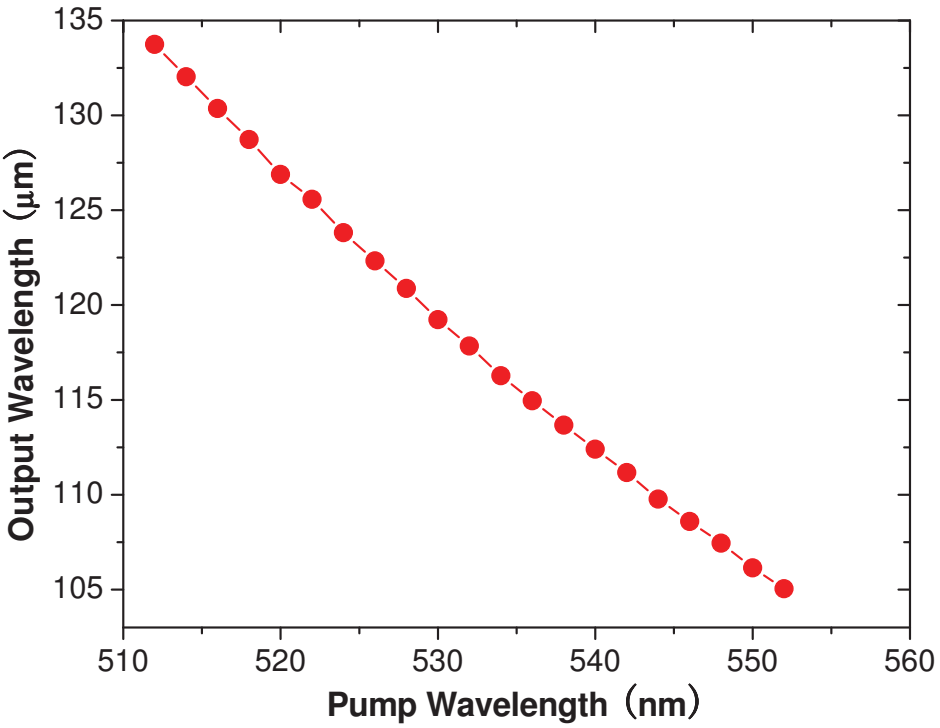

Figure 6.6: An illustration of the tuning characteristics.

By scanning a Si-based etalon, THz wavelength was measured to be 121 μm, which agrees well with the designed value of 118 μm (see inset to Fig. 6.5).

The THz frequency is determined by not only the phase-matching condition of the pump, signal and idler from the OPO, but also the QPM condition due to the presence of the alternatively-inverted AFB KTP plates. The THz output

frequency is given by $\nu = \nu_{i1} - \nu i2$, where ν_{i1} and ν_{i2} are the frequencies of the idler beams generated by the OPO. Since the pump wavelength of the OPO is 532 nm, the THz frequency is calculated to be 2.55 THz, which is close to 2.54 THz (118 μm). In addition, to explore the tunability of the THz generation, we varied the pump wavelength within the range of 512-552 nm. Fig. 6.6 illustrates the tuning characteristics. According to Fig. 6.6, the THz output wavelength can be tuned in the range of 105.0-133.7 μm, corresponding to the frequency range of 2.244-2.857 THz.

In conclusion, we have demonstrated a singly-resonant OPO based on AFB periodically-inverted KTP plates. Such a noncritical-phase-matched OPO had a threshold, measured to be $8MW/cm^2$. We have generated THz waves by mixing the dual-idler output of the OPO in GaP stacks. We have achieved a tuning range of 2.244-2.857 THz. Besides the collinear configuration, one could use such an OPO output to generate a THz wave under the surface-emitting geometry [47].

6.3 Simultaneous Generation of Multiple THz Frequencies

Terahertz (THz) frequency comb has been used for terahertz spectrum analyzer [76] and high accuracy, high-resolution terahertz spectroscopy [77]. In addition, dual-wavelength THz generated by quantum cascade laser (QCL) is promising for attractive application in dual-wavelength THz imaging [78]. Compared with QCL, THz generation based on DFG can work at room temperature. Provided with multi-wavelength pump beam, THz frequency comb could be achieved from DFG. In the first section of this chapter, as a first step to achieve this goal, we have discussed

about the results on a singly resonant OPO with the dual-signal and dual-idler wavelengths around 1 μm. It was achieved through periodically orientated KTP stacks based on AFB technology, which can simultaneously compensate spatial walk-off. The dual-signal was confined in the cavity for resonance such that the dual-idler was coupled outside as the output beam.

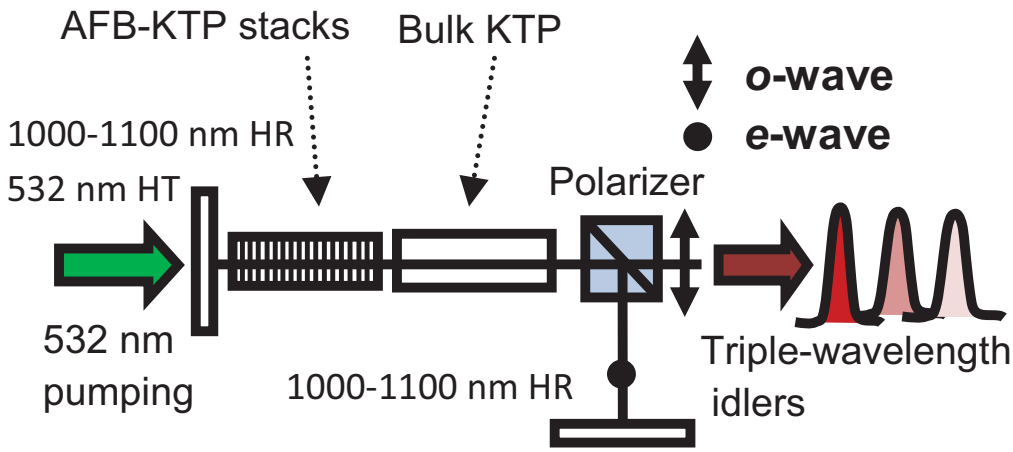

Figure 6.7: The experimental setup of triple-wavelength idlers OPO based on AFB-KTP stacks and bulk KTP.

In this section, we report our results on the triple-wavelength OPO and its application in generating THz radiation with multiple frequencies. The dual and triple-wavelength THz frequency radiation is generated through DFG pumped by the triple-wavelength idlers in GaP and GaSe crystals. This is made possible by inserting another bulk KTP crystal beside the AFB KTP stacks which are placed inside the OPO cavity.

The experimental setup for the singly resonant triple-wavelength OPO, as shown in Fig. 6.7, is quite similar with the setup in Fig. 6.1. The AFB KTP stacks consist

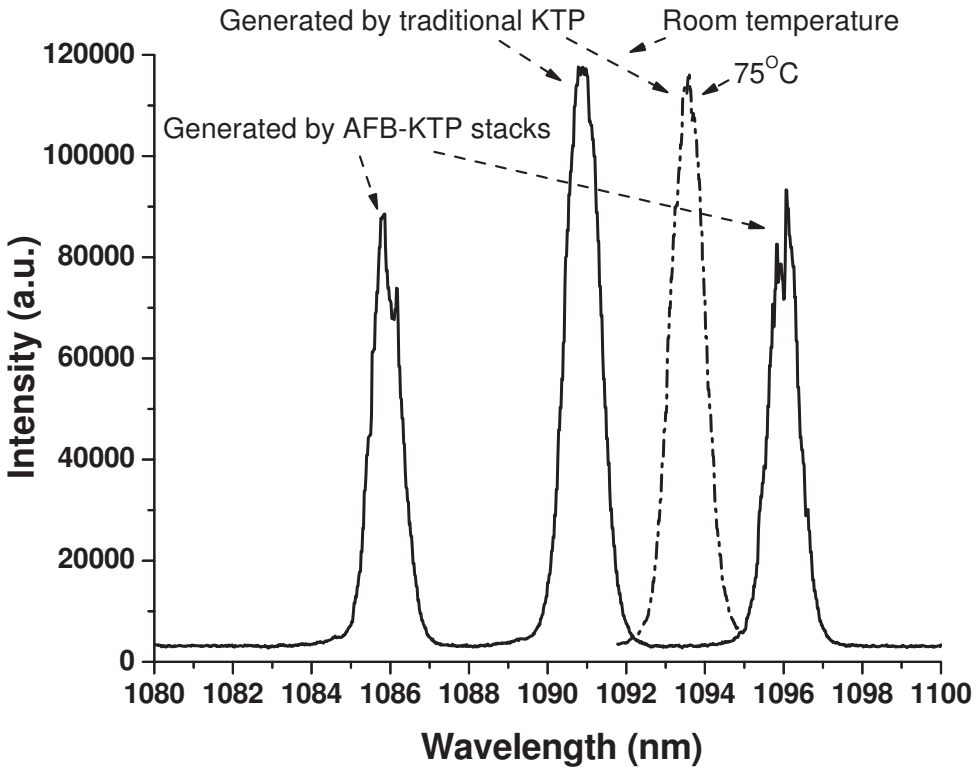

Figure 6.8: Spectrum of the triple-wavelength idlers.

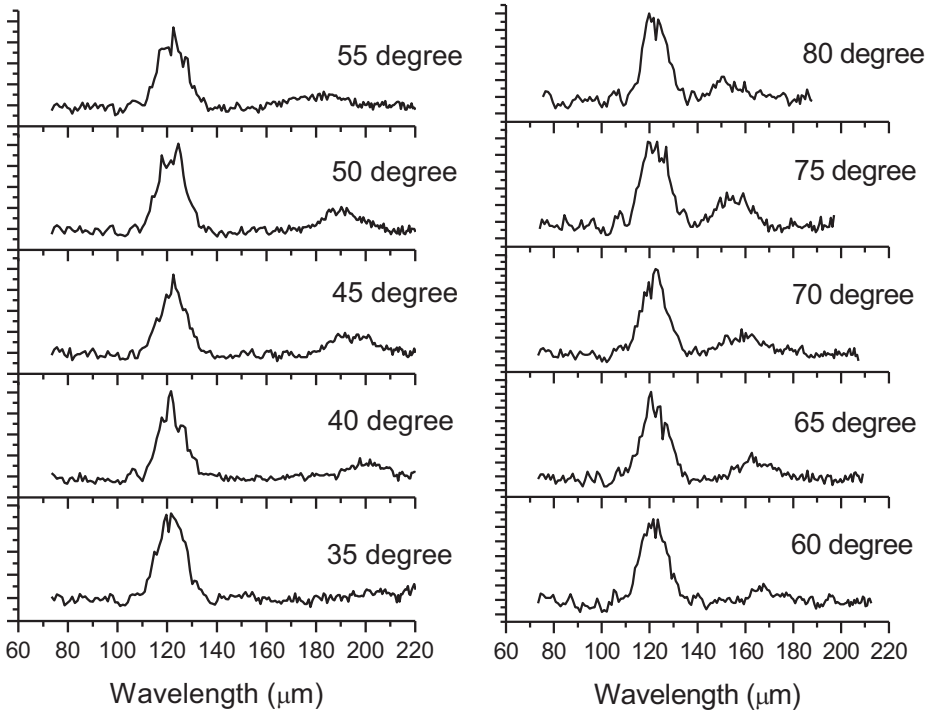

Figure 6.9: Spectra of the tunable THz comb generated from 2pc GaP Stack.

of 20 x-cut KTP plates, each of which has a thickness of 1.19±0.01 mm. The total interaction length is thus 23.8 mm and the composite stacks have a clear aperture of 5.6 mm×10.5 mm. All the z axes of the stacks were periodically switched and were adhesive-free-bonded together as a composite such that the QPM condition ($\Delta kl = \pm\pi$) could be achieved. In this way, the intrinsic signal and idler wavelengths that satisfied the phase matching condition in bulk KTP would split into dual-signal and dual-idler wavelengths. Beside the composite stacks, a x-cut bulk KTP crystal (5 mm×5 mm aperture, 20 mm length) was also placed in the cavity. As a result, the third set of signal and idler wavelengths could be generated. In addition, the bulk crystal was fixed in an oven so that the wavelength could be tuned through changing the temperature. The two cavity mirrors both have high-reflection coating between 1000 and 1100 nm and the input mirror is also high transmission coated at 532 nm which is the pump wavelength of the OPO. To ensure the oscillations only at the signal wavelengths, a cubic polarizer was placed inside the cavity. It reflects almost all of the *e*-polarized signal beams (R > 99%) such that the signals are confined inside the cavity whereas the *o*-polarized idler beams are coupled outside the cavity as the emitting beams. Figure 6.8 shows the spectrum of the triple-wavelength idlers at the room temperature. The wavelength generated by bulk KTP crystal located at the middle position between the dual-wavelength generated by the AFB-KTP stacks. The reason, as we mentioned before, is due to the periodically rotation of the x-cut KTP plates in the stacks. Besides, we also plotted the spectrum as we applied temperature-tuning for the bulk KTP crystal when the temperature was set at 75°C.

To generate THz comb, the triple-wavelength idlers were directed onto the GaP stacks. The stacks were composed of two piece of GaP plate, each of which had

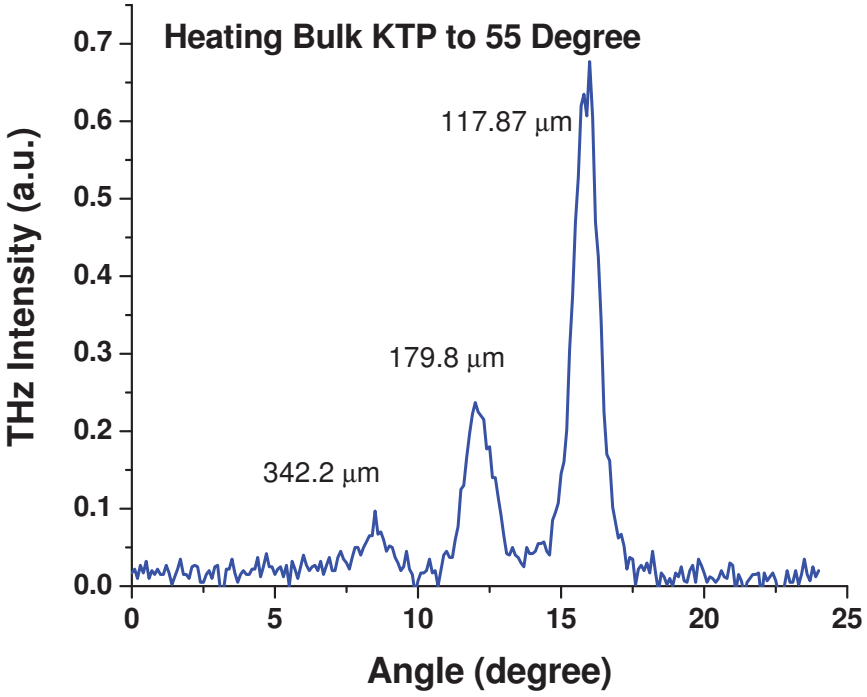

Figure 6.10: Spectra of the THz generation as a function of phase match angle based on GaSe crystal.

been cut along the (110) plane and had a thickness of 663 μm. The two plates were stacked along the same direction. THz radiations were then measured by using the homemade THz spectrometer. The measured spectra are shown in Fig. 6.9. The THz radiation at around 120 μm was generated by the DFG pumped by two idlers at 1085.9 nm and 1096.1 nm. Meanwhile, the other tunable THz radiation was generated by the DFG pumped by idler at 1085.9 nm and the third idler generated by the bulk KTP. As we changed the temperature from 35°C to 80°C, the THz

wavelengths were measured to shift from 198 μm to 142 μm. It is mentioned that we did not observe the third THz wavelength due to the limitation of the grating we used in the spectrometer.

When we directed the triple-wavelength beams to the GaSe crystal, we measured all the three THz wavelengths generated by all the three idlers. As GaSe is uniaxial birefringent crystal, the phase matching angles for each THz wavelength is different. We measured the THz intensity relative to the θ angle between the wave vector direction and z-axis of GaSe, shown in Fig. 6.10. We set 55°C for the bulk KTP so that the triple-wavelength idlers are 1085.9 nm, 1092.5 nm, and 1096.1 nm, respectively. Based on the Sellmeier equation of GaSe crystal, the triple-wavelength THz wavelengths are 117.87 μm (2.545 THz), 179.8 μm (1.668 THz) and 342.2 μm (0.8767 THz), respectively.

Chapter 7

THz Generation Pumped by Yb:YAG Laser

In previous chapters, we have demonstrated several compact and potable terahertz source based on difference-frequency generation (DFG) pumped by dual-frequency sources either from solid-state laser or optical parametric oscillator. Compared with quantum cascade laser, these sources can completely work at room temperature. Besides, due to the availability of more than 100 Nd-doped laser mediums, almost any THz wavelength could be achieved simply by choosing two different laser mediums that can emit different wavelengths. Moreover, some Nd-doped laser mediums could emit dual-wavelength simultaneously such that the size of the THz source could be further reduced. However, there are very few mediums of this kind and the frequency difference between the two wavelengths is always fixed. Nevertheless, it has been proposed that based on laser medium with broad emission bandwidth, dual-frequency emission could be achieved by using intracavity etalon [33, 79]. Indeed, THz generation has been demonstrated pumped by dual-frequency from Nd:

LSB laser [33]. Compared with Nd-doped laser mediums, Yb-doped crystals have several advantages for dual-frequency generation [42, 80]. For example, the Yb: YAG crystal can easily provide emission bandwidth with more than 10 nm [81, 82]. Thus, it is possible to achieve dual-wavelength oscillation with large frequency interval, resulting in much wider tunability in THz frequency. Besides, the ratio of heat generated to absorbed energy in Yb: YAG is around one third of that in Nd: YAG. As a result, Yb: YAG is more promising for high power systems such that they can work as more powerful pump sources for THz generation [83, 84]. In recent years, Yb: YAG crystal has been very successful as the gain medium for high power solid-state lasers, especially after the introduction of disk laser technology [85]. It now become not difficult to achieve disk laser with output power of more than 1kW [86]. Besides, even high power (several tens of watt) ultrafast laser has been demonstrated and become commercialized based on Yb: YAG [87]. Moreover, the ceramic Yb: YAG medium have been successfully fabricated and used in solid-state laser [88, 89, 90]. Compared with traditional Yb: YAG crystal, the ceramic medium can have higher doping rate for Yb ion. As a result, the pump absorption coefficient of the crystal can be dramatically improved. In addition, the ceramic medium can also have wider emission bandwidth. Thus, the ceramic medium would be more feasible for the experiment THz generation with wider tunability.

In this chapter, we will discuss the first demonstration of terahertz generation by mixing dual-frequency pulses from a compact Q-switched Yb: YAG solid-state laser [91]. The dual-frequency emission is successfully achieved through inserting a 50 m thick etalon into the laser cavity. The wavelength interval can reach 6.1 nm, corresponding to 1.65 THz in frequency. Besides, we would also like to discuss about other novel approach to achieve THz tunability based on the advantages of

Yb: YAG crystal and Yb: YAG ceramic material.

7.1 Dual-Frequency Yb:YAG Laser

Our proposed approach would be similar to the design on the Nd: LSB laser [33]. An etalon will be inserted into the cavity of Yb: YAG laser and choose dual-wavelength or even triple-wavelength within the emission spectrum of the crystal. The laser output radiation will then be used as the pump for THz DFG and will be expected to obtain efficient output power in THz region. In this proposed experiment, a Yb: YAG rod will be used as the laser gain medium.

Figure 7.1 shows our theoretical design of dual-wavelength generation by inserting an etalon into the laser cavity. In the last sub figure, it is illustrated that the dual-wavelength could be successfully chosen.

The experimental setup for the compact dual-frequency Q-switched Yb: YAG laser is shown in Fig. 7.2. The laser crystal used in the experiment is a 5% Yb-doped YAG crystal with 5 mm diameter and 5 mm length. To match the absorption band of Yb: YAG, we used a 940 nm laser diode which can emit the light through a pigtail multi-mode fiber. The 940 nm pump light is then reshaped through the coupling optics and focused onto the region adjacent to the input surface of Yb: YAG crystal. The input surface, functioning as the back reflector of the laser cavity, has a high reflection (HR) coating centered at 1030 nm and a high transmission (HT) coating at 940 nm (T$>$ 90%). On the contrary, the exit surface of the crystal is anti-reflection coated at 1030 nm. The output coupler is a concave mirror with curvature of 5 cm. The transmittance of the output coupler was chosen to be T=2% such that the emission bandwidth of laser medium could be sufficiently broad. Besides, to

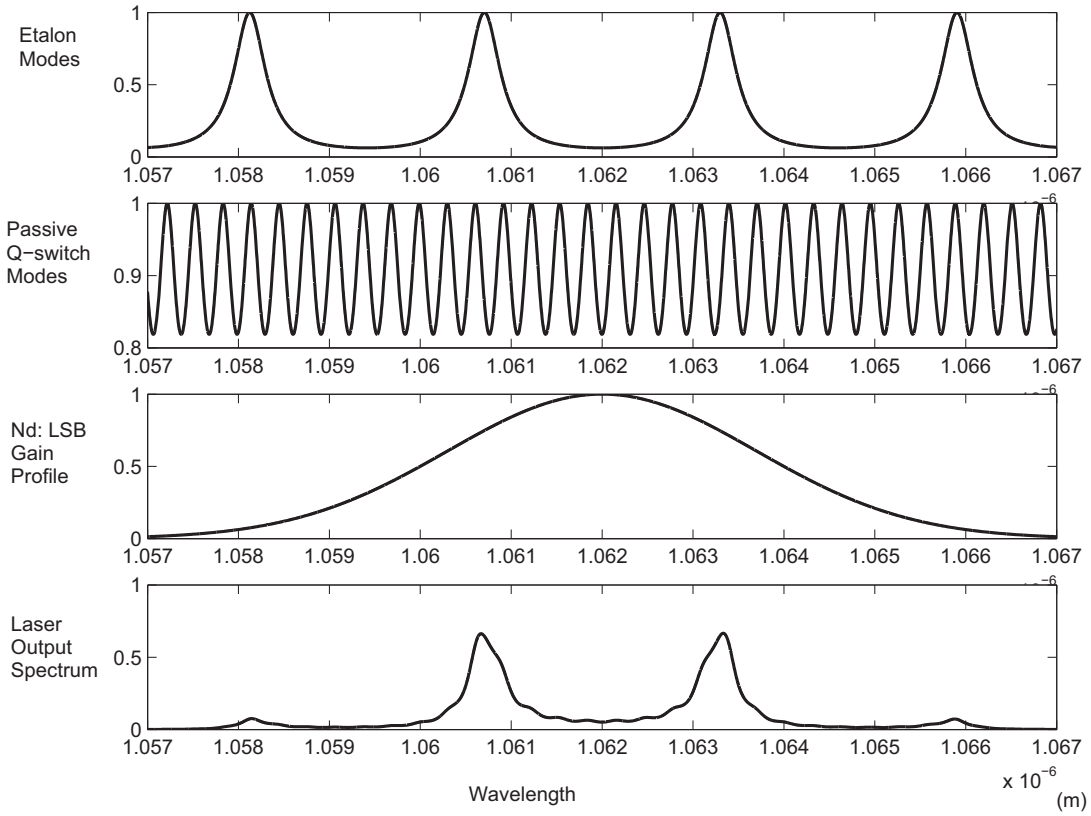

Figure 7.1: Design of dual-wavelength emission in laser with broad bandwidth emission bandwidth by inserting etalon.

operate the laser in pulsed mode, an acoustic-optic Q-switch was placed inside the cavity. In addition, a solid etalon was used which is the key component to ensure the dual-frequency oscillation. In this experiment, we chose a 50 μm thick uncoated YAG etalon with a free spectrum range (FSR) of 1.65 THz. We tested the one-pass transmittance of etalon by using a FTIR spectrometer. The dependence of the transmittance showed as a periodically modulated curve and the transmittance dip went down to around 72.5%. Once placed into the laser cavity, the laser spectrum

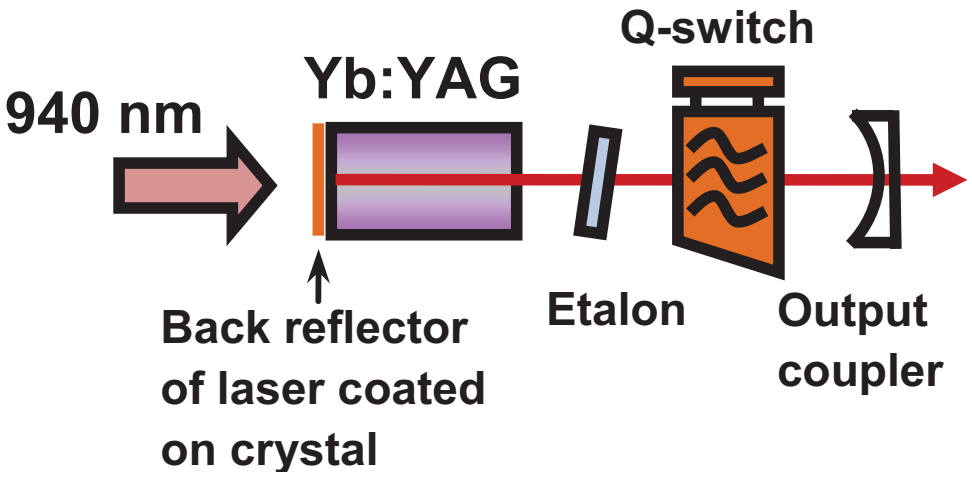

Figure 7.2: The experimental setup of dual-frequency Q-switched Yb: YAG laser by inserting etalon.

would be determined by the superposition of the laser emission spectrum multiplied by the modulated spectrum caused by etalon. It is observed that if two transmission peaks located within the profile of the laser emission spectrum, the laser could operate in dual-frequency mode. In order to do this, we can tilt the etalon inside the cavity such that the frequency of the transmission peaks could shift a little relative to the center frequency of the laser emission spectrum. At the tilting angle of around 6°, we achieved Q-switch dual-frequency emission at 1035.6 nm and 1041.7 nm, see Fig. 7.3. At the pump of power of 8.67 W, we achieved 262 mW dual-frequency average power. The low conversion efficiency is attributed to additional reflection loss introduced by the tilted etalon. The conversion efficiency could be improved by using laser crystals with broader emission spectrum in which the tilting of etalon is not necessary.

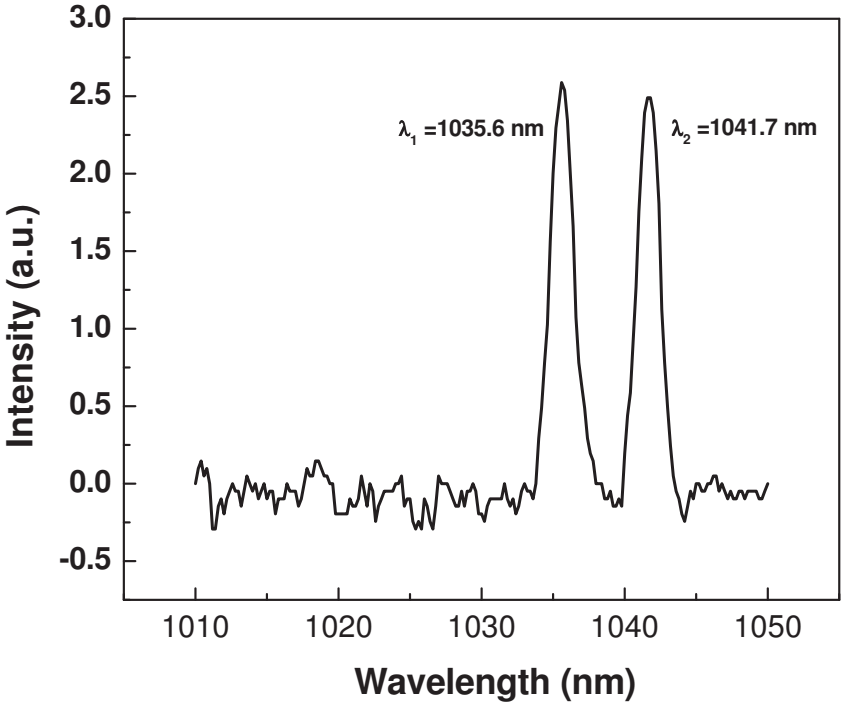

Figure 7.3: Dual-frequency spectrum of Yb:YAG laser.

7.2 THz Source Based on Yb:YAG Laser

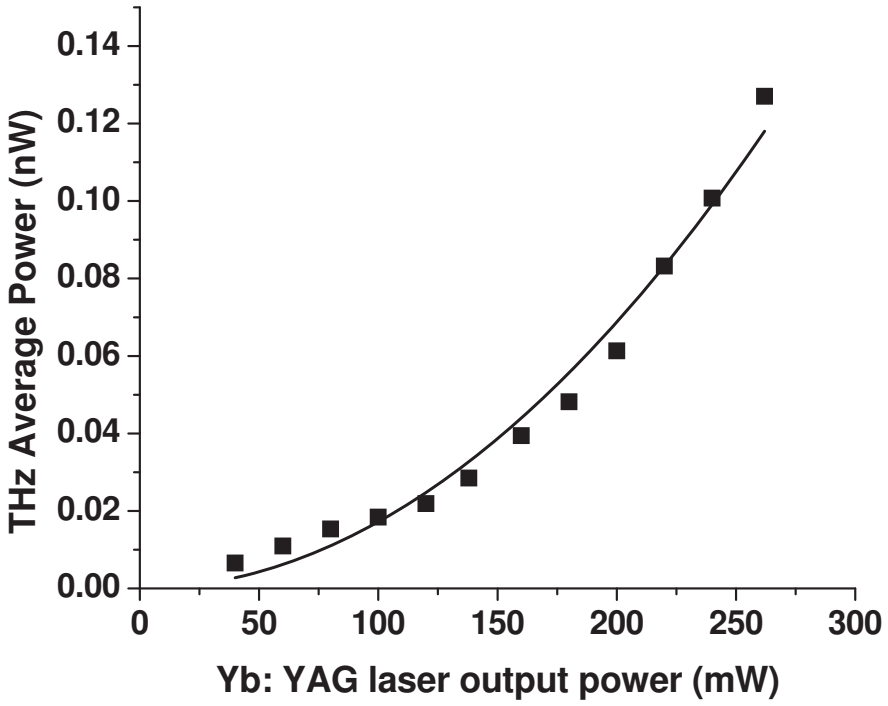

Figure 7.4: THz power dependence vs. corresponding laser pump power.

To generate THz wave, the dual-frequency beam was focused and directed onto GaP crystal. Each of the GaP plates used in the experiment was cut and polished along the [110] direction. The diameter of each plate is 48.5 mm and the thickness is 663 μm. In the experiment, we used two GaP plates and stacked them along the same direction such that the total interaction length is 1.326 mm. At the pump power of 262 mW, we generated THz wave at 1.65 THz with an average power

of 0.127 nW. The THz power dependence is shown in Fig. 7.4. The solid curve corresponds to the quadratic fitting. Obviously, the dependence is quadratic which is the typical characteristic of DFG. Besides, we have also measured the polarization of the THz radiation as a function of the azimuthal angle of a THz polarizer which shows as the dependence of *sin* function. It is mentioned that Yb: YAG crystal is a laser medium suitable for high average power systems. Nowadays, the high power Yb: YAG disk laser system is widely used in laser processing industry. Thus, it is possible to do THz power scaling by using higher pump source or intracavity scheme.

7.3 Tunable THz Source

As the Yb: YAG crystal has emission bandwidth as wide as several tens of nm, it is feasible to achieve dual-wavelength generation with different wavelength intervals simply by choosing etalons with different thicknesses. As a result, it is possible to achieve any THz wavelength based on DFG pumped by Yb: YAG laser. Besides, we can also achieve tunable single-frequency Yb: YAG laser by using some frequency-selection component, such as prism, birefringent filter, grating etc. If we have another laser with fixed wavelength, it can then be mixed with the tunable frequency from Yb: YAG laser such that the tunable THz generation could also be achieved.

7.3.1 Tunable Etalon

Apart from the 50 μm thick YAG etalon, we also have 4 other etalons with their thicknesses and the corresponding THz frequencies listed in Table 7.1. As is known

Etalon Material	Thickness	THz Frequency
Fused silica	200 μm	0.502 THz
YAG	100 μm	0.82 THz
Fused silica	88 μm	1.143 THz
YAG	50 μm	1.65 THz
Fused silica	50 μm	2.011 THz

Table 7.1: THz frequency as a function of etalon thicknesses.

to all, the etalon effect will introduce the modulation of transmittance as a function of wavelength or frequency. The wavelength interval between the adjacent transmittance peaks is determined by $\lambda_0^2/(2nl)$, where λ_0 is the center wavelength of the transmittance peaks, n is the index of the etalon material and l is the thickness of the etalon. Thus, when the etalon material is chosen, the only parameter that could be changed is the thickness of the etalon. In order to generating dual-wavelength laser radiations with different wavelength intervals, we can simply choose different etalon thicknesses. In addition, apart from solid etalons, there is also air-gap etalon that could be used in our research. In order to achieve continuous frequency tuning for THz radiation, we can also continuously tune the air gap distance within the etalon.

7.3.2 Yb:YAG and Nd:YLF

As shown in Fig. 3.4 in chapter 3, we could use two separate laser crystal and drive them to generate two separate laser wavelengths for DFG. In Fig. 3.4, we used two Nd: YLF crystals and generate two wavelengths at 1047 nm and 1053 nm, respectively. However, the two wavelengths are fixed in these two laser crystals such that the THz frequency cannot be tunable. Nevertheless, the Yb: YAG is a

promising laser medium for wavelength tunable lasers. We proposed a novel design for tunable THz source, shown in Fig. 7.5. One of the two Nd: YLF crystals has been replaced by a Yb: YAG rod. Besides, we introduced an additional birefringent filter into the cavity of Yb: YAG laser such that the emission wavelength of Yb: YAG laser could be tunable. Correspondingly, the frequency of THz radiation could be varied based on DFG.

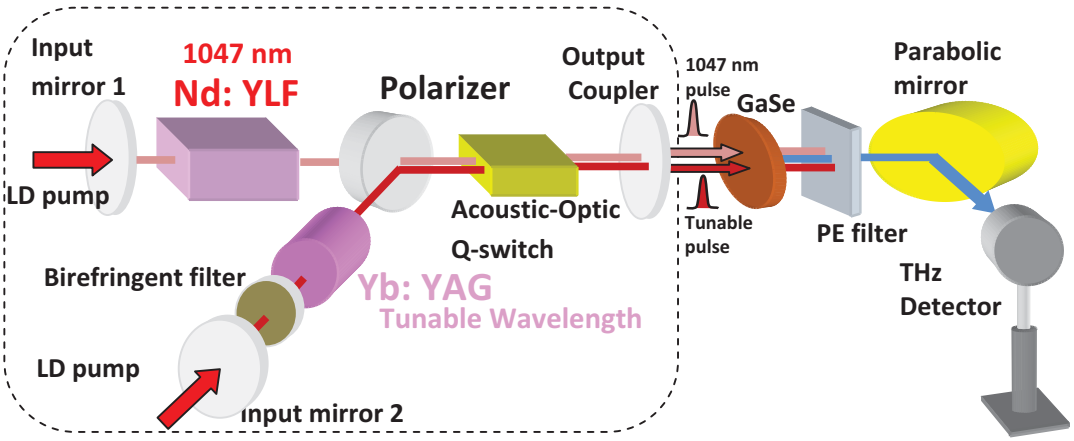

Figure 7.5: Schematic plot of tunable THz source based on Nd: YLF and Yb: YAG lasers.

7.4 Multiple-Frequency Ceramic Yb:YAG Laser

Multi-wavelength lasers have potential applications including aerosol lidar, optical imaging etc. Specifically, if the output frequencies have identical interval, the application could be extended to frequency comb and cascaded frequency down-conversion for terahertz generation. Recently, it has been observed that multiple idler-waves were generated through an intracavity cascaded parametric process

pumped by a single pump wavelength [92]. It is thus expected that the cascaded DFG is possible if we can pump the frequency converter by using multi-wavelength laser with output wavelengths of identical frequency interval.

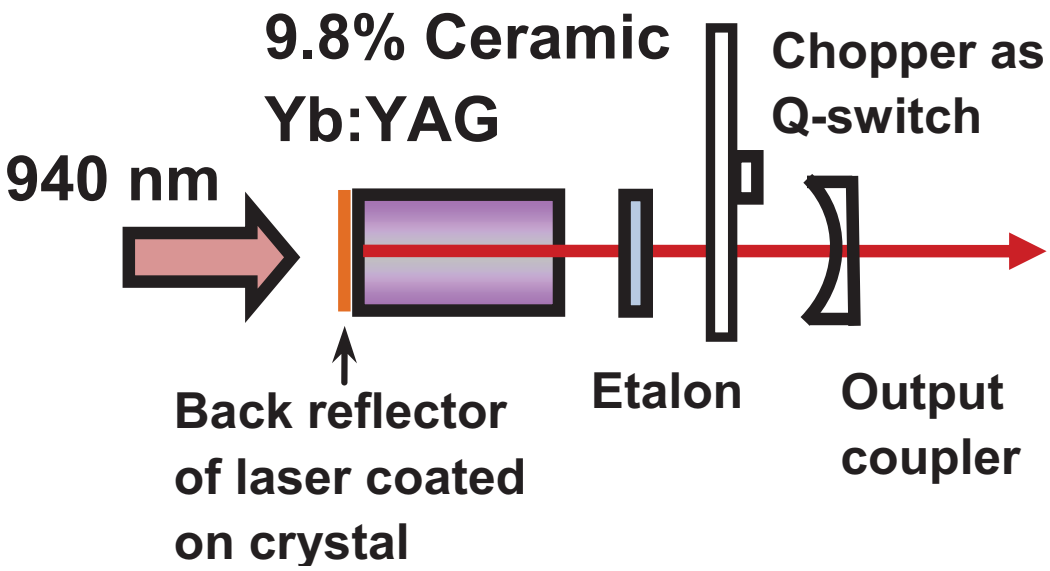

Figure 7.6: The experimental setup of multi-wavelength Q-switched ceramic Yb: YAG laser.

In this section, we will discuss the demonstration of a novel multi-wavelength solid-state laser. Based on the broad emission bandwidth of some special laser crystals, we can achieve multi-wavelength lasing by using interference filters inside laser cavity. This is made possible by inserting etalons into the cavity. It is mentioned that this approach is similar with how we designed the dual-wavelength Yb: YAG laser. However, for multi-wavelength radiation generation, we need the emission bandwidth of the laser medium to be much wider. The emission bandwidth could be improved by increasing the doping rate of the ion. However, due to the reason

that most of the laser crystals cannot be doped with Nd^{3+} ion at very high doping rate, the Nd-doped laser medium have very narrow emission bandwidth. Thus, the Nd-doped crystals are not suitable candidate for achieving multi-wavelength generation. Nevertheless, the Yb-doped laser crystals are not confronted with this problem and can be doped at a much higher doping rate. Moreover, it has recently been demonstrated that the ceramic Yb: YAG crystal can provide better performance. Indeed, the 9.8% Yb-doped ceramic YAG crystal is capable of emitting radiation around 1 μm with an emission bandwidth of more than 100 nm wide [89].

Figure 7.6 shows our experimental setup for the multi-wavelength ceramic Yb: YAG solid-state laser. The laser gain medium is a 9.8% Yb-doped ceramic YAG crystal rod. It has a diameter of 5 mm and a length of 5 mm. The input surface, operating as the back reflector of the laser, is high-reflection (HR) coated between 1000 nm and 1100nm, whereas the exit surface is anti-reflection (AR) coated between 1000 nm and 1100 nm. Besides, to ensure efficient pumping, the input surface is also high-transmission (HT) coated at 940 nm ($T \approx 90\%$). To achieve multi-wavelength operation, we used five etalons with different thicknesses, see Table 7.1. The output coupler is a concave mirror (curvature 5 cm) with a coupling coefficient of T=2% at 1030 nm. In addition, we placed a chopper inside the cavity such that the laser could operate at Q-switched mode. In the experiment, chopping rate was set at 2.3 kHz.

By using etalon with different thicknesses, we have achieved laser emission with multi-wavelength spectra. Here, we show the multi-wavelength spectra by inserting the etalon with thickness of 200 μm and 88 μm, shown in Fig. 7.7. In the Fig.

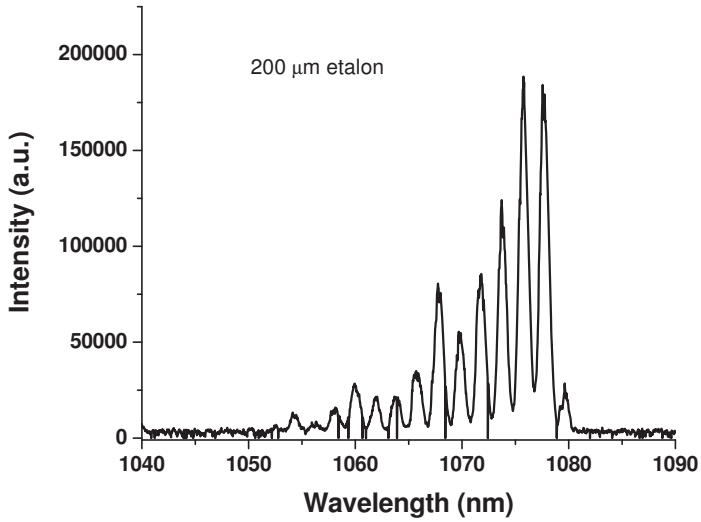

(a)

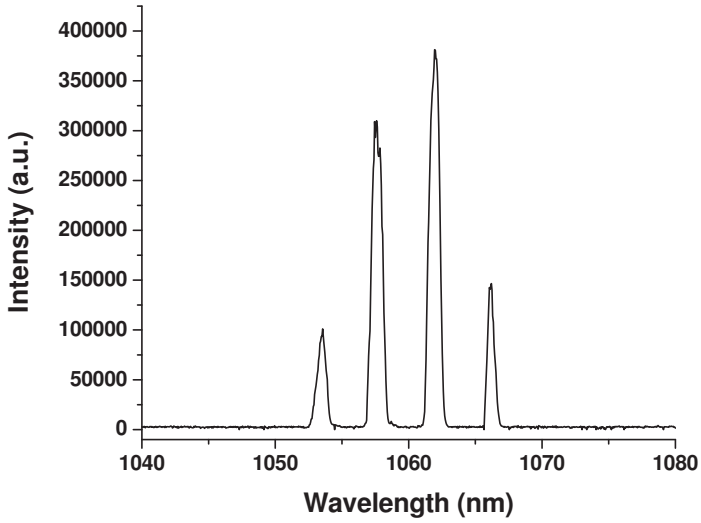

(b)

Figure 7.7: Spectra of ceramic Yb:YAG laser with intracavity etalon. (a) 14 emission peaks by inserting 200μm etalon; (b) 4 emission peaks by inserting 88μm etalon.

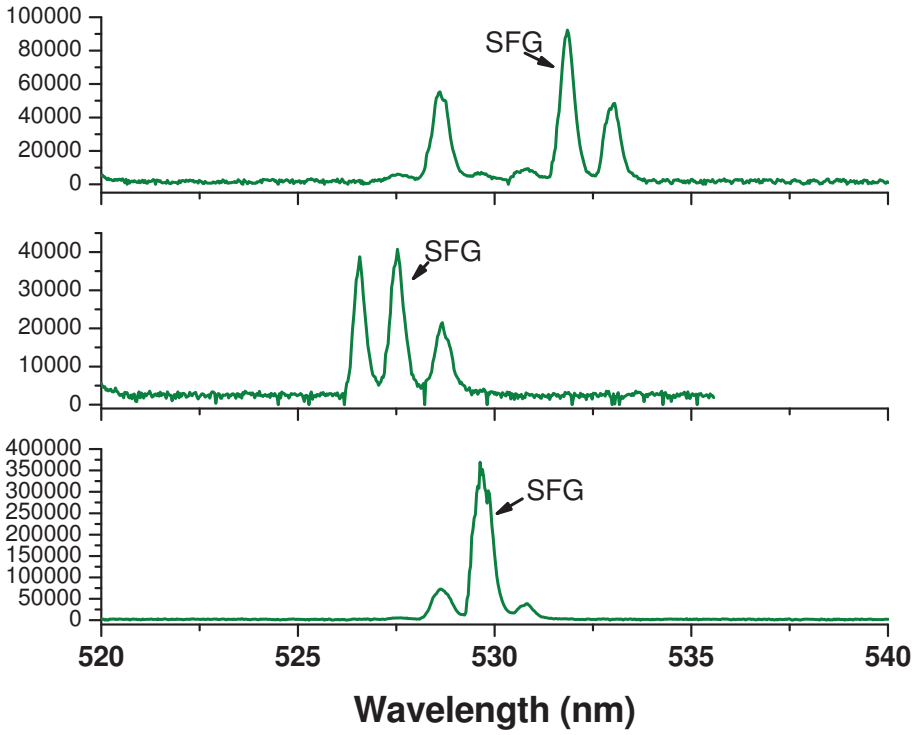

Figure 7.8: Spectra of SFG pumped by the multi-wavelength beam.

7.7 (b), the wavelengths of the four peaks were measured to be 1053.68 nm, 1057.8 nm, 1062.13 nm and 1066.34 nm, respectively. Because of the filtering effect of the etalon, the frequency interval among the four wavelengths should be identical. In the experiment, the frequency interval (or be called FSR) was measured to be 1.14 THz, which agreed well with the theoretical value of 1.143 THz. At the 940 nm pump power of 5.63 W, we have achieved the Q-switched multi-wavelength output of 637 mW. At the repetition rate of 2.3 kHz, the pulsewidth was measured to be around 80 ns. In order to test the synchronization of the laser pulses at different wavelengths,

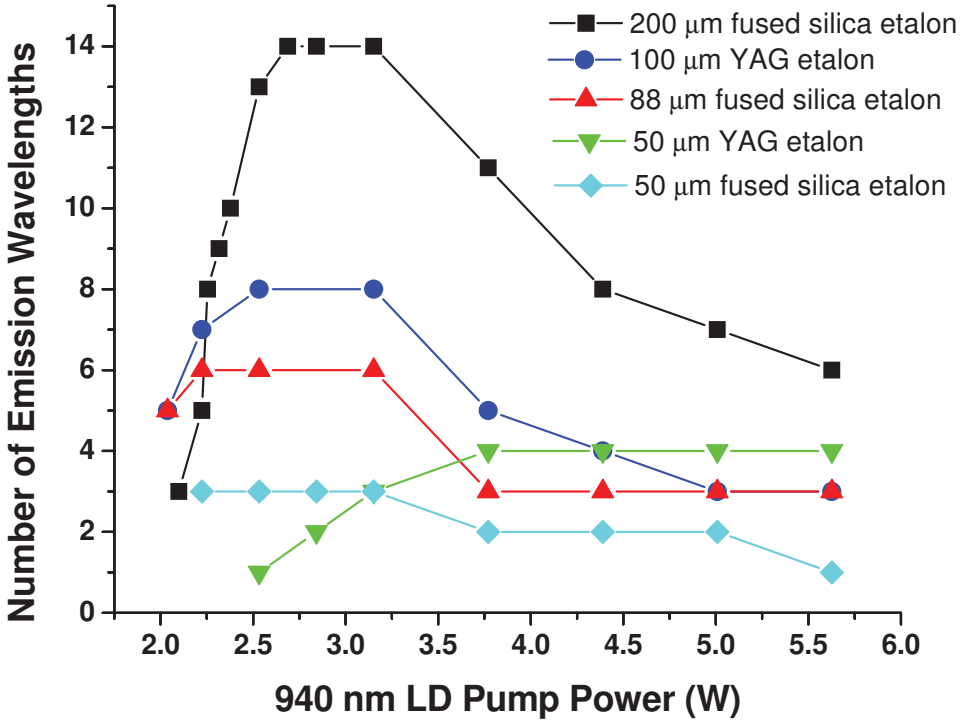

Figure 7.9: Number of emission wavelengths relative to the 940 nm pump power.

we directed the beam to a KTP crystal ($\theta = 90°, \varphi = 23.5°$) and tried to measure the spectrum of Type-II sum-frequency generation (SFG). We measured the second harmonic generation (SHG) of the four fundamental wavelengths at 526.84 nm, 528.9 nm, 531.06 nm and 533.17 nm. Besides, the SFG wavelengths were also measured at 527.53 nm, 529.69 nm and 531.85 nm, see Fig. 7.8. Thus, such a frequency mixing experiment provided as a proof for our expectation that the pulse trains at the different wavelengths have been synchronized.

As we studied the continuous-wave multi-wavelength operation based on the five different etalons, we have also investigated the variations of the number of emission wavelengths as we changed the power of 940 nm pump, see Fig. 7.9. The thresholds of the lasers were around the pump power of 2 W. It is noted that we could achieve as many as 14 emission wavelengths as we used the 200 μm thick etalon which has the shortest frequency interval. In addition, as we increased the pump power, the number of the emission wavelengths would decrease. This, we believe, is due to the nonuniform gain at different wavelengths within the emission band of ceramic Yb: YAG. As the pump level is higher relative to the threshold, the gain competition among different wavelengths would become more severe. Thus, some emitted wavelength with weaker gain would be suppressed.

Chapter 8

Conclusion and Future Work

8.1 Conclusion

In this dissertation, we have investigated several approaches to solve the biggest barrier in the current THz technology - lack of portable and efficient THz source that can operate at room temperature. Based on the technology of difference frequency generation (DFG), we have demonstrated several compact THz sources which can completely work at room temperature. The contributions of this research belong to two main fields. In one field, we have proposed and demonstrated a number of novel ways to achieve lasers or coherent sources with synchronized dual-frequency pulses output. These coherent sources are either solid-state lasers or optical parametric oscillator (OPO). Because solid-state lasers and OPO are two common types of products in laser industry, our sources are thus promising to be converted to product. Besides, in the other field, we have utilized these dual-frequency sources for THz generation. As these dual-frequency sources are all designed to be rather compact, our THz generation setups are all very compact. In addition, we also

demonstrated some novel approaches for the process of DFG. In the following part, we will summarize all the contributions in this dissertation.

In the following part, we will summarize the contributions presented in this dissertation.

In Chapter 2, a novel compact and portable THz source has been demonstrated with the size as small as 12" × 6" × 4" ($30.48cm \times 15.24cm \times 10.16cm$). This research was based on the interesting property of Nd: YLF laser crystal, which has two adjacent emission wavelengths at 1047 nm and 1053 nm, respectively. The corresponding THz wave at 1.64 THz (182.42 μm) efficiently generated with an output power of about 1 μW, corresponding to a dynamic range of 4120 by using a detector that can operate at room temperature.

In Chapter 3, one approach of THz source power scaling and frequency tuning was proposed and demonstrated. Compared with the setup in Chapter 2, we modified the laser cavity design by introducing two laser crystals, each of which functioned as the gain medium for one of two separate laser emission wavelengths. This design dramatically reduced the gain competition problem appearing in the experiment of Chapter 2 and improved the average output power of THz wave by about 4.5 times. Moreover, it also added the flexibility of choosing all most all kinds of laser crystals. For example, it is not needed to choose the single laser crystal that could emit two adjacent wavelengths. Any laser crystal that could emit one single wavelength could become the candidate for the laser cavity. The only requirement is that the difference between the two wavelengths emitted from these two laser crystal is in the range of THz wavelength.

In Chapter 4, a novel THz source based on intracavity DFG scheme has been proposed and demonstrated. In the conventional way, the nonlinear crystal is placed

inside the laser cavity such that the conversion efficiency of DFG could be dramatically improved due to the much higher intracavity intensity. In our design, the multi-layer GaP stack functioned both as the output coupler of laser cavity and the intracavity nonlinear optical medium for DFG. Besides, as the GaP stack was fabricated only through optical stacking without bonding. The wafer could be aligned according to the coherence length of DFG at different THz wavelength based on quasi-phase-matching technology.

In Chapter 5, we introduced the research on the first demonstration of THz generation pumped by using dual-frequency passively Q-switched solid-state laser. Because it is widely known that passively Q-switched laser has very serious problem of time jitter among the pulses, the synchronization of pulses from two lasers would thus believed to be impossible. We successfully introduced a novel design and reduced the inter pulse jitter time by a factor of 20. THz wave was successfully generated pumped by the pulses from two passively Q-switched lasers based on DFG. Besides, the best application of passively Q-switched laser is designed into extreme compact laser, namely microchip laser. Thus, based on our results, one important implication is the possibility of making microchip THz source.

In Chapter 6, we have achieved a singly resonant optical parametric oscillator (OPO) based on adhesive-free bonded KTP crystal. This oscillator has the superior advantages of compensating walk-off and resonating dual-signal wavelengths based on QPM. THz wave generation at 2.54 THz was demonstrated by mixing the dual-idler emitted from the OPO. Besides, the tunability of this THz source was also demonstrated with the tuning range between 2.19-2.77 THz.

In Chapter 7, we proposed and demonstrated another compact THz source by using dual-frequency Q-switched Yb: YAG laser as the pump source. The advantage

of this source is its compactness and the potential to be tunable. As we can use etalon with different thicknesses, it is possible to choose dual-wavelength laser emissions with different wavelength interval such that the THz wavelength could be tunable. Besides, if we use the air-gap etalon which is capable of changing the gap thickness, the THz wavelength could also be tunable accordingly.

8.2 Future Work

It would be interesting to explore more about compact THz source in the following fields.

(I) For the compact THz source introduced in Chapter 2, it would be very interesting to design a prototype which could be realized by placing the whole system into a package or be fixed onto a breadboard.

(II) As the intracavity scheme is the best way to achieve the most efficient THz generation, it would be needed to spend more efforts on the improvement of this technique. One approach is to use bonded GaP stack with anti-reflection coating at both pump laser wavelength and THz wavelength such that the insertion loss could be reduced for the laser cavity. As a result, the conversion efficiency of THz generation could be dramatically improved.

(III) It is worthwhile to explore more about the research of THz generation pumped by using dual-frequency passively Q-switched laser. In our previous work, the timing jitter has been reduced by more than 20 times. However, the timing jitter has not been completely removed. Thus, new technology is still needed to solve the problem of jitter. Besides, in the experiment of Chapter 5, the two Nd: YLF lasers shared the same passive Q-switch. In the pulses sequence, because we used the first

pulse from 1047 nm Nd: YLF laser as the trigger signal, the second pulse at 1047 nm could be successfully synchronized with the pulse at 1053 nm. However, the first trigger pulse had no contribution to the process of THz generation and would thus reduce the conversion efficiency. As a result, more efforts could be spent to solve this problem.

(IV) For the research of tunable THz source, we have proposed two approaches in the section 7.3 of Chapter 7. It would be very meaningful to demonstrate these two ideas in experiment.

Appendix A

QPM Condition for Crystal with Several Layers

A.1 Introduction

As is known to all, the quasi-phase-matching (QPM) condition is determined by the expression $\Delta kl = \pm\pi$, where l is the thickness of each inverted domain in periodically poled crystals. In our experiments, l is the thickness of each KTP plate in the AFB-KTP stack. This expression is obtained through the Fourier Transform when calculating the equations for the phase matching conditions. However, this result is only valid when treating crystals with large number of periodic structures, like the periodically poled crystals with thousands of inverted domains. As this number is very small, this expression $\Delta kl = \pm\pi$ will become invalid. For example, if the crystal only has two layers being inverted (optical axis in positive direction in one layer and optical axis in negative direction in the other layer), the accurate expression will be determined by $\frac{\Delta kl}{2} = \tan(\frac{\Delta kl}{4})$. In the following part, I will show

how we get this expression. In addition, the following calculation is done without any Fourier Transform. It is noted that this way to derive the Coupled-Wave Equations is also used by Xiaodong in Ref. [93].

A.2 Derivation

We take the process of SHG for example [94]. The second-harmonic field is then if

$$\frac{dE_2}{dz} = \Gamma d(z) \exp(-j\Delta k z) \tag{A.1}$$

where $\Gamma = j\omega E_1^2/n_2 c$. $d(z)$ is the spatially varying nonlinear coefficient. In the crystal with $2N$ periodically inverted layers, $d(z)$ equals d_{eff} in the $(2i-1)th$ layer and $d(z)$ equals $-d_{eff}$ in the $(2i)th$ layer, where $i = 1, 2, 3.....N$. The Δk is the wave vector mismatch and defined by

$$\Delta k = k_2 - 2k_1 \tag{A.2}$$

where k_2 and k_1 are the wave vectors at the fundamental and the second harmonic, respectively. Integrating (A.1), we can find the second harmonic filed at the end of the crystal at the length of L, by

$$E_2(L) = \Gamma \int_0^L d(z) \exp(-j\Delta k z) dz \tag{A.3}$$

Because $d(z)$ equals d_{eff} in the $(2i-1)th$ layer and $d(z)$ equals $-d_{eff}$ in the

$(2i)th$ layer, where $i = 1, 2, 3.....N.$, $E_2(L)$ is then

$$\begin{aligned} E_2(L) = \Gamma \textstyle\int_0^{\frac{L}{2N}} d_{eff} \exp(-j\Delta kz)dz + \Gamma \int_{\frac{L}{2N}}^{\frac{L}{N}} (-d_{eff}) \exp(-j\Delta kz)dz + \cdots \\ +\Gamma \textstyle\int_{\frac{L}{2N}(2i-2)}^{\frac{L}{2N}(2i-1)} d_{eff} \exp(-j\Delta kz)dz + \Gamma \int_{\frac{L}{2N}(2i-1)}^{\frac{L}{2N}(2i)} (-d_{eff}) \exp(-j\Delta kz)dz + \cdots \\ +\Gamma \textstyle\int_{\frac{L}{2N}(2N-2)}^{\frac{L}{2N}(2N-1)} d_{eff} \exp(-j\Delta kz)dz + \Gamma \int_{\frac{L}{2N}(2N-1)}^{L} (-d_{eff}) \exp(-j\Delta kz)dz, \\ where\ i = 1, 2, 3.....N \end{aligned} \tag{A.4}$$

$$\rightarrow E_2(L) = \frac{\Gamma d_{eff}}{j\Delta k}(1 - 2\exp(-j\Delta k\frac{L}{2N}) + \exp(-j\Delta k\frac{L}{N})) \cdot \sum_{i=1}^{N} \exp(-j\Delta k\frac{L}{N}(i-1)) \tag{A.5}$$

$$\rightarrow E_2(L) = \frac{\Gamma d_{eff}}{j\Delta k}(1 - \exp(-j\Delta k\frac{L}{2N}))^2 \cdot \sum_{i=1}^{N} \exp(-j\Delta k\frac{L}{N}(i-1)) \tag{A.6}$$

Take the absolute value of $E_2(L)$, then

$$|E_2(L)| = \frac{\Gamma d_{eff}}{\Delta k} \left|1 - \exp(-j\Delta k\frac{L}{2N})\right|^2 \cdot \left|\sum_{i=1}^{N} \exp(-j\Delta k\frac{L}{N}(i-1))\right| \tag{A.7}$$

Using the mathematic sum property of Geometric progression, (A.7) become

$$|E_2(L)| = \frac{\Gamma d_{eff}}{\Delta k} \left|1 - \exp(-j\Delta k\frac{L}{2})\right|^2 \cdot \left|\frac{1 - \exp(-j\Delta kL)}{1 - \exp(-j\Delta k\frac{L}{N})}\right| \tag{A.8}$$

Expanding (A.8), we have

$$|E_2(L)| = 4\Gamma d_{eff} \frac{\left[\sin(\Delta k\frac{L}{4N})\right]^2}{|\Delta k|} \cdot \left|\frac{\sin(\Delta k\frac{L}{2})}{\sin(\Delta k\frac{L}{2N})}\right| \tag{A.9}$$

A.3 In crystal with only 2 layers

When $N = 1$, the crystal has only two layers. Then expression (A.9) reduced to

$$|E_2(L)| = 4\Gamma d_{eff} \frac{\left[\sin(\Delta k\frac{L}{4})\right]^2}{|\Delta k|} \tag{A.10}$$

Now, we know the relationship between $|E_2(L)|$ and Δk. To find the phase matching condition, we can simply look for the value of Δk when $|E_2(L)|$ is maximized. To do this, we can calculate the derivative of $|E_2(L)|$ and set it to be zero

$$\frac{d\,|E_2(L)|}{d\Delta k} = 0 \tag{A.11}$$

$$\rightarrow \frac{d\,|E_2(L)|}{d\Delta k} = \Gamma d_{eff} \frac{4 \cdot 2\sin(\Delta k\frac{L}{4})\cos(\Delta k\frac{L}{2}) \cdot \frac{L}{4} \cdot \Delta k - 4\sin^2(\Delta k\frac{L}{4})}{\Delta k^2} = 0 \tag{A.12}$$

$$\rightarrow 2 \cdot \cos(\Delta k\frac{L}{2}) \cdot \frac{L}{4} \cdot \Delta k - \sin(\Delta k\frac{L}{4}) = 0 \tag{A.13}$$

We then have the relationship, as

$$\frac{\Delta k L}{2} = \tan(\Delta k\frac{L}{4}) \tag{A.14}$$

This relationship is different from $\Delta kl = \pm\pi$.

To illustrate this difference, we can plot the figure showing the value of $|E_2(L)|$ as a function of Δk, see Fig. A.1. We take KTP as an example and the composite crystal is made up of two layers. The thickness of each layers is 22.5 mm. As a result, the total length of crystal $L = 45mm$ and the thickness of each layer $l = 22.5mm$.

The result is shown in Fig. A.1. The two red lines show the positions of Δk determined by $\Delta kl = \pm\pi$. We can see that the red lines are shifted from the peak values of $|E_2(L)|$. On the contrary, the peak position is determined by the expression (A.14). As a result, if we use the expression of $\Delta kl = \pm\pi$ in the design of stacked KTP with two layers, we cannot get the precise result. For example, for the thickness 22.5 mm of each layer, the frequency difference between the dual-signal will be 100.7 GHz. However, the frequency difference determined by $\Delta kl = \pm\pi$ is 135 GHz. The error is about 35%, which cannot be neglected.

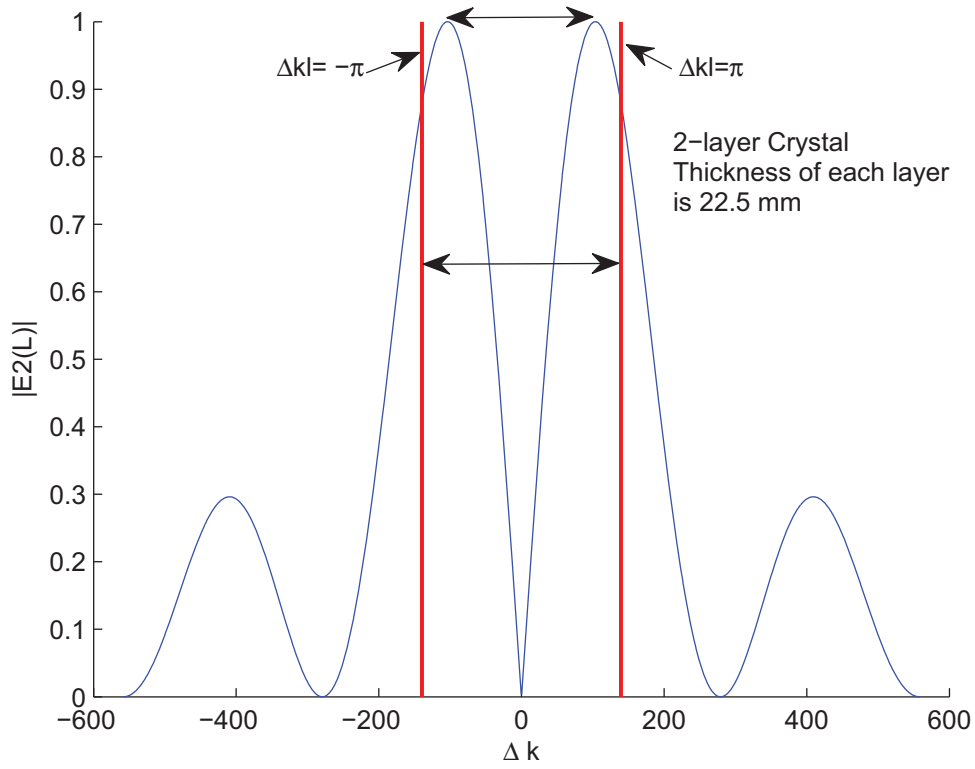

Figure A.1: Amplitude of SHG as a function of Δk; 2 layer crystal.

A.4 In crystal with more than 2 layers

As $N > 1$, we will have to see equations (A.9) again

$$|E_2(L)| = 4\Gamma d_{eff} \frac{\left[\sin(\Delta k \frac{L}{4N})\right]^2}{|\Delta k|} \cdot \left| \frac{\sin(\Delta k \frac{L}{2})}{\sin(\Delta k \frac{L}{2N})} \right| \tag{A.15}$$

When N is a large number, $\left| \frac{\sin(\Delta k \frac{L}{2})}{\sin(\Delta k \frac{L}{2N})} \right|$ will play a dominant role in determining the maximum value of $|E_2(L)|$. $\left| \frac{\sin(\Delta k \frac{L}{2})}{\sin(\Delta k \frac{L}{2N})} \right|$ is maximized when $\Delta k \frac{L}{2N} = \pm m\pi, m = 1, 2.....$ In the composite crystal, $\frac{L}{2N} = l$, where l is the length of each layer. Here, we take the first order and choose $m = 1$. Thus, $\left| \frac{\sin(\Delta k \frac{L}{2})}{\sin(\Delta k \frac{L}{2N})} \right|$ is maximized when

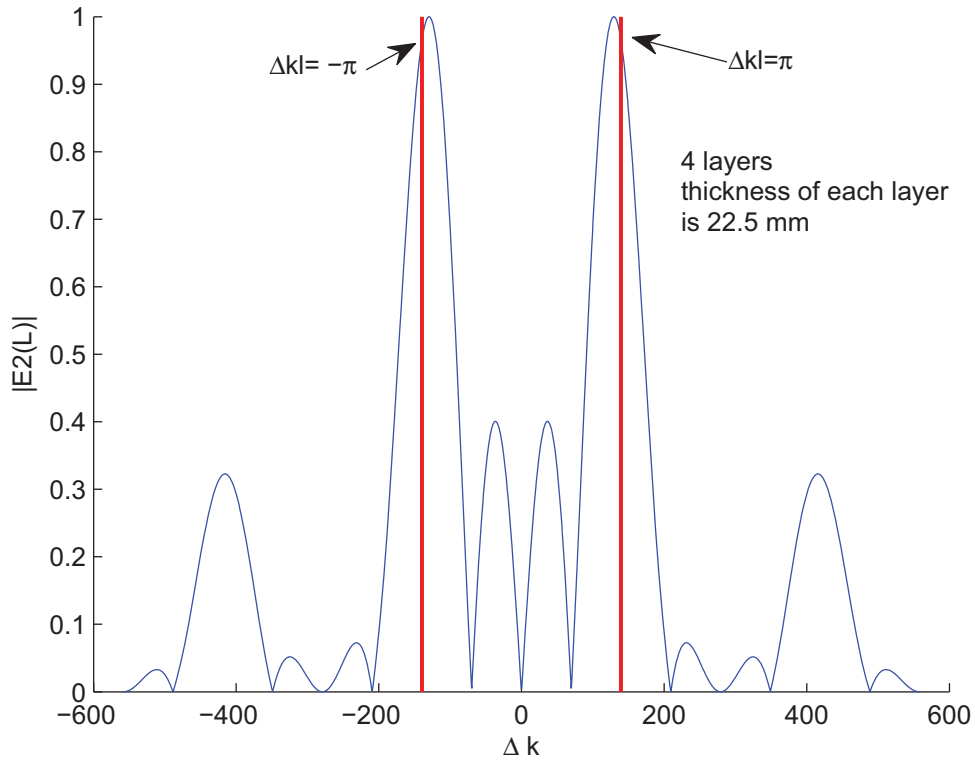

Figure A.2: Amplitude of SHG as a function of Δk; 4 layer crystal.

$\Delta kl = \pm\pi$. We plot the value of $|E_2(L)|$ in crystals with 4 layer and 6 layer in Fig. A.2 and Fig. A.3, respectively. The thickness of each layer in these crystals are the same. We can see that when the number of layers N is larger, the position of $|E_2(L)|$ is become closer and closer with the position of Δk determined by $\Delta kl = \pm\pi$.

We also estimated the error by calculating the frequency difference between the dual-signal in OPO. In crystal with 4 layers, the error reduced to 7.7%. In addition, in crystal with 6 layers, the error reduced further to 3.2%, which means that the expression of $\Delta kl = \pm\pi$ is already very precise.

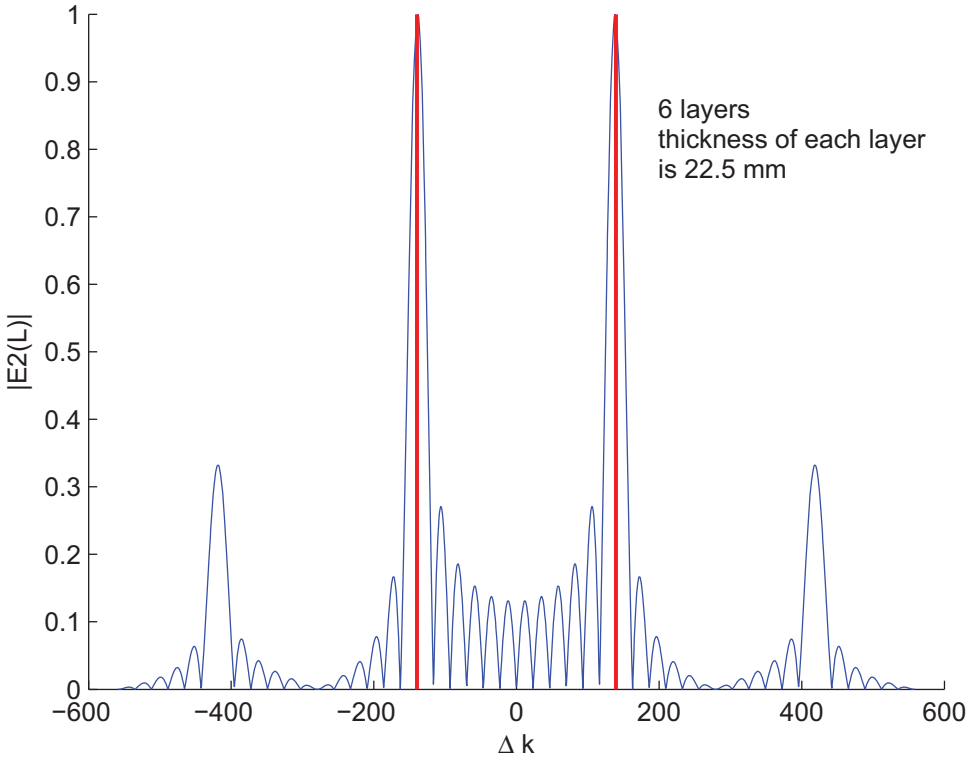

Figure A.3: Amplitude of SHG as a function of Δk; 6 layer crystal.

Bibliography

[1] B. Ferguson and X. C. Zhang. Materials for terahertz science and technology. *Nature Materials*, 1(1):26–33, 2002.

[2] A. Dobroiu, C. Otani, and K. Kawase. Terahertz-wave sources and imaging applications. *Measurement Science and Technology*, 17(11):R161–R174, 2006.

[3] Renbo Song, Wei Shi, and Y. J. Ding. Direct measurements of resonance peaks of dna's and proteins using widely-tunable monochromatic thz source. volume vol.1 of *2003 IEEE LEOS Annual Meeting Conference Proceedings (IEEE Cat. No.03CH37460)*, page 238 vol.1, Piscataway, NJ, USA, 2003. IEEE.

[4] Yun-Shik Lee. *Principles of Terahertz Science and Technology*. Springer Publishing Company, Incorporated, 2008.

[5] X. D. Mu, I. B. Zotova, and Y. J. Ding. Power scaling on efficient generation of ultrafast terahertz pulses. *IEEE Journal of Selected Topics in Quantum Electronics*, 14(2):315–332, 2008.

[6] Xu Xie, Jianming Dai, and X. C. Zhang. Coherent control of thz wave generation in ambient air. *Physical Review Letters*, 96(7):075005, 2006.

[7] W. Shi, Y. J. J. Ding, X. D. Mu, and N. Fernelius. Tunable and coherent nanosecond radiation in the range of 2.7-28.7 μm based on difference-frequency generation in gallium selenide. *Applied Physics Letters*, 80(21):3889–3891, 2002.

[8] W. Shi, Y. J. J. Ding, N. Fernelius, and K. Vodopyanov. Efficient, tunable, and coherent 0.18-5.27-THz source based on GaSe crystal. *Optics Letters*, 27(16):1454–1456, 2002.

[9] W. Shi and Y. J. J. Ding. A monochromatic and high-power terahertz source tunable in the ranges of 2.7-38.4 and 58.2-3540 μm for variety of potential applications. *Applied Physics Letters*, 84(10):1635–1637, 2004.

[10] W. Shi, Y. J. J. Ding, and P. G. Schunemann. Coherent terahertz waves based on difference-frequency generation in an annealed zinc-germanium phosphide crystal: improvements on tuning ranges and peak powers. *Optics Communications*, 233(1-3):183–189, 2004.

[11] W. Shi and Y. J. J. Ding. Continuously tunable and coherent terahertz radiation by means of phase-matched difference-frequency generation in zinc germanium phosphide. *Applied Physics Letters*, 83(5):848–850, 2003.

[12] W. Shi, Y. J. Ding, N. Fernelius, and K. Vodopyanov. Efficient, tunable, and coherent 0.18-5.27-THz source based on GaSe crystal (vol 27, pg 1454, 2002). *Optics Letters*, 28(2):136–136, 2003.

[13] W. Shi, Y. J. Ding, N. Fernelius, and F. K. Hopkins. Observation of difference-frequency generation by mixing of terahertz and near-infrared laser beams in a GaSe crystal. *Applied Physics Letters*, 88(10):101101, 2006.

[14] W. Shi and Y. J. Ding. Tunable terahertz waves generated by mixing two copropagating infrared beams in GaP. *Optics Letters*, 30(9):1030–1032, 2005.

[15] W. Shi and Y. J. Ding. Designs of terahertz waveguides for efficient parametric terahertz generation. *Applied Physics Letters*, 82(25):4435–4437, 2003.

[16] W. Shi and Y. J. J. Ding. Generation of backward terahertz waves in GaSe crystals. *Optics Letters*, 30(14):1861–1863, 2005.

[17] Y. J. Ding and W. Shi. Efficient THz generation and frequency upconversion in GaP crystals. *Solid-State Electronics*, 50(6):1128–1136, 2006.

[18] Y. Jiang, D. Li, Y. J. J. Ding, and I. B. Zotova. Terahertz generation based on parametric conversion: from saturation of conversion efficiency to back conversion. *Optics Letters*, 36(9):1608–1610, 2011.

[19] Y. Jiang, Y. J. Ding, and I. B. Zotova. Power scaling of widely-tunable monochromatic terahertz radiation by stacking high-resistivity GaP plates. *Applied Physics Letters*, 96(3):031101, 2010.

[20] Y. Jiang, Y. J. Ding, and I. B. Zotova. Power scaling of coherent terahertz pulses by stacking GaAs wafers. *Applied Physics Letters*, 93(24):241102, 2008.

[21] Y. Jiang and Y. J. Ding. Efficient terahertz generation from two collinearly propagating CO_2 laser pulses. *Applied Physics Letters*, 91(9):091108, 2007.

[22] G. B. Xu, X. D. Mu, Y. J. Ding, and I. B. Zotova. Efficient generation of backward terahertz pulses from multiperiod periodically poled lithium niobate. *Optics Letters*, 34(7):995–997, 2009.

[23] F. Capasso, K. Mohammed, and A. Y. Cho. Resonant tunneling through double barriers, perpendicular quantum transport phenomena in superlattices, and their device applications. *Ieee Journal of Quantum Electronics*, 22(9):1853–1869, 1986.

[24] J. Faist, F. Capasso, D. L. Sivco, C. Sirtori, A. L. Hutchinson, and A. Y. Cho. Quantum cascade laser. *Science*, 264(5158):553–556, 1994.

[25] J. Faist, F. Capasso, C. Sirtori, D. L. Sivco, J. N. Baillargeon, A. L. Hutchinson, S. N. G. Chu, and A. Y. Cho. High power mid-infrared (lambda greater than or similar to-5 mu m) quantum cascade lasers operating above room temperature. *Applied Physics Letters*, 68(26):3680–3682, 1996.

[26] R. Kohler, A. Tredicucci, F. Beltram, H. E. Beere, E. H. Linfield, A. G. Davies, D. A. Ritchie, R. C. Iotti, and F. Rossi. Terahertz semiconductor-heterostructure laser. *Nature*, 417(6885):156–159, 2002.

[27] B. S. Williams, S. Kumar, Q. Hu, and J. L. Reno. Operation of terahertz quantum-cascade lasers at 164 k in pulsed mode and at 117 k in continuous-wave mode. *Optics Express*, 13(9):3331–3339, 2005.

[28] M. A. Belkin, F. Capasso, A. Belyanin, D. L. Sivco, A. Y. Cho, D. C. Oakley, C. J. Vineis, and G. W. Turner. Terahertz quantum-cascade-laser source based on intracavity difference-frequency generation. *Nature Photonics*, 1(5):288–292, 2007.

[29] J. E. Schaar, K. L. Vodopyanov, and M. M. Fejer. Intracavity terahertz-wave generation in a synchronously pumped optical parametric oscillator using quasi-phase-matched GaAs. *Optics Letters*, 32(10):1284–1286, 2007.

[30] K. Kawase, M. Sato, T. Taniuchi, and H. Ito. Coherent tunable THz-wave generation from $LiNbO_3$ with monolithic grating coupler. *Applied Physics Letters*, 68(18):2483–2485, 1996.

[31] S. Kumar, B. S. Williams, Q. Hu, and J. L. Reno. 1.9 THz quantum-cascade lasers with one-well injector. *Applied Physics Letters*, 88(12):121123, 2006.

[32] G. Sun and R. A. Soref. Si-based quantum staircase terahertz lasers. *Microelectronics Journal*, 34(5-8):391–393, 2003.

[33] U. Willer, R. Wilk, W. Schippers, S. Bottger, D. Nodop, T. Schossig, W. Schade, M. Mikulics, M. Koch, M. Walther, H. Niemann, and B. Guttler. A novel THz source based on a two-color Nd: LSB microchip-laser and a LT-GaAsSb photomixer. *Applied Physics B-Lasers and Optics*, 87(1):13–16, 2007.

[34] E. R. Brown, F. W. Smith, and K. A. McIntosh. Coherent millimeter-wave generation by heterodyne conversion in low-temperature-grown GaAs photoconductors. *Journal of Applied Physics*, 73(3):1480–1484, 1993.

[35] P. Zhao, S. Ragam, Y. J. Ding, and I. B. Zotova. Compact and portable terahertz source by mixing two frequencies generated simultaneously by a single solid-state laser. *Optics Letters*, 35(23):3979–3981, 2010.

[36] A. W. M. Lee, Q. Qin, S. Kumar, B. S. Williams, and Q. Hu. Real-time terahertz imaging over a standoff distance ($>$ 25 meters). *Applied Physics Letters*, 89(14):141125, 2006.

[37] H. Q. Sun, Y. J. J. Ding, and I. B. Zotova. Thz spectroscopy by frequency-tuning monochromatic THz source: From single species to gas mixtures. *IEEE Sensors Journal*, 10(3):621–629, 2010.

[38] T. Kleine-Ostmann, R. Wilk, F. Rutz, M. Koch, H. Niemann, B. Guttler, K. Brandhorst, and J. Grunenberg. Probing noncovalent interactions in biomolecular crystals with terahertz spectroscopy. *Chemphyschem*, 9(4):544–547, 2008.

[39] B. Frei and J. E. Balmer. 1553 nm wavelength selection in a diode-laser-pumped $Nd:YLF$ laser. *Applied Optics*, 33(30):6942–6946, 1994.

[40] H. Zbinden and J. E. Balmer. Q-switched Nd-YLF laser end pumped by a diode-laser bar. *Optics Letters*, 15(18):1014–1016, 1990.

[41] B. Wu, P. P. Jiang, D. Z. Yang, T. Chen, J. Kong, and Y. H. Shen. Compact dual-wavelength $Nd : GdVO_4$ laser working at 1063 and 1065 nm. *Optics Express*, 17(8):6004–6009, 2009.

[42] W Koechner and M Bass. *Solid-State Lasers*. Springer Publishing Company, Incorporated, 2003.

[43] D. N. Nikogosyan. *Nonlinear Optical Crystals*. Springer Publishing Company, Incorporated, 2005.

[44] Q. Qin, B. S. Williams, S. Kumar, J. L. Reno, and Q. Hu. Tuning a terahertz wire laser. *Nature Photonics*, 3(12):732–737, 2009.

[45] P. Zhao, S. Ragam, Y. J. J. Ding, and I. B. Zotova. Power scalability and frequency agility of compact terahertz source based on frequency mixing from solid-state lasers. *Applied Physics Letters*, 98(13):131106, 2011.

[46] F. Trager. *Handbook of Lasers and Optics*. Springer, New York, 2008.

[47] Y. Avetisyan, Y. Sasaki, and H. Ito. Analysis of THz-wave surface-emitted difference-frequency generation in periodically poled lithium niobate waveguide. *Applied Physics B-Lasers and Optics*, 73(5-6):511–514, 2001.

[48] Y. J. Ding. Efficient generation of high-frequency terahertz waves from highly lossy second-order nonlinear medium at polariton resonance under transverse-pumping geometry. *Optics Letters*, 35(2):262–264, 2010.

[49] P. Zhao, S. Ragam, Y. J. J. Ding, and I. B. Zotova. Terahertz intracavity generation from output coupler consisting of stacked GaP plates. *Applied Physics Letters*, 101(2):021107, 2012.

[50] Pu Zhao, Srinivasa Ragam, Yujie J. Ding, and Ioulia B. Zotova. Intracavity terahertz generation in laser output coupler made from stacked GaP plates. In *CLEO: QELS-Fundamental Science*, page JW2A.41. Optical Society of America, 2012.

[51] R. Smith. Theory of intracavity optical second-harmonic generation. *IEEE Journal of Quantum Electronics*, 6(4):215–223, 1970.

[52] E. C. Honea, C. A. Ebbers, R. J. Beach, J. A. Speth, J. A. Skidmore, M. A. Emanuel, and S. A. Payne. Analysis of an intracavity-doubled diode-pumped

Q-switched Nd: YAG laser producing more than 100 W of power at 0.532 μm. *Optics Letters*, 23(15):1203–1205, 1998.

[53] D. G. Xu, Y. Y. Wang, H. F. Li, J. Q. Yao, and Y. H. Tsang. 104 w high stability green laser generation by using diode laser pumped intracavity frequency-doubling Q-switched composite ceramic Nd: YAG laser. *Optics Express*, 15(7):3991–3997, 2007.

[54] D. J. M. Stothard, T. J. Edwards, D. Walsh, C. L. Thomson, C. F. Rae, M. H. Dunn, and P. G. Browne. Line-narrowed, compact, and coherent source of widely tunable terahertz radiation. *Applied Physics Letters*, 92(14):141105, 2008.

[55] M. Scheller, J. M. Yarborough, J. V. Moloney, M. Fallahi, M. Koch, and S. W. Koch. Room temperature continuous wave milliwatt terahertz source. *Optics Express*, 18(26):27112–27117, 2010.

[56] E. B. Petersen, W. Shi, A. Chavez-Pirson, N. Peyghambarian, and A. T. Cooney. Efficient parametric terahertz generation in quasi-phase-matched GaP through cavity enhanced difference-frequency generation. *Applied Physics Letters*, 98(12):121119, 2011.

[57] L. A. Coldren and S. W. Corzine. *Diode Lasers and Photonic Integrated Circuits*. John Wiley & Sons, New York, 1995.

[58] J. J. Zayhowski and C. Dill. Diode-pumped passively Q-switched picosecond microchip lasers. *Optics Letters*, 19(18):1427–1429, 1994.

[59] P. Zhao, S. Ragam, Y. J. J. Ding, and I. B. Zotova. Investigation of terahertz generation from passively Q-switched dual-frequency laser pulses. *Optics Letters*, 36(24):4818–4820, 2011.

[60] J. F. Noxon. Nitrogen dioxide in the stratosphere and troposphere measured by ground-based absorption spectroscopy. *Science*, 189(4202):547–549, 1975.

[61] J. B. Khurgin, F. Jin, G. Solyar, C. C. Wang, and S. Trivedi. Cost-effective low timing jitter passively Q-switched diode-pumped solid-state laser with composite pumping pulses. *Applied Optics*, 41(6):1095–1097, 2002.

[62] B. Cole, L. Goldberg, C. W. Trussell, A. Hays, B. W. Schilling, and C. McIntosh. Reduction of timing jitter in a Q-Switched Nd:YAG laser by direct bleaching of a Cr^{4+}:YAG saturable absorber. *Optics Express*, 17(3):1766–1771, 2009.

[63] T. Hakulinen, R. Koskinen, and O. G. Okhotnikov. Low jitter Q-switched fiber laser using optically driven surface-normal saturable absorber modulator. *Optics Express*, 16(12):8720–8726, 2008.

[64] A. Steinmetz, D. Nodop, A. Martin, J. Limpert, and A. Tunnermann. Reduction of timing jitter in passively Q-switched microchip lasers using self-injection seeding. *Optics Letters*, 35(17):2885–2887, 2010.

[65] X. J. Wang and Z. Y. Xu. Timing jitter reduction and single-frequency operation in an acousto-optic Q-switched Cr,Nd: YAG laser. *Applied Optics*, 45(33):8477–8483, 2006.

[66] V. K. Bagdasarov, N. N. Denisov, A. A. Malyutin, and I. A. Chigaev. Pulse synchronisation in passively Q-switched lasers emitting at 1.053 and 1.064 μm. *Quantum Electronics*, 39(10):887–890, 2009.

[67] H. P. H. Cheng, P. Tidemand-Lichtenberg, O. B. Jensen, P. E. Andersen, P. M. Petersen, and C. Pedersen. Experimental investigation of relative timing jitter in passively synchronized Q-switched lasers. *Optics Letters*, 36(3):415–417, 2011.

[68] P. Tidemand-Lichtenberg, J. Janousek, R. Melich, J. L. Mortensen, and P. Buchhave. Synchronization of 1064 and 1342 nm pulses using passive saturable absorbers. *Optics Communications*, 241(4-6):487–492, 2004.

[69] U. Sharma, C. S. Kim, and J. U. Kang. Highly stable tunable dual-wavelength Q-switched fiber laser for DIAL applications. *IEEE Photonics Technology Letters*, 16(5):1277–1279, 2004.

[70] R. Diaz, S. C. Chan, and J. M. Liu. Lidar detection using a dual-frequency source. *Optics Letters*, 31(24):3600–3602, 2006.

[71] F. Ganikhanov, S. Carrasco, X. S. Xie, M. Katz, W. Seitz, and D. Kopf. Broadly tunable dual-wavelength light source for coherent anti-Stokes Raman scattering microscopy. *Optics Letters*, 31(9):1292–1294, 2006.

[72] K. Miyamoto and H. Ito. Wavelength-agile mid-infrared (5-10 μm) generation using a galvano-controlled $KTiOPO_4$ optical parametric oscillator. *Optics Letters*, 32(3):274–276, 2007.

[73] H. Ito, K. Suizu, T. Yamashita, A. Nawahara, and T. Sato. Random frequency accessible broad tunable terahertz-wave source using phase-matched 4-dimethylamino-n-methyl-4-stilbazolium tosylate crystal. *Japanese Journal of Applied Physics Part 1-Regular Papers Brief Communications & Review Papers*, 46(11):7321–7324, 2007.

[74] X. D. Mu, H. Meissner, and H. C. Lee. Optical parametric oscillations of 2 μm in multiple-layer bonded walk-off compensated KTP stacks. *Optics Letters*, 35(3):387–389, 2010.

[75] Pu Zhao, Srinivasa Ragam, Yujie J. Ding, Ioulia B. Zotova, Xiaodong Mu, Huai-Chuan Lee, Stephanie K. Meissner, and Helmuth Meissner. Singly resonant optical parametric oscillator based on adhesive-free-bonded periodically inverted $KTiOPO_4$ plates: terahertz generation by mixing a pair of idler waves. *Optics Letters*, 37(7):1283–1285, 2012.

[76] S. Yokoyama, R. Nakamura, M. Nose, T. Araki, and T. Yasui. Terahertz spectrum analyzer based on a terahertz frequency comb. *Optics Express*, 16(17):13052–13061, 2008.

[77] T. Yasui, Y. Kabetani, E. Saneyoshi, S. Yokoyama, and T. Araki. Terahertz frequency comb by multifrequency-heterodyning photoconductive detection for high-accuracy, high-resolution terahertz spectroscopy. *Applied Physics Letters*, 88(24):241104, 2006.

[78] G. Scalari, L. Sirigu, R. Terazzi, C. Walther, M. I. Amanti, M. Giovannini, N. Hoyler, J. Faist, M. L. Sadowski, H. Beere, D. Ritchie, L. A. Dunbar, and

R. Houdre. Multi-wavelength operation and vertical emission in THz quantum-cascade lasers. *Journal of Applied Physics*, 101(8):081726, 2007.

[79] A. A. Sirotkin, S. V. Garnov, A. I. Zagumennyi, Y. D. Zavartsev, S. A. Kutovoi, V. I. Vlasov, L. Di Labio, W. Luthy, T. Feurer, and I. A. Shcherbakov. New lasers based on c-cut vanadat crystals. *Laser Physics*, 19(5):1083–1091, 2009.

[80] D. Zimmermann, D. Bollmann, I. Rohde, D. Theisen-Kunde, and R. Brinkmann. Compact, Q-switched Yb:YAG laser with a new longitudinal pumping concept. In *Lasers and Electro-Optics Europe, 2005. CLEO/Europe. 2005 Conference on*, page 78, june 2005.

[81] H. Z. Cao, H. Y. Peng, M. H. Zhang, Y. Q. Chen, B. Zhang, B. L. Chen, J. Zhang, T. H. Wu, X. M. Zhao, and H. M. Tan. Laser diode array (LDA) end-pumped multi-watt Yb:YAG 1030 nm laser. *Optica Applicata*, 40(3):653–656, 2010.

[82] V. V. Ter-Mikirtychev, M. A. Dubinskii, and V. A. Fromzel. Q-switched, TEM_{00}-mode, diode-pumped Yb^{3+}: YAG laser with extended tunability. *Optics Communications*, 197(4-6):403–411, 2001.

[83] W. F. Krupke. Ytterbium solid-state lasers - the first decade. *IEEE Journal of Selected Topics in Quantum Electronics*, 6(6):1287–1296, 2000.

[84] P. Lacovara, H. K. Choi, C. A. Wang, R. L. Aggarwal, and T. Y. Fan. Room-temperature diode-pumped Yb-YAG laser. *Optics Letters*, 16(14):1089–1091, 1991.

[85] A. Giesen, H. Hugel, A. Voss, K. Wittig, U. Brauch, and H. Opower. Scalable concept for diode-pumped high-power solid-state lasers. *Applied Physics B-Lasers and Optics*, 58(5):365–372, 1994.

[86] C. Stewen, K. Contag, M. Larionov, A. Giesen, and H. Hugel. A 1-kw CW thin disc laser. *IEEE Journal of Selected Topics in Quantum Electronics*, 6(4):650–657, 2000.

[87] E. Innerhofer, T. Sudmeyer, F. Brunner, R. Haring, A. Aschwanden, R. Paschotta, C. Honninger, M. Kumkar, and U. Keller. 60-w average power in 810-fs pulses from a thin-disk Yb: YAG laser. *Optics Letters*, 28(5):367–369, 2003.

[88] J. R. Lu, K. Ueda, H. Yagi, T. Yanagitani, Y. Akiyama, and A. A. Kaminskii. Neodymium doped yttrium aluminum garnet ($Y_3Al_5O_{12}$) nanocrystalline ceramics - a new generation of solid state laser and optical materials. *Journal of Alloys and Compounds*, 341(1-2):220–225, 2002.

[89] Shinki Nakamura, Hiroaki Yoshioka, Takayo Ogawa, and Satoshi Wada. Broadly Tunable Yb^{3+}-Doped $Y_3Al_5O_{12}$ Ceramic Laser at Room Temperature. *Japanese Journal of Applied Physics*, 48(6):060205, 2009.

[90] S. Nakamura, Yu. Matsubara, T. Ogawa, and S. Wada. High-Power and Highly Efficient $Yb^{3+} - doped Y_3Al_5O_{12}$ Ceramic Laser at Room Temperature. In *Lasers and Electro-Optics - Pacific Rim, 2007. CLEO/Pacific Rim 2007. Conference on*, pages 1 –2, aug. 2007.

[91] Pu Zhao, Srinivasa Ragam, Yujie J. Ding, and Ioulia B. Zotova. Generation of terahertz pulses by mixing dual-frequency pulses from Yb:YAG laser. In *CLEO: QELS-Fundamental Science*, page QF3G.2. Optical Society of America, 2012.

[92] David A Walsh, Peter G Browne, Malcolm H Dunn, and Cameron F Rae. Intracavity parametric generation of nanosecond terahertz radiation using quasi-phase-matching. *Optics Express*, 18(13):13951–13963, Jun 2010.

[93] Xiaodong Mu, Helmuth E. Meissner, and Huai-Chuan Lee. Multilayer walk-off corrected nonlinear optical devices - engineering of quasi-noncritical phase-matching to all wavelengths. In *Conference on Lasers and Electro-Optics/International Quantum Electronics Conference*, page CMJ2. Optical Society of America, 2009.

[94] M.M. Fejer, G.A. Magel, D.H. Jundt, and R.L. Byer. Quasi-phase-matched second harmonic generation: tuning and tolerances. *Quantum Electronics, IEEE Journal of*, 28(11):2631 –2654, 1992.

Invention and Publication List

Patent

1. **Pu Zhao**, Srinivasa Ragam and Yujie J. Ding, "Terahertz Source", US patent (US 20120044959), (2012).

Journal Papers

1. **Pu Zhao**, Srinivasa Ragam, Yujie J. Ding and Ioulia B. Zotova, "Terahertz intracavity generation from output coupler consisting of stacked GaP Plates", *Applied Physics Letters*, 101, 021107 (2012).

2. **Pu Zhao**, Srinivasa Ragam, Yujie J. Ding, Ioulia B. Zotova, Xiaodong Mu, Huai-Chuan Lee, Stephanie K. Meissner, and Helmuth Meissner, "Singly-resonant optical parametric oscillator based in adhesive-free-bonded periodically-inverted $KTiOPO_4$ plates: oscillation at four wavelengths and terahertz generation", *Optics Letters*, 37, 1283-1285 (2012).

3. **Pu Zhao**, Srinivasa Ragam, Yujie J. Ding and Ioulia B. Zotova, "Investigation of terahertz generation from passively Q-switched dual-frequency laser pulses", *Optics Letters*, 36, 4818-4820 (2011).

4. **Pu Zhao**, Srinivasa Ragam, Yujie J. Ding and Ioulia B. Zotova, "Power scalability and frequency agility of compact terahertz source based on frequency mixing from solid-state lasers", *Applied Physics Letters*, 98, 131106 (2011) .

5. **Pu Zhao**, Srinivasa Ragam, Yujie J. Ding and Ioulia B. Zotova, "Compact and portable terahertz source by mixing two frequencies generated simultaneously by a single solid-state laser", *Optics Letters*, 35, 3979-3981 (2010).

6. **Pu Zhao**, Yujie J. Ding and Ioulia B. Zotova, "Power scaling of blue and red light based on frequency mixing inside adhesive-free bond composite Nd:YAG laser cavity", *Optics Communications*, 283, 1905-1908 (2010).

Conference Papers

1. **Pu Zhao**, Srinivasa Ragam, Lei Wang, Yujie J. Ding, Ioulia B. Zotova and et al., "Simultaneous Generation of Multiple THz Frequencies Tunable for Novel Applications," in Conference of CLEO 2012, paper CTu1B.8.

2. **Pu Zhao**, Srinivasa Ragam, Yujie J. Ding and Ioulia B. Zotova, "Intracavity terahertz generation in laser output coupler made from stacked GaP plates," in Conference of CLEO 2012, paper JW2A.41.

3. **Pu Zhao**, Srinivasa Ragam, Yujie J. Ding and Ioulia B. Zotova, "Generation of Terahertz Pulses by Mixing Dual-Frequency Pulses from Yb:YAG Laser," in Conference of CLEO 2012, paper QF3G.2.

4. **Pu Zhao**, Srinivasa Ragam, Yujie J. Ding and Ioulia B. Zotova, "Compact and Portable Terahertz Source by Mixing Two Frequencies Generated Simultaneously by Single Solid-State Laser," in Conference of CLEO 2011, paper CMFF4.

5. Srinivasa Ragam, **Pu Zhao**, Yujie J. Ding and Ioulia B. Zotova, "Power Scaling of Actively Q-Switched Synchronized Dual-Frequency Laser Pulses based on Two Nd: YLF Crystals," in Conference of CLEO 2011, paper CMP4.

6. **Pu Zhao**, Srinivasa Ragam, Yujie J. Ding and Ioulia B. Zotova, "Demonstration of Terahertz Generation by Mixing Passively Q-Switched Dual-Frequency Nd:YLF Laser Pulses," in Conference of CLEO 2011, paper QTuB5.

7. **Pu Zhao**, Srinivasa Ragam, Yujie J. Ding, et al., "Singly-Resonant Optical Parametric Oscillator in Adhesive- Free-Bonded Periodically Inverted $KTiOPO_4$ Plates: Achieving Oscillations at Dual Wavelengths," in Conference of CLEO 2011, paper CMR2.

8. **Pu Zhao**, Yujie J. Ding, and Ioulia B. Zotova , "Synchronized dual-frequency pulses from Q-switched compact Nd:YLF laser cavities," in Conference of CLEO 2010, paper JTuD109.

9. **Pu Zhao**, Yujie J. Ding, and Ioulia B. Zotova , "Power scaling of coherent blue light source based on frequency tripling inside adhesive-free bond composite Nd:YAG laser cavity," in Conference of CLEO 2010, paper JTuD113.

10. Baigang Zhang, **Pu Zhao**, Yujie J. Ding, and Ioulia B. Zotova , "Ultrabroadband second-Harmonic generation in slant-stripe-type periodically-poled $RbTiOPO_4$," in Conference of CLEO 2009, paper JWA126.

Vita

Pu Zhao received his B.E. degree in electronic science and technology and B.A. degree in English from Tianjin University, Tianjin, China in 2004. He also received his M.E. degree in physical electronics from Tianjin University in 2007. He is currently pursuing the Ph.D degree in electrical engineering at Lehigh University, Bethlehem, Pennsylvania.

His research interest lies in terahertz generation, nonlinear optics, diode pumped solid-state lasers, intracavity frequency doubling and tripling, optical parametric oscillator (OPO), optical frequency conversion, quasi-phase-matching technology.